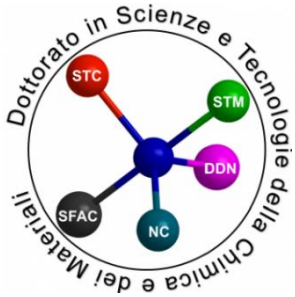

University of Genova
Doctoral School in Science and Technology of
Chemistry and Materials
(*XXXII cycle*)

Heterogeneous Nucleation in Semicrystalline Polymers

Bao Wang

Tutor: Prof. Dario Cavallo

Thesis defense day: 20 March 2020

Contents

Chapter 1. Summary and Outline

Nucleation of polymer crystals is a key issue in polymer science and technology. Indeed, it is of outmost importance for industrial application of semicrystalline polymers, since the nucleation rate often dictates the processing time of the products, and strongly affects the resulting mechanical or optical properties of the material. Despite this a comprehensive understanding of the phenomenon is still lacking, as testified for instance by the fact that the scouting of new heterogeneous nucleating agents for polymers is still mostly driven by empiricism. With this thesis, we aim to provide novel quantitative approaches to quantify the heterogeneous nucleation efficiency of different surfaces in various, industrially relevant, systems, such as polymer/fiber composites or nucleated polymers. The presented results are a contribution towards the clarification of the mechanism of heterogeneous nucleation in semicrystalline polymers.

1.1 Summary

The nucleation process of biodegradable poly(lactide) on a series of fibers, including commercially available fibers, natural fibers and a custom-spun fiber of stereocomplex enantiomeric PLA blend, was studied by polarized optical microscope during crystallization. The nucleation ability of different fiber substrates was derived and compared in the light of classical heterogeneous nucleation theory, by considering the interfacial free energy difference parameter, $\Delta\sigma$, directly related to the nucleation barrier. The role of fiber surface topography and chemical interactions between the fiber substrate and the crystallizing polymer in promoting the nucleation was investigated and discussed in detail. While a general effect of surface roughness on lowering the heterogeneous nucleation energy barrier can be deduced, the role of chemical interactions between the fiber substrate and the crystallizing polymer cannot be neglected.

Furthermore, a novel approach was proposed to quantitatively evaluate the nucleation efficiency of several additives for isotactic polypropylene (i-PP), using droplets containing nucleating agents (i.e., sodium benzoate, NA11, quinacridone quinone) dispersed in an immiscible polystyrene matrix. The crystallization was investigated by isothermal step crystallization and melting with Differential Scanning Calorimetry (DSC). Moreover, self-nucleation of neat i-PP droplets is also studied in detail, enabling to derive an “intrinsic” nucleation efficiency scale based on the ratio of the free energy barrier, ΔG^*, of

heterogeneous nucleation on different substrates with respect to that of self-nucleation, which is found equivalent to the secondary nucleation barrier for crystal growth. Having established the interfacial free energy difference parameter ($\Delta\sigma$) governing the heterogeneous nucleation kinetics of i-PP onto different substrates, a simple correlation curve useful to describe non-isothermal fractionated crystallization of i-PP/PS blends with droplet morphology was constructed.

Finally, we propose a Differential Scanning Calorimetry (DSC) approach for the quantitative investigation of isotactic poly(1-butene) Form II-on-Form I cross-nucleation. Seeds of trigonal Form I crystal were produced in PB1 samples, and their amount and characteristic size were varied by using different crystallization conditions. DSC isothermal and non-isothermal crystallization measurements of Form I seeded samples were performed, highlighting a clear nucleation effect of the stable polymorph on Form II. Moreover, the nucleating efficiency is highly dependent on the content of Form I seeds, more specifically, on the area of Form I spherulites per unit of sample volume. Depending on the seeding and crystallization conditions, Form II crystallization is controlled either by nucleation on foreign heterogeneous surfaces or on Form I crystals.

1.2 Outline of the Thesis

In Chapter 2, some general concepts about polymer crystallization, with emphasis on the nucleation step, required for the comprehension of the present thesis, are provided. In particular, the related thermodynamic and kinetics aspects involved in the process are described.

Chapter 3 tackles a very common nucleation phenomenon in polymer/fiber composites. The nucleation process of poly(lactide) on various fiber substrates was studies. The contribution to nucleation of fiber surface roughness and chemical interaction between PLA and the fiber substrates were investigated and discussed in detail.

A new method to quantitatively evaluate the nucleation efficiency of nucleating agents towards polypropylene is proposed in Chapter 4. With respect to the empirical nucleation efficiency method proposed in the literature, in this chapter, we quantify a model-based parameter, the interfacial free energy barrier, potentially useful for the industrial scouting of efficient nucleating agents.

In addition, a particular nucleation phenomenon, known as cross-nucleation, was re-examined by Differential Scanning Calorimetry method. The approach, described in Chapter 5, shows its advantage to study cross-nucleation in polymorphic systems in which

morphological evidences are not sufficiently informative.

The most important achievements of the whole investigation, together with some perspectives for future work, are summarized in Chapter 6.

Chapter 2. General Introduction

2.1 The Phenomenon of Polymer Crystallization

The phenomenon of polymer crystallization has always been one of the most important and fascinating aspects of polymer physics. It is well known that the physical properties of polymers can be directly related to crystalline structure and morphology. Long chain polymers have low diffusion coefficients and high viscosities which significantly affect the crystalline structure and the morphology of the resulting polymer crystals. Theories for polymer crystallization were originally developed by adapting the theories developed for description of crystallization of small molecules and metals.[1, 2] However, the intrinsic differences between those materials and long chain polymers often led to unsatisfactory predictions in terms of the experimental results.

In the last decades, nucleation and growth mechanism of polymer crystals, including the corresponding kinetics, have been investigated intensively since the discovery of the chain folding in polyethylene single crystal in 1957 by Till, Keller, and Fischer.[3-6] Up to now, the most successful and widely accepted theory which describe polymer crystal growth was proposed by Hoffman and Lauritzen,[7-10] now known as Hoffman–Lauritzen (HL) theory and based on secondary nucleation at the lateral growth front of lamellar polymer crystals. One of the advantages of the HL theory is that it provides an analytical form to connect microscopic parameters with macroscopic quantities. However, Sadler-Gilmer[11, 12] argued that the secondary nucleation barrier is completely an “entropy barrier” without any enthalpic contribution. Furthermore, some other nucleation models (e.g. chain sliding diffusion theory, intramolecular nucleation) were developed by Hikosaka[13-15] and Hu[16, 17] *et al*. Recently additional crystallization/growth models have been put forward, i.e., the mesophase model by Strobl,[18-21] a continuum coarse-grained model by Muthukumar [22, 23] and the molecular nucleation model by Wunderlich.[24-26]

Polymer crystallization features in the development of polymer science and the corresponding theories have been debated for more than fifty years; however, new models or theories are still being proposed nowadays, which indicates that the field itself is essentially complex and robustly vital. Open questions remaining in this field, and controversial opinions still deserve further discussion.

2.2 Primary Nucleation

Polymer crystallization is a first order phase transition of a supercooled liquid, and in order for this thermodynamically favored transformation to occur, two separate processes are required, i.e., the stable phase has to nucleate and then grow within the metastable phase. The nucleation step is an activated process that relies on microscopic fluctuations to produce a critical size nucleus of the new phase, also called primary nucleus.

2.2.1 Nucleation Theory Concepts

Nucleation requires a particular molecular chain arrangement to form the new phase. In the case of polymer crystallization from the melt, the chain segments must approach themselves to distances commensurate to those characteristics of the crystalline unit cell, and must possess the right conformation, as the crystal symmetry imposes. From a thermodynamic point of view, the chain segments with those attributes form a crystalline aggregate which varies the system free energy according to:

$$\Delta G = \Delta H - T\Delta S \tag{2.1}$$

where ΔH and ΔS are the enthalpy and entropy of crystallization, respectively. The thermodynamic equilibrium condition between the melt and the crystals is verified when ΔG is equal to zero, i.e., when the temperature of the system is the melting temperature, T_m. Crystallization becomes possible as soon as ΔG assumes negative values.

Any crystal must have its beginning as a small crystal with a large specific surface area. Therefore, Equation 2.1 can also be written by explicitly expressing the surface and volume contributions to the Gibbs free energy:

$$\Delta G = V\Delta g + \sum_i A_i \sigma_i \tag{2.2}$$

where V is the volume and A_i is the i-th surface of the aggregate, σ_i represents the (positive) surface free energy of the relative surface, and Δg is the bulk free energy change per unit volume associated to the formation of a new crystal. At temperatures above T_m, crystallization is thermodynamically impossible, while below T_m it becomes possible, but its occurrence depends on the competition between these two energy terms. As such, the ΔG exhibits a maximum with respect to the crystalline aggregate size, as shown in Figure 2.1. The maximum in ΔG corresponds to the critical size that the new crystal must attain in order to become a nucleus. Clusters smaller than r^* are called subcritical nuclei or embryos, they are unstable and tend to disappear from the system, since their growth is linked to an increase

of ΔG. Aggregates that exceed r^* are called supercritical nuclei as long as their ΔG is still positive: their growth to sizes exceeding the minimum stability requirement is thermodynamically favored. Nuclei with a negative ΔG are called stable nuclei or small crystals. The larger the critical nucleus size, the longer will be the time needed for the nucleation process.[27]

The classical concept of crystal nucleation was developed by Gibbs[28], Volmer[29], and Kossel[30], based on the assumption that fluctuations in the supercooled phase can overcome the nucleation barrier caused by the formation of the crystal surfaces. The probability of the presence of a nucleus of given size at constant volume and energy is, according to Boltzmann's law, a function of the change in entropy, proportional to $\exp(\Delta S/k)$. At constant pressure and temperature, the probability for the presence of a nucleus of given size is proportional to $\exp(-\Delta G/kT)$. The rate of nucleation I^* has been derived on these assumptions by Turnbull and Fisher[31] using absolute reaction rate theory[32] to be:

$$I^* = (NkT/h)exp\left[-\left(\Delta G^* + \Delta G_\eta\right)/kT\right] \tag{2.3}$$

The rate of nucleation is given in nuclei per second, and refers to the number of un-crystallized elements N able to participate in nucleation of a nucleus of critical size.

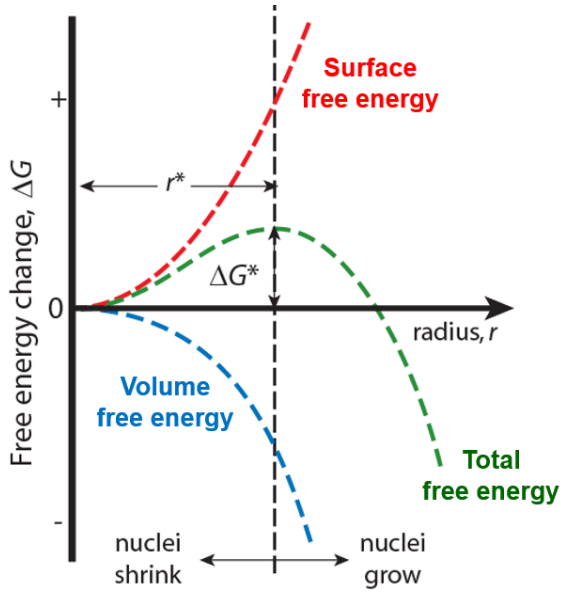

Figure 2.1 Schematic representation of the change in ΔG as a function of crystalline aggregate size, illustrating the nucleation process.

After this brief introduction on the primary nucleus, we will illustrate the nucleation phenomena usually occur in semi-crystalline polymers: homogeneous nucleation, heterogeneous nucleation and self-nucleation.

2.2.2 Homogeneous Nucleation

If there are no preformed nuclei or foreign surfaces in the polymer melt, the primary nucleation is called homogeneous nucleation. The process occurs as the result of random fluctuations of order in the melt. Considering a spherical nucleus with radius *r*, the free energy change associated to its formation is:

$$\Delta G = -\frac{4}{3}\pi r^3 \Delta g + 4\pi r^2 \sigma \tag{2.4}$$

The trend of this function is the same of that showed in Figure 2.1. The function $\Delta G = \Delta G(r)$ has a maximum for *r* equal to r^*, the critical nucleus dimension, given by:

$$r^* = \frac{2\sigma}{\Delta g} = \frac{2\sigma T_m}{\Delta h^o \Delta T} \tag{2.5}$$

where Δh^0 is the enthalpy of crystallization at the equilibrium melting point T_m and ΔT is the supercooling degree ($\Delta T = T_m - T$). The related value of the critical free energy variation, $\Delta G(r^*)$ can be computed as:

$$\Delta G^* = \frac{16}{3}\pi \frac{\sigma^3}{\Delta g^2} = \frac{16}{3}\pi \frac{\sigma^3 T_m^2}{(\Delta h^o)^2 (\Delta T)^2} \tag{2.6}$$

From Equation 2.4 and 2.5, it can be deduced that both the critical dimension and the size of the energetic barrier increase with the crystallization temperature. Therefore, the probability of nucleation drastically decreases at temperature near T_m.

In the case of polymers, we must consider a different geometry for the nucleating crystal, given the fact that this is built by the successive addition of adjacent segments of polymer chains. The simplest choice is that of a prismatic nucleus with quadratic cross section. For this geometry, and taking into account chain folding, we have to use two different surface free-energies: that of the bases (σ_e) and of the lateral surfaces (σ) of the parallelepiped. Then, the equation for the change in the free energy of crystallization becomes:

$$\Delta G = 4al\sigma + 2a^2\sigma_e - a^2 l \Delta g \tag{2.7}$$

where *a* and *l* are the cluster dimensions. In general, σ_e is 5 to 20 times the value of σ. Also, this function has a maximum (ΔG^*) in correspondence of the critical dimensions a^* and l^*:

$$a^* = \frac{4\sigma T_m}{\Delta T \Delta h^o} \tag{2.8}$$

$$l^* = \frac{4\sigma_e T_m}{\Delta T \Delta h^o} \tag{2.9}$$

$$\Delta G^* = \frac{32\sigma\sigma_e T_m^2}{(\Delta h^o)^2(\Delta T)^2} \tag{2.10}$$

The inverse dependence of the critical dimensions on the supercooling is the same as in the previously introduced model of the spherical nucleus.

Although predicted, homogeneous nucleation in polymers is rarely observed since requires particularly pure samples and extremely large supercooling.[33] In practical (and industrial) conditions, much lower supercooling is needed to observe nucleation and crystallization, due to the ubiquitous presence of foreign materials' surfaces on which heterogeneous nucleation favorably occurs. As a matter of fact, homogeneous nucleation can effectively play a role only at very low crystallization temperatures, often close to the polymer's glass transition. In order to be able to attain such large undercoolings, two methods have so far been adopted.

The first is based on subdividing the sample in a number of domains which is much larger than the number of possible nucleating impurities in bulk samples. This procedure increases the probability of finding relatively pure polymer domains which would then nucleate homogeneously, if the effect of the domain interfaces is not of importance. Several systems showing this behavior have been investigated,[34-38] going from immiscible blends with sea-island morphology,[39-42] suspension of micrometer/sub-micrometer size droplets,[43-45] block-copolymer nanodomains[46-48], infiltrated polymers within alumina nano-porous materials[36] and dewetted droplets on a substrate[49, 50]. The small domain size and the large undercoolings effectively make nucleation the rate-determining step in the overall crystallization process. As such, the domains crystallize one-by-one, following a first-order crystallization kinetics, with the rate constant typically scaling with the domain volume (see Figure 2.2(a)).[49]

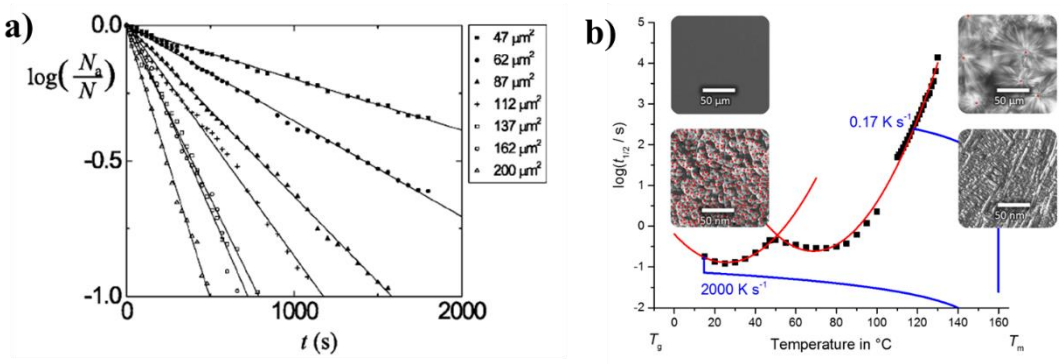

Figure 2.2 (a) Logarithm of the uncrystallized fraction of dewetted polyethyleneoxide droplets as a function of time, during isothermal crystallization at -5 °C. Data for droplet of different base area (hence volume) are shown;[49] (b) Crystallization of i-PP at low and high supercooling. The blue curves indicate two representative linear cooling rates. Images in the inset show meaningful morphologies obtained in the

two distinct nucleation regime (top image optical microscopy, bottom image AFM), with the red dots indicating nuclei position[51].

A different way to observe and study homogeneous nucleation is provided by the recently developed fast scanning chip-based calorimeters[52, 53]. Being able to cool and heat small polymer samples at previously unattained rates of several hundreds of thousands of K per seconds, the complete range of undercoolings can now be achieved for the large majority of polymers.[54] It has thus been showed that several semicrystalline polymers exhibit a bimodal-temperature dependence of the overall crystallization kinetics, with two maxima in the rate at distinct high and low crystallization temperature. Ex-situ optical or atomic force microscopy analysis revealed a striking change in the morphology of the sample, depending on the crystallization temperature region. At crystallization temperatures corresponding to the low-temperature maximum, the crystals lack any spherulitic superstructure, and the nucleation density exceeds the one measured at high temperatures by several orders of magnitude (Figure 2.2(b))[55]. Therefore it is deduced that the crystallization process at large undercoolings is dominated by the occurrence of homogeneous nucleation[51].

2.2.3 Heterogeneous Nucleation

In the modern plastic technology, the addition of additives (nucleating agents, colorants, fillers, etc.) has a very important role because it allows tuning and improving the properties of the material. In the case of nucleation, an extremely small quantity of foreign particles may be responsible for the heterogeneous nucleation, and it is very difficult to purify a material to such an extent that these particles are absent, or to reduce their number by a substantial amount. But if particular compounds that act as nucleating agents are added in the polymer voluntarily, it’s possible to exploit them in order to increase the crystallization rate (thus reducing the processing times) and improve mechanical or optical properties.

A heterogeneous nucleation path makes use of foreign preexisting surfaces to reduce the free energy opposing primary nucleation. In the presence of heterogeneous substrates in the polymer melt, there is the availability solid surfaces on which the embryos can form. Several different types of heterogeneity (extraneous solids, cavities, surfaces wetted by the nucleus, container walls, already formed crystal surfaces, etc.) can enhance the formation of stable embryos and have important implications for polymer crystallization. A brief analysis is presented in the following.

In the case of a nucleus which wets a foreign surface and assumes the shape of a spherical cap of radius r, as shown in Figure 2.3, the critical radius and the energy barrier to nucleation are given by:

$$r^* = \frac{2\sigma_{\alpha\beta}}{\Delta g} \tag{2.11}$$

$$\Delta G^*_{het} = \Delta G^* f(\theta) = \Delta G^* \frac{(2+\cos\theta)(1-\cos\theta)^2}{4} \tag{2.12}$$

where ΔG^* is the energy barrier for the homogeneous nucleation case, from Equation 2.12, and θ is the contact angle between the crystal, the melt and the substrate, obtained from the equilibrium of the surface tensions components parallel to the interface.

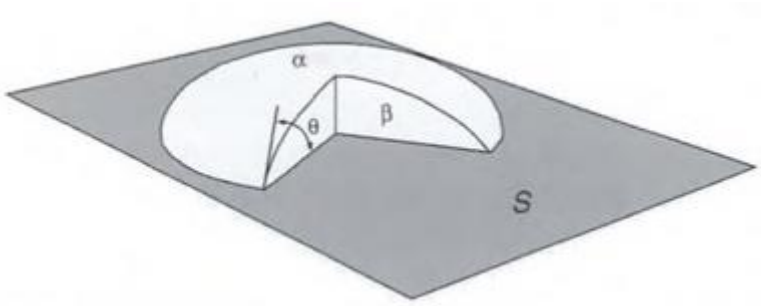

Figure 2.3 Schematic example of heterogeneous nucleation on a flat substrate: α is the melt polymer phase, β is the nucleus phase and *S* is the substrate.[56]

Instead, considering a cylindrical nucleus of height h and radius r, forming on the substrate, we obtain:

$$r^* = \frac{2\sigma_{\alpha\beta}}{\Delta g} = h^* \tag{2.13}$$

$$\Delta G^*_{het} = \frac{4\pi\sigma^3_{\alpha\beta}}{\Delta g^2} \tag{2.14}$$

From Equation 2.11 and 2.13 we can note that r^* has the same dependence on Δg, as predicted from Equation 2.5 for the homogeneous nucleation of spherical clusters. Thus, the main role of a nucleating heterogeneity is to reduce the barrier for nucleation, caused by the surface interfacial free energy. Moreover, Equation 2.12 and 2.14 show that ΔG^*_{het} is inversely proportional to the Δg and directly proportional to the cube of the surface free energy for both nucleus geometries. The general result is that $\Delta G^*_{het} = f(\theta)\Delta G^*$, with $f(\theta)$ varying between zero and unity: the formation of a heterogeneous nucleus is less energetically costly with respect to a homogeneous one. However, the crystallization temperature dependence of the energy barrier for creating the critical-size nucleus is identical in both cases.

Another classical approach assumes the formation of prismatic embryos with rectangular cross section and height in the direction of the chain axis on a flat surface, as showed in Figure 2.4.

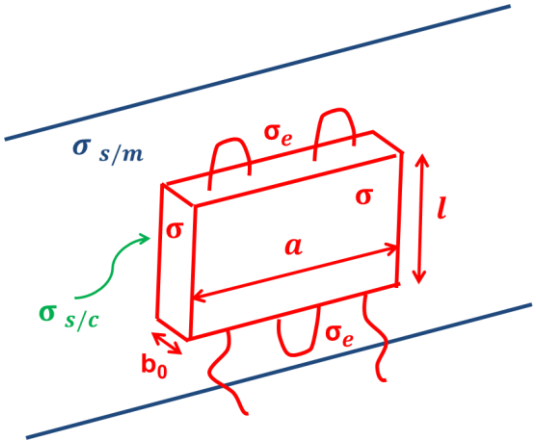

Figure 2.4 Scheme of the heterogeneous nucleation, the blue lines represent the surface of the heterogeneous nucleus on which the embryo is formed.

The equation that describes this nucleation modality is simply a modification of the homogeneous nucleation case. The change in the Gibbs energy has the form:

$$\Delta G_{het} = -abl\Delta g + 2bl\sigma + al\Delta\sigma + 2ab\sigma_e \tag{2.15}$$

where σ is the free energy of the lateral surfaces in contact with the supercooled melt, σ_e is the free energy of the surfaces perpendicular to the chain direction and $\Delta\sigma$ is the interfacial free energy difference, given by:

$$\Delta\sigma = \sigma + \sigma_{s/c} - \sigma_{s/m} \tag{2.16}$$

In which $\sigma_{s/c}$ is the crystal-substrate interfacial energy and $\sigma_{s/m}$ is the melt-substrate interfacial energy. Therefore, $\Delta\sigma$ can be brought down to the surface tension properties of the substrate, polymer crystal and polymer melt. Thus, $\Delta\sigma$ is a convenient way to define the nucleating ability of the substrate toward the polymer melt. In fact, this parameter is related to the critical dimensions of the heterogeneous nucleus and the associated free energy barrier:

$$b^* = \frac{2\Delta\sigma T_m}{\Delta T \Delta h^o} \tag{2.17}$$

$$\Delta G^*_{het} = \frac{16\sigma\sigma_e\Delta\sigma T_m^2}{(\Delta h^o)^2(\Delta T)^2} \tag{2.18}$$

The energetic barrier that must be overcome for the formation of the nucleus on the substrate is lower than the one needed for homogenous nucleation, only when the following inequality is true:

$$\Delta\sigma = \sigma + \sigma_{s/c} - \sigma_{s/m} \leq 2\sigma \tag{2.19}$$

However, the free energy barrier for the formation of the nucleus of critical size is not the only parameter one has to take into account for the description of the nucleation rate. Indeed,

especially at large supercooling, the activation energy for segmental transport across the phase boundary, (ΔG_η), can become of importance. Thus, the total energy barrier that must be overcome by the nucleating segments is given by the sum of ΔG^* and ΔG_η [57] and the equation for the rate of nucleation is given by:

$$I = I_0 \, exp\left(-\frac{\Delta G^* + \Delta G_\eta}{kT}\right) \tag{2.20}$$

where I_0 is a temperature independent frequency term and k is the Boltzmann's constant. Equation 2.19 will be used and discussed more extensively later in this thesis.

In practical (and industrial) conditions, relatively low supercoolings are needed to observe nucleation and crystallization, due to the occurrence of heterogeneous nucleation. For example, heterogeneous nucleation is often encountered at the interface with the fiber surfaces in polymer-fiber composites. In this case, the density of nuclei at the interface is so high that the lateral development of the spherulites is hindered, so that crystal growth can only proceed perpendicular to the substrate surface forming a columnar growth region that extend towards the spherulitic matrix, typically indicated as "transcrystalline" morphology (Figure 2.5a)[58] . The lower the free energy barrier for heterogeneous nucleation at the fiber's surface the lower the undercooling at which transcrystalline morphology can be appreciated [59].

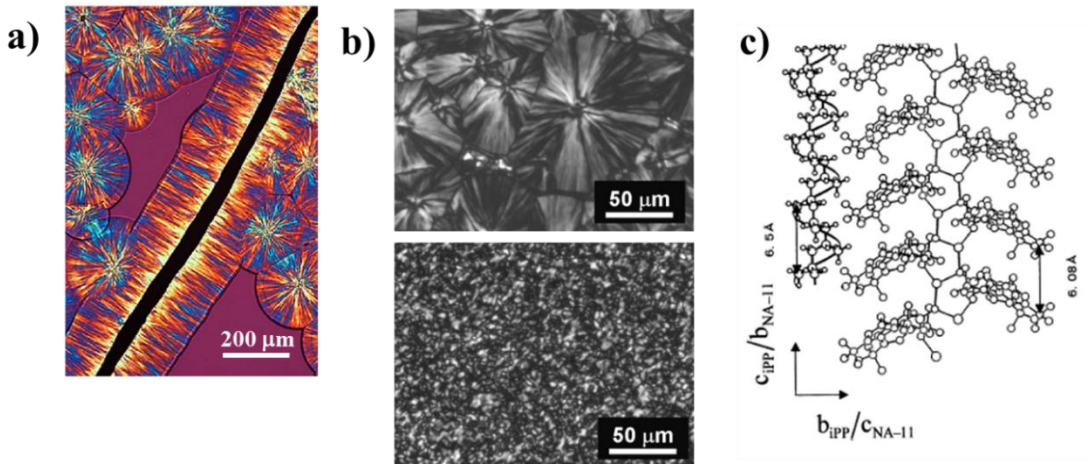

Figure 2.5 (a) Transcrystalline morphology obtained during isothermal crystallization of i-PP on the surface of carbon nanotube macroscopic fiber;[60] (b) spherulitic morphology of compression molded i-PP either neat (top image) or containing a benzenetrisamide nucleating agent (bottom image)[61]; (c) structural matching between i-PP and an organophosphate derivative nucleating agent (NA-11)[62].

Another, industrially relevant, example of heterogeneous nucleation is constituted by nucleating agents (NA), i.e., particular compounds that are voluntarily added to the polymer in order to increase the crystallization rate, thus reducing the processing times and improving

mechanical or optical properties. The most widely investigated NAs are those for isotactic polypropylene (i-PP), for which a plethora or organic and inorganic compounds with various efficient has been identified[63]. An example of the striking effect of added nucleating on the polymer morphology is shown in Figure 2.5(b), where the polarized optical micrographs of compression molded neat isotactic polypropylene is compared to that of the same material containing 0.13 wt% of a benzenetrisamide type nucleant[61].

It has been recognized that the existence of epitaxy, given by the dimensional matching between the spacing of particular lattice planes of the nucleating substrate and the crystallizing polymer is highly beneficial for the occurrence of heterogeneous nucleation. An example of disclosed epitaxial relationship between i-PP and an organophosphate nucleating agent is shown in Figure 2.5(c). The helical pitch of i-PP (c-axis) is very close to the periodicity of the NA unit cell along the b-axis. Despite very important, epitaxy is yet not the sole criterion which determines the nucleating ability of a substrate. The research on more efficient heterogeneous nucleating agents is thus still mostly empirical.

2.2.4 Self-Nucleation

Self-nucleation is a special nucleation process in semicrystalline polymers, which implies nucleation by a “memory” of the original crystalline morphology that survives the melting process. Despite being known from the dawn of polymer crystallization studies, the intimate nature of self-nuclei is still not unequivocally established. In particular, self-nuclei are considered as stable crystalline remains or as a “kinetic” memory of the crystalline state due to the slow relaxation of local chain orientation.

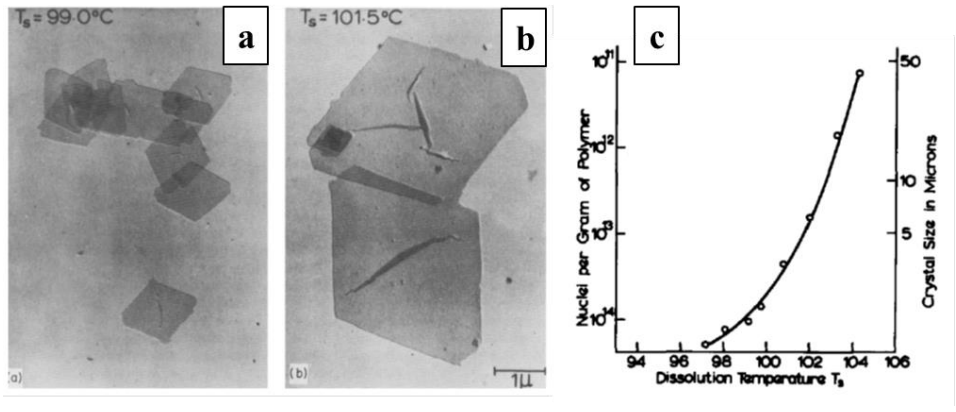

Figure 2.6 Electron micrographs of crystals grown at 80 °C from a 0.1 wt% solution of polyethylene in xylene after seeding at 99 °C (a) and 101.5 °C (b); (c) effect of dissolution temperature on the number of nuclei and final crystal size.

Blundell and Keller were the first to recognize the occurrence of self-nucleation, or self-seeding, in 1966[64, 65]. By dissolving previously crystallized polyethylene single crystals in

poor solvents at low temperatures, they discovered that the number of nuclei per gram of polymer increases exponentially with decreasing dissolution/self-nucleation temperature (T_s) (see Figure 2.6) The recrystallized crystals all have similar sizes, indicating they all nucleate at the same time. Moreover, the high molecular weight fraction of the polyethylene chains was found to be particularly active in self-nucleation, while parameters such as the solution concentration or the chosen crystallization temperature had little effect on the phenomenon.

Self-nucleation is also of fundamental importance for crystallization from the molten state. In this case, the spherulitic morphology is significantly affected by the melt treatment. Indeed, many early studies reported a decrease of the spherulite size with decreasing melt temperature for various polymers, such as polyethylene,[66] poly(ethylene terephthalate), isotactic polypropylene and Nylon 6.[67] An early attempt to probe the effect of self-nucleation on the crystallization kinetics of bulk polymers was made using dilatometry by Vidotto et al.[68]

More than two decades after this first study, a seminal work was presented by Lotz et al., [69] who adapted self-nucleation procedures with differential scanning calorimetry (DSC). After the creation of a crystalline standard state, by cooling at constant rate from a temperature 30 - 40 °C above the observed melting point, the polymer crystals are brought to a given melt temperature and kept there for a chosen period of time (this temperature is denoted Ts or self-nucleation temperature). Afterwards, the impact of this self-nucleation step on the nucleation process during the subsequent re-crystallization is evaluated, and the procedure is repeated for different self-nucleation temperatures. The presence of self-nuclei is indirectly observed by measuring the much faster crystallization rate, i.e., the increase in crystallization peak temperature, which is proportional to the number of seeds left in the melt. According to Lotz et al.[69] the explored self-nucleation temperature range can be divided in different Domains, on the basis of the effect on crystallization and subsequent melting behavior of the polymer crystals. With reference to Figure 2.7, which shows the typical outcome of a DSC self-nucleation experiment, the different Domains will be discussed. A more comprehensive review of polymer self-nucleation can be found in [70].

Domain I, at the highest temperatures, is characterized by the absence of self-nucleation effects, i.e., by complete melting and erasure of any crystalline memory. At these self-nucleation temperatures, the nucleation density stays constant at its minimum value. When the self-nucleation temperature is lowered, we encounter Domain II, where the thermal conditioning at T_s is able to leave self-nuclei in the system, but not to anneal possible crystal remnants. Domain II is identified clearly from the re-crystallization curves, since the

crystallization peak temperature shows a strong increase with decreasing T_s. Finally, *Domain III* manifests annealing of the remaining un-molten crystals during the self-nucleation step. These crystals which have thickened are detected by the melting of the recrystallized specimen, as a small sharp melting peak at temperatures higher than the main endotherm.

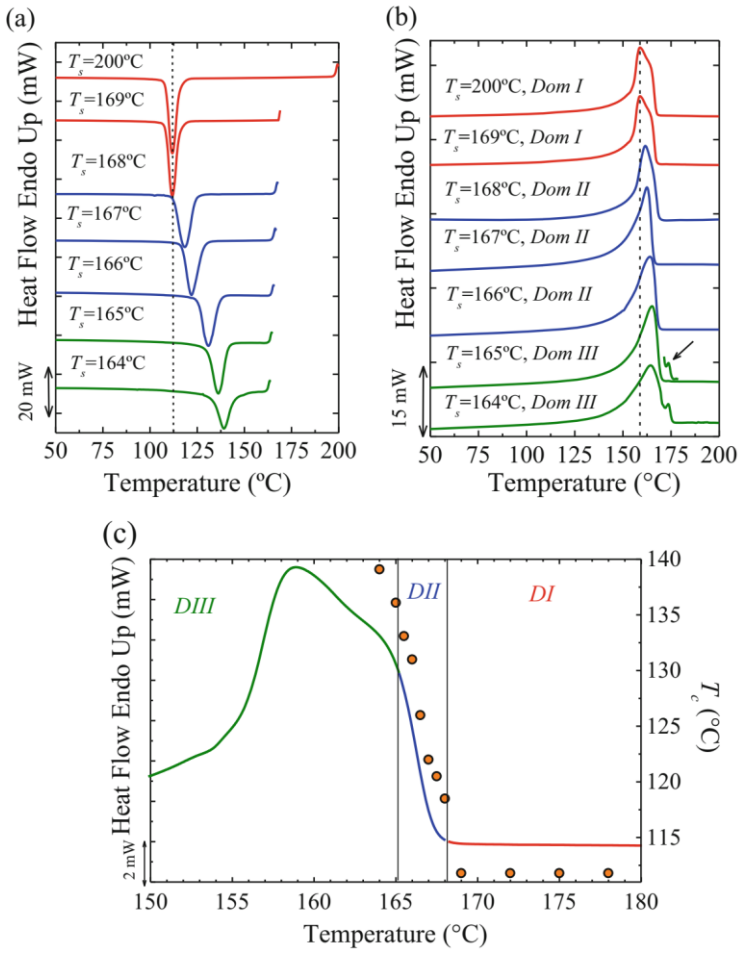

Figure 2.7 (a) DSC cooling scans for isotactic polypropylene after 5 minutes at the indicated T_s; (b) subsequent heating scans after the cooling runs shown in (a); (c) representation of the self-nucleation domains for PP homopolymer superimposed on top of a standard DSC melting trace. Data points represent crystallization temperature peaks (right-hand y-axis) as a function of T_s value (x-axis).[70]

In recent works, it has been found that random copolymers of ethylene display memory of crystallization even at temperatures ~ 40 degrees above their equilibrium melting points. This unusual strong melt memory of copolymers is in sharp contrast with the behavior of linear polyethylene fractions that, independent of molar mass, display a region of self-nucleation at temperatures well below the equilibrium melting temperature.[71] The copolymer's strong memory is associated with the process of sequence partitioning during crystallization. Because branches longer than methyl are excluded from the crystal, the crystallization of random copolymers evolves through a process of sequence length selection by which long ethylene sequences are selected first, and other shorter sequences of suitable length will need

to diffuse through the entangled melt to the crystal front in order to propagate lamellar crystallites. The path of selecting and dragging ethylene sequences to build copolymer crystallites generates a complex topology of knots, loops, ties and other entanglements in the intercrystalline regions, especially at high levels of transformation, which is responsible for the unusual strong melt-memory observed in random ethylene copolymers.

It is believed that when the crystallites of ethylene copolymers melt, clusters from the initial crystalline ethylene sequences remain in close proximity because segmental melt diffusion to randomize all sequences is hampered by branches and the constrained intercrystalline topology. These clusters are effective self-nuclei and only fully dissolve into a homogeneous melt at temperatures well above the equilibrium melting point. The strong melt memory of random copolymers was also observed in Monte Carlo simulations carried out by Wu and co-workers and was interpreted as a state with weak liquid-liquid phase separation.[72]

Self-nucleation has also been explained within a thermodynamic context. On the basis of the multi-step path to polymer crystallization postulated by Strobl,[19] Muthukumar has considered the heterogeneous melt as a hypothetical metastable intermediate melt state in the path between the melt and the crystalline state, and has derived a general expression for the nucleation rate using a standard reaction kinetics scheme and accounting for the transitions between the crystalline, heterogeneous, and homogeneous states.[73]

Recent experiments have demonstrated that the presence of self-nuclei in a polymer melt can lead to different rheological properties[74, 75] and dielectric permittivity[76] with respect to the fully homogeneous state (Domain I). These findings suggest that the structure of self-nucleated melt is related to chain clusters, persisting in the melt due to interactions between chain segments in the regions of the melt where crystallites were previously present. Nevertheless, the exact nature of self-nuclei, despite extensive research in the last decades, still remains elusive.

2.3 Transcrystallinity on Fiber Surface

Semicrystalline polymers are usually reinforced by various types of organic or inorganic fillers, like fibers etc., to form composites with improved mechanical properties. It is well known that these reinforcements can result in changes in morphology and crystallinity of the interphase regions. Embedded fiber in polymer matrix may act as heterogeneous substrates and crystallization occurs along the interface with sufficiently high density of nuclei. These nuclei will further hinder the lateral extension and force crystal growth in one direction,

namely perpendicularly to the fiber surfaces and result in a columnar crystalline layer, known as transcrystallinity (TC) or transcrystalline layers (TCL), with limited thickness.[77-81] Figure 2.8 shows a typical transcrystalline layer of PLLA on Carbon fiber and it is clear that the growth of the TCL proceeds perpendicularly to the fiber surface until the growing front impinges with spherulites nucleated in the bulk.[82]

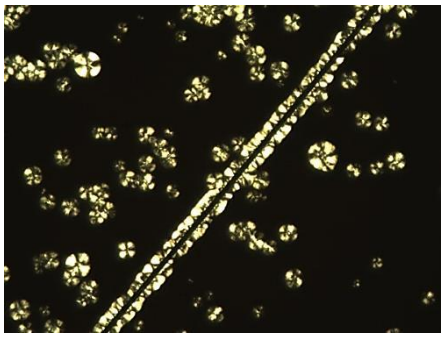

Figure 2.8 Micrograph showing isothermal crystallization of PLLA/Carbon fiber composite at 110 °C (5 min).

Single fiber-polymer composites are often used for the study of TC, that is, single or several fibers are embedded in polymer melt to prepare “model” composites. The composites are heated to temperature where the matrix melts but fibers do not, then the samples are cooled for isothermal or nonisothermal crystallization. TC has been reported to occur in several semicrystalline polymers such as isotactic polypropylene, polyethylene, poly (ether ether ketone), poly (phenylene sulfide) and polyamide, etc. in contact with carbon fiber,[83] glass fibers,[84] aramid fibers,[85] natural fibers[86] and so on. The formation of transcrystalline layer has significant influence on the performances of fiber/matrix interfaces, and hence affects largely the mechanical properties of composites. Although TC plays an important role to improve the properties of some fiber/polymer interfaces and composites, the mechanism controlling TC layers occurrence is not fully understood and there are no clear rules which manage to predict the appearance of TC in a particular fiber/matrix system. Meanwhile, the effects of TC on the interfaces and properties of composites still remains in dispute. Felix [87] reported that TC can improve stress transfer at the interface, and consequently, the mechanical properties of the composites, whereas some other researchers claimed that it has no, or negligible, effect on these properties. [88] Moreover, for the formation of TC, many factors, such as the fiber material type (mainly its topography and the chemical interaction with matrix), matrix material type, and thermal protocols, have all been reported to affect TC in these composites to some extent.[88]

Since Jenckel et al.[89] described transcrystalline for the first time in 1952, more and more researchers have joined in the investigation of TCL. Many efforts have been made to study

TC in different composites, however, the formation and growth mechanisms of TC are still unclear and its effect on the properties of composites and their interfaces remains controversial. Hence, deeper and more detailed studies of the specific role of TC interfaces must be performed before general conclusions can be drawn.

2.4 Nucleating Agents for Isotactic Polypropylene

Nucleating agents (NAs) are common polymer additives, widely used for speeding up processing and tuning the final mechanical properties. A wide variety of substances can act as nucleating agents, e.g., natural minerals, organic or inorganic salts, organic components, other polymers, or the same polymer to be nucleated in a cross-linked form. In principle, a chemical similarity to the matrix is not required.

The reasons for choosing isotactic polypropylene as an example material for matrix are various. Due to its wide application range, the modification of the property profile with NAs is of interest. In addition, the quantity of production and the applications makes it both technically and economically very relevant, and it exhibits an interesting polymorphism with four crystal modifications, i.e., α, β, γ, and mesomorphic[90]. For i-PP, two physically distinct classes of nucleating agents (NAs) exist: particulate systems (examples include talc, sodium benzoate, organophosphates, etc.), and soluble systems, which dissolve in the polymer melt upon heating and phase separate upon cooling (examples are sorbitol derivatives and benzene-trisamides).[91] Moreover, another useful classification of NAs is based on the specific crystalline structure they induce upon crystallization: α (monoclinic) and γ (orthorhombic) or β (hexagonal). Wittmann and Lotz[92] suggested that any substrate with a periodicity of ~5 Å, matching the (010) face of i-PP monoclinic face, can be a potential α-nucleant for i-PP, as shown in Figure 2.9. In the same way, substrates with a periodicity (or the c axis of the unit cell dimension) of 6.5 Å, which matches the (110) face of i-PP, can be a potential β-nucleating agent.

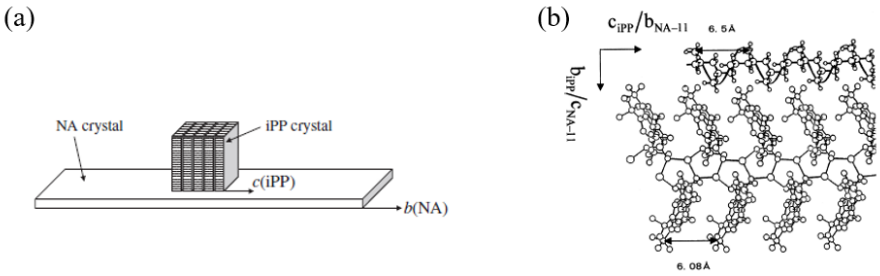

Figure 2.9 (a) Structural matching between i-PP and NA-11 (organophosphate derivative nucleating agent) by a schematic view[93] and (b) through the view of chemical structure within the space[94].

An important improvement in the classification of the nucleating efficiency of these substances was put forward by Lotz et al.[95, 96] They proposed an empirical efficiency scale based on the DSC analysis. Compared to earlier methods based solely on the difference of the absolute T_c of the nucleated polymer with respect to the T_c of the blank polymer, they introduce an "upper reference bound" to T_c. The maximum crystallization temperature is obtained by "self-nucleation" of the blank polymer, a procedure in which the original polymer crystals are molten at low temperatures, leaving some residual order in the polymer melt, which greatly enhances the recrystallization behavior. The self-nucleated polymer is considered as the ideally nucleated sample. Thus, the blank polymer crystallizes at the lowest temperature, whereas the best self-nucleated polymer crystallizes at the highest temperature, and the T_c of the nucleated polymer must be within this range. Therefore, a nucleation efficiency scale is conveniently defined attributing a value of 0 and 100 % to the neat and self-nucleated polymer, respectively. In this way, any additive can be characterized by a percentage which expresses its efficiency in nucleating the particular polymer. In Table 2.1, the Lotz's efficiency classification for some common i-PP NAs is reported.

This scale gives several practice advantages, but it's not an absolute or intrinsic one, since it requires standardization of certain experimental variables, like the cooling rate, and depends on the particular polymer grade used. In particular the lowest crystallization temperature (the blank polymer T_c) is clearly a material characteristic, which depends on the density of unknown nucleating impurities within the polymer used.

Table 2.1 Crystallization temperatures of i-PP/NA compounds and nucleation efficiency (NE) for some NAs at various concentrations.[96]

Nucleating agents and concentration	T_ciPP/°C	Nucleation efficiency *NE*/%
4-biphenyl carboxylic acid, 2%	128.8	66
2-naphtoic acid, 1%	127.8	62
Nicotinic acid, 1%	125.7	52
Thymin, 1%	125.3	50
DBS (dibenzylidene sorbitol), 0.4%	123.2	41
9-anthracene carboxylic acid, 1%	122.7	38
Talc, 1%	121.4	32
Sodium benzoate, 1%	121.2	31
9-fluorene carboxylic acid, 1%	118.4	18
2-hydroxy 3-naphtoic acid, 1%	116.0	7
2,4-(bis butylamine)6-hydroxy, 1,3,5 triazine, 1%	115.5	5

2.5 Cross-Nucleation

Polymorphism, which is the ability of a given substance to acquire different ordered arrangements in the solid state, *i.e.*, to crystallize in different structures, is a ubiquitous phenomenon in nature and material science. Basically, all the types of crystallizable compounds may exhibit polymorphism: it is found both in complex organic molecules,[97] in simple molecules such as water,[98] and even in single chemical elements, *e.g.*, sulfur and phosphorus. Clearly, the different structures of the same substance, *i.e.*, the polymorphs, can display remarkably different physical properties, including melting point, solubility, electrical properties, etc. A striking example is the one of the polymorphs (also referred to as allotropes) of the carbon element: diamond and graphite. Their differences in mechanical properties, *e.g.*, hardness, and electrical conductivity are self-evident.

Different crystallization pathways can be recognized when dealing with polymorphic substances. A common observation is the so-called Ostwald's Rule of Stages,[99] according to which a phase transition occurs through steps of increasing thermodynamic stability, i.e., from the least to the most stable polymorph in successive stages. If suitable thermodynamic and kinetics conditions are met, two (or more) polymorphs can also form concomitantly, *i.e.*, they nucleate independently and grow simultaneously in the same melt/supersaturated solution. Finally, a faster growing polymorph can nucleate heterogeneously on the surface of another one, without requiring any phase transition between them. This latter scheme has recently been referred to as cross-nucleation. Yu was the first to discuss the nucleation of one polymorph by another in small organic molecules. [100] He reported the examples of two hexitols, D-mannitol and D-sorbitol. Melt crystallization of D-mannitol proceeds via the nucleation of a metastable δ-polymorph, followed by the nucleation of a more stable α-polymorph on the surface of the δ-spherulites (see Figure 2.10). In his experiments, the new α

-polymorph grows faster than the δ-one Instead, for what concerns D-sorbitol, the melt was seeded with crystals of the stable γ-form. The crystallization around the seed occurred in the metastable E polymorph.[100] Already from these first examples, it was clear that seeds of one polymorph can nucleate another crystal structure of either higher or lower thermodynamic stability, provided it grows faster than the original polymorph.

The new phenomenon, termed cross-nucleation, was further investigated in spontaneous and seeded crystallization of 5-methyl-2-[(2-nitrophenyl)amino]-3-thiophenecarbonitrile, [101] named ROY for the red, orange and yellow crystals of its ten polymorphs.[102] Extensive, and sometime selective cross-nucleation between ROY polymorphs was found. An example is provided in Figure 2.10, which show a seed of the Y04 polymorph which cross-nucleate the fast growing R05 phase and is then engulfed by the newborn spherulite.

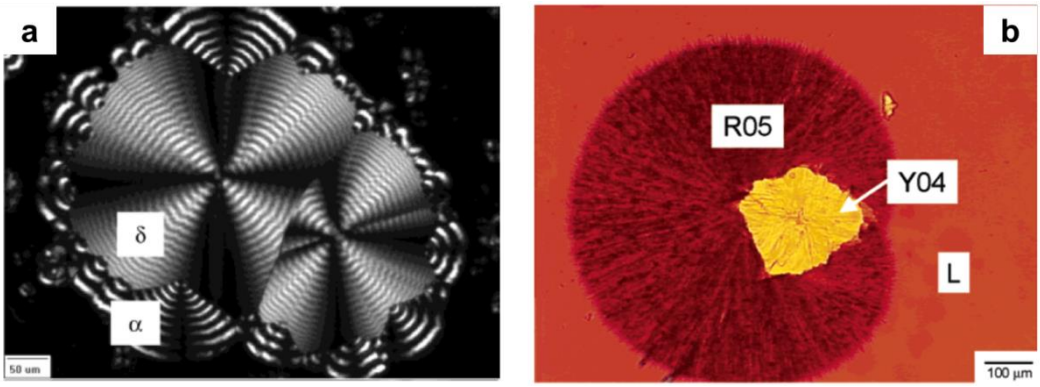

Figure 2.10 (a) Cross-nucleation in D-mannitol, *α*-phase nucleating on *δ*-polymorph; (b) cross-nucleation between ROY polymorphs: R05 nucleating on Y04. Adapted with permission from[100, 101].

The study of ROY polymorphs confirms that thermodynamic stability is not the governing factor for cross-nucleation, *i.e.*, the "daughter" phase can either be of higher or lower stability than the "parent" one. On the other hand, the new cross-nucleating polymorph always grow faster than (or at least as fast as) the initial one. This is a necessary, but not sufficient condition to observe nucleation. In fact, for instance, Y04 grows the slowest of all polymorphs at room temperature, but only R and R05 phases were observed to nucleate on it. This selectivity of the cross-nucleation process is apparently not related to epitaxy, since no evident lattice matching is found for any couple of cross-nucleating polymorphs. On the other hand, solution crystallization of a steroid provides evidence that epitaxy can play a role in cross-nucleation between polymorphs, both for the case of metastable-on-stable[103] and vice-versa.[104] However, changing the composition of the solvent mixture leads to the occurrence of cross-nucleation of the metastable polymorph on the stable one without any preferred orientation, *i.e.*, lacking epitaxial relationship between the two phases.[103] It can thus be concluded that epitaxy is not a fundamental requirement for cross-nucleation to

happen.

Although the occurrence of cross-nucleation was observed in polymers before than in small organic molecules, the phenomenon did not receive much attention in polymer literature. The first observation of cross-nucleation in polymers dates back to 1977, when Lovinger et al. described the peculiar "growth-transformation" occurring in an i-PP sample solidified in a temperature gradient or isothermally (see Figure 2.11).[105] The authors describe the initiation of a spherulite of the trigonal β-phase (more birefringent than the α-phase) at the growth front of the monoclinic α-phase, and named the process "growth transformation". The sudden change in the growing structure was interpreted as an "accidental discrepancy" at the tip of the growing lamella causing the chains to pack in a different mode, which eventually can be preserved and overtake the original structure because of its faster growth rate.

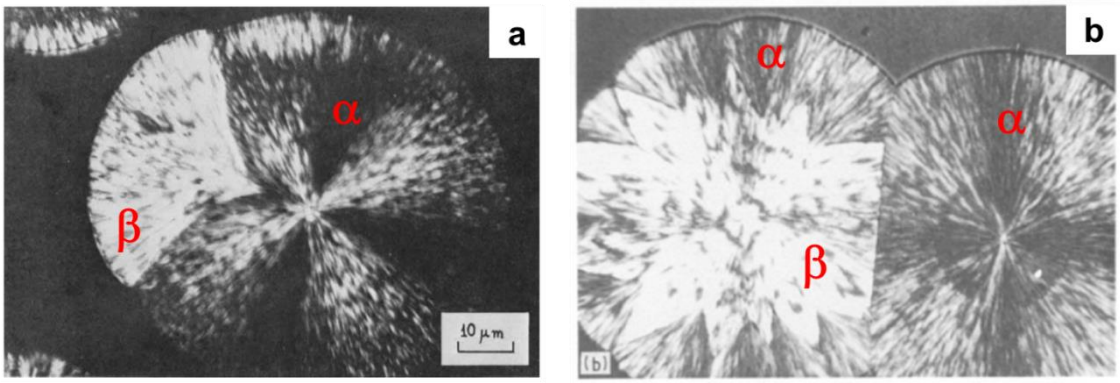

Figure 2.11 *α*-to-*β* (a) and β-to-α (b) growth transition (or cross-nucleation) in isotactic polypropylene. Adapted with permission from [105, 106].

Recently, Cavallo investigated this special nucleation phenomenon in isotactic polybutene,[107] isotactic polypropylene[108] and polypivalolactone[109] melts. Large seeded form I PBu spherulites serve as nucleation sites for small Form II crystal. In Figure 2.12, the number of Form II nuclei increases with time, and further studies shows that cross-nucleation rates decrease exponentially with increasing crystallization temperature and the energy barrier of cross-nucleation is just half of that in typical homogeneous nucleation. Moreover, Cavallo studied the cross-nucleation of α phase on δ phase crystal in polypivalolactone melt,[109] showing a cross-nucleation kinetics with a relatively low nucleation barrier, which is comparable to that for secondary nucleation of the parent polymorph.

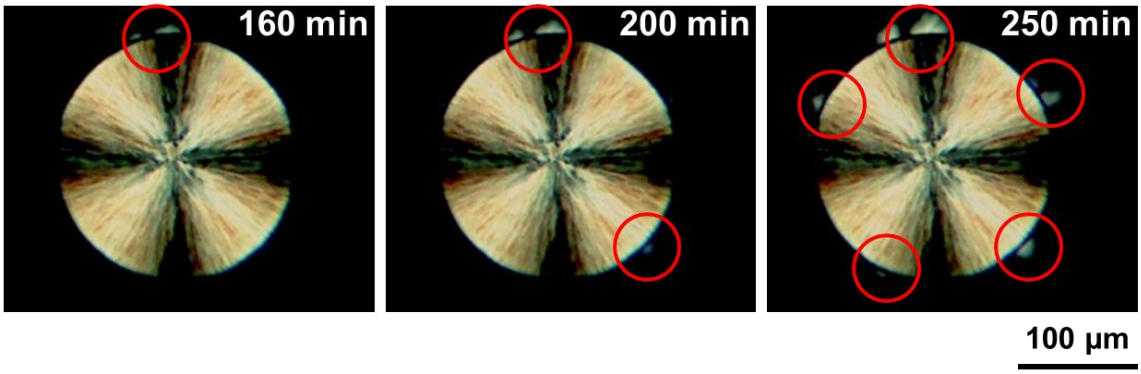

Figure 2.12 Example of cross-nucleation kinetics at a crystallization temperature of 105 °C. Large Form I spherulites serve as nucleation sites for small Form II crystals which are indicated by the red circles. Adapted with permission from [107].

However, an abnormal temperature dependence of cross-nucleation kinetics in polypropylene melt was observed by Cavallo,[108] where the rate of cross-nucleation of the monoclinic α phase on the trigonal β phase crystals increases with increasing temperature. This behavior is contrary to that of the heterogeneous nucleation kinetics of the same crystal on various solid substrates, and also to the previously reported cases of cross-nucleation rate of other polymorphic systems, which exhibit the expected decrease with temperature. The results are explained as a manifestation of a kinetic competition between α-on-β cross-nucleation and growth of β-crystalline seeds. These new finding indicates that further theoretical efforts are needed to include the cross-nucleation phenomenon in the framework of a comprehensive understanding of polymorphic crystallization.

Chapter 3. Nucleation of Poly(lactide) on the Surface of Different Fibers

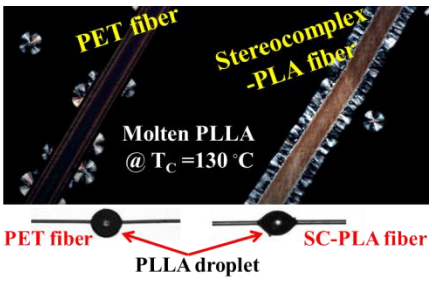

3.1 Introduction

Fiber composites of semicrystalline polymers are able to develop, under certain conditions, a highly oriented crystalline layer with molecular chain axis parallel to fiber axis at the fiber/matrix interface.[88, 110, 111] This peculiar morphology is addressed as transcrystalline layer (TCL), and is typically associated to the high nucleating ability of the embedded fibers' surface.[59, 112-119] The formation of TCL is of technological importance, because it can significantly influence the mechanical properties of the product.[120-126] In fact, TCL presents a higher Young's modulus compared with the bulk materials, despite a lower strain at break.[127, 128] Moreover, the presence of TCL can effectively improve the adhesion between the polymer and the fiber, thus increasing the flexural modulus and strength of the composites.[120]

Although TCL has significant implication for the properties of fiber-reinforced composites, the exact mechanism for its development is not fully univocally ascertained. A major role in the formation of the transcrystalline layer has been attributed to fiber's surface chemistry,[129-131] topography,[111, 128] or residual stresses at the fiber/matrix interface, generated during cooling due to the mismatch in the thermal expansion coefficients of the two materials.[59, 80, 112-117, 132, 133] Clearly, the transcrystalline layer forms as a consequence of extremely high surface nucleation density on the fiber, which hinders the later development of the spherulites and thus forces crystal growth to proceed perpendicular to the fiber long axis only. Therefore, understanding of fiber induced nucleation is essential.

Several detailed investigations on fiber induced nucleation have been reported. [58, 134] In particular, Wang et al.[59, 112-117] investigated the nucleation of polypropylene on different fibers, including polytetrafluoroethylene (PTFE) fiber, carbon fiber, poly(p-phenylene benzobisoxazole) (PBO) fiber and Kevlar. The fiber nucleation ability was

characterized on the basis of the interfacial free energy difference, $\Delta\sigma$, a parameter expressing the magnitude of the heterogeneous nucleation barrier. Moreover, such value was found to be closely correlated to the maximum temperature for transcrystalline layer formation, T_{max}. Ishida and Bussi studied the crystallization phenomenon of ultrahigh-modulus polyethylene fiber reinforced polyethylene (PE) composites, finding an extremely low $\Delta\sigma$, around 0.3 mJ/m^2. The excellent nucleation ability was attributed to the perfect matching between the lattice parameters of the polymer/fiber system.[58]

However, fiber induced nucleation studies are still scarce and mainly limited to polyolefins, despite the increasing importance of bio-based polymers and composites. Poly(lactide) (PLA) is an aliphatic polyester with good biocompatibility and biodegradability. It has received much attention in recent years because of its potential in replacing the widely used petroleum-based polymers.[135-145]

There are two different enantiomeric forms of lactide, i.e., L-lactide and D-lactide, which allows preparing stereocomplexes having different properties with adjustment of L/D ratios in the synthesis mixture.[146-148] Moreover, Ikada et al. reported that a blend of the poly(L-lactide) (PLLA) and poly(D-lactide) (PDLA) can develop co-crystals, containing both enantiomeric chains in the unit cell, defined as stereocomplex.[149-153] The stereocomplex crystals possess a melting temperature 40 - 50 °C above that of the “homocrystals” of neat PLLA or PDLA and exhibit better mechanical properties and slower biodegradation rate.[147, 148, 154-160] Of particular interest is the ability of stereocomplex crystals (SC) to enhance the crystallization kinetics of slow-crystallizing PLA homocrystals. It has been shown that SC surfaces can efficiently nucleate the lower melting homocrystals, although epitaxy between the two crystalline structures is probably not involved.[124, 155, 161-164] Given the higher melting point of stereocomplex crystals and their spinnability to give oriented fibers, the design of an all-poly(lactide) biobased polymer-fiber composite could be devised, possibly leading to mechanical reinforcement of the brittle PLA.

In this work, the nucleation process of poly(lactide) (PLA) on a series of fibers was studied in-situ by means of polarized optical microscope (POM). Several commercially available fibers (i.e., carbon, PET, Kevlar, and glass fibers) and natural fibers (i.e., hemp, linen and cellulose fibers) are employed and compared to lab-made stereocomplex enantiomeric PLA blend fibers. The nucleating efficiency of the various heterogeneous substrates was quantitatively compared on the basis of the derived interfacial free energy difference, $\Delta\sigma$, and the maximum temperature for transcrystalline layer formation, T_{max}. On the basis of the results some general insights and considerations on the mechanism of fiber

induced nucleation are proposed.

3.2 Experimental

3.2.1 Materials and Fibers

Samples of poly(L-lactide) (PLLA) and poly(D-lactide) (PDLA) in pellet form were kindly provided by Purac Biochem (Gorinchem, The Netherlands). PLLA sample has a molecular weight of 226 kg/mol, a melt flow index (MFI) of 6.9 g/10min and shows a nominal melting point of 175.4 °C. The SC fiber was extruded from PLLA/PDLA blend with a ratio of 1:1. Detailed information on the fiber preparation procedure and equipment can be found elsewhere.[164] After extrusion, the SC fiber was annealed at 200 ºC for 1 h, in order to obtain pure stereocomplex crystal.

As comparison, some commercial fibers (i.e., carbon, Kevlar, PET and glass fibers) and natural fibers (i.e., hemp, linen and cellulose fibers) were employed. Fibers were kindly provided by various composite and textile industries and used as received. Glass fibers have been previously sized, while all the other fibers did not receive any surface treatment.

3.2.2 Methods

The PLLA films were prepared by compressing PLLA pellets on a hot stage at 210 °C, and the thickness of the film was adjusted to about 30 - 50 μm.

The thermal protocol adopted for sample preparation and crystallization experiments was controlled by a calibrated Mettler Toledo FP-82 microscope hot-stage. A piece of PLLA thin film (10 mm × 10 mm) was heated to 190 °C on a glass slide and then a single fiber was manually introduced into the film, and the single fiber-polymer composite what then covered with a microscope cover glass. The composites were then heated to 200 °C and held there for 3 min to eliminate any residual thermal-mechanical history potentially affecting the crystallization. Subsequently, the composites were cooled down to selected temperatures and allowed to crystallize for adequate time. The scheme of the temperature protocol is depicted in Figure 3.1. The crystallization process was observed in-situ by using a Polyvar-Pol optical microscope under crossed polarizers. Micrographs were acquired with a computer-controlled digital camera (Optika).

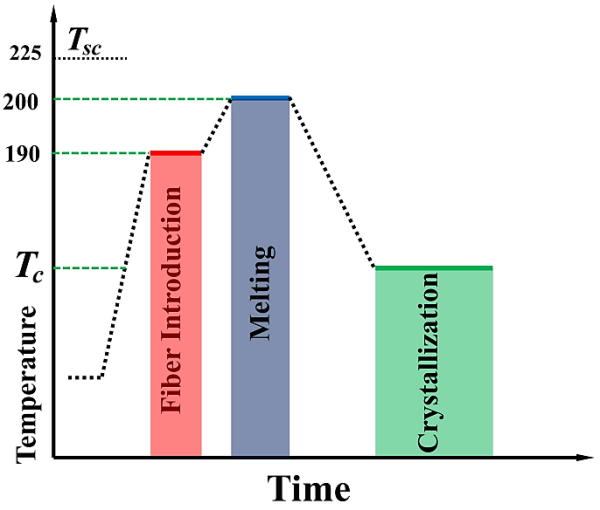

Figure 3.1 Schematic diagram of the applied thermal history. The melting point of SC fibers (T_{sc}) is indicated by dotted lines on the y-axis.

3.2.3 AFM Characterization of Fibers' Surface

In order to quantitatively characterize the surface topography of the different fiber AFM measurements have been performed. For this purpose, a Dimension Icon AFM from Bruker equipped with Nanoscope V controller was used in tapping mode. The measurements were carried out using a silicon TESP-V2 tip with 10 nm nominal radius and 125 μm cantilever length. The operating frequency was 320 kHz and the scan rate was between 0.4 - 0.7 Hz/s. AFM measurements were done with 512 scan lines and target amplitude of around 0.9 V. The representative AFM height profiles of each investigated fiber surface were extracted after second order flatten. Moreover, the root mean square roughness (RMS or R_q) were determined using 10 independent zones of 1 μm^2 on the fiber surface. The R_q values were extracted from 5 μm × 5 μm AFM height images derived after second order flatten using NanoScope Analysis software version 1.90.

3.2.4 Fiber-PLA Adhesion Properties

The interaction between PLA melt and the fibers surfaces was tentatively probed with contact angle measurements. Droplets of PLLA on the fibers were created according to the following procedure. SC, Kevlar, PET and glass fibers were supported on a "U-shaped" aluminum frame, and PLLA fibers (made from the same polymer used as matrix in the nucleation experiments) were tied to them at room temperature, creating several small knots. The frame was then put in an oven kept at a temperature of 210 °C, which is high enough to melt the PLLA "knots" while keeping the fibers unaffected. Several holding times in the oven were employed; an equilibrium shape of the molten PLLA droplet on the fiber was attained

after 5 min. The fiber holder was then quickly extracted from the oven, and the PLLA droplet solidifies by cooling to room temperature. The contact angle of PLLA on different nucleating fibers was finally measured by using a Nordtest tensiometer, with a digital camera equipped with suitable magnifying objective to visualize the solid PLLA droplet/fiber assembly. The angles are measured on both right and left sides of the droplets and the presented results are the mean value of about 20 different droplets.

3.3 Results and Discussion

3.3.1 Morphology Investigation

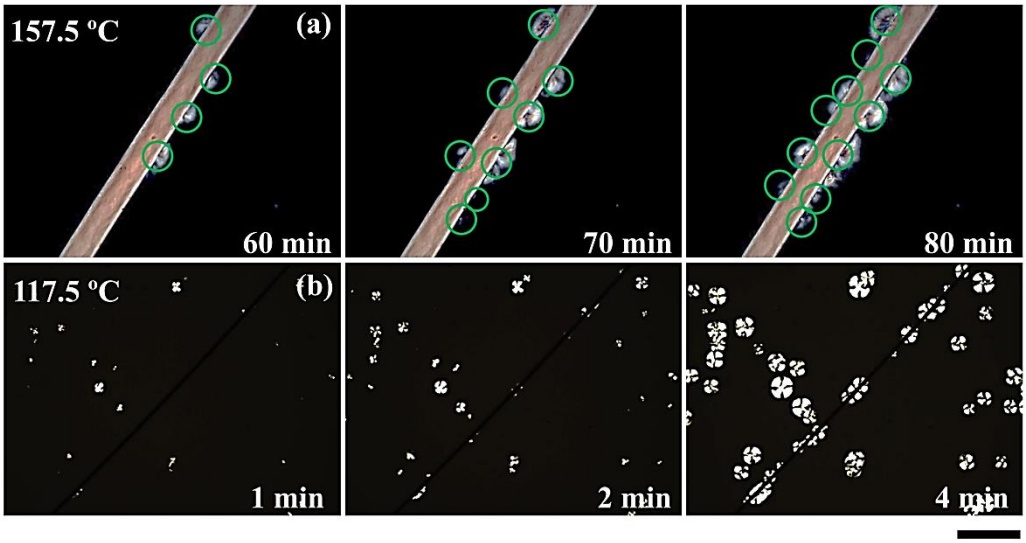

Figure 3.2 Optical micrographs after the indicated crystallization times for PLLA with embedded SC fiber (a) and carbon fiber (b). Crystallization temperatures are 157.5 and 117.5 °C, respectively. Some PLLA nuclei are highlighted, to help the visualization. Scale bar: 100 μm.

Two typical examples of time-resolved polarized optical microscopy images, acquired during the isothermal nucleation process of PLLA onto the SC and the carbon fiber are shown in Figure 3.2. A sporadic nucleation process can be appreciated, with the number of nuclei on the surface of both fibers increasing gradually with crystallization time. Similar nucleation process is also observed for other fibers and shown in Figure 3.3. The relatively low nucleation density enables one to observe the growth of the individual nuclei, which develop into distinguishable spherulites and are therefore amenable to direct counting. We note that the very different crystallization temperatures employed for the two fibers (40 °C) is related to the different nucleation ability. However, due to their different diameters and the different experimental time scales, the relatively nucleation efficiency cannot be grasped from the POM micrographs.

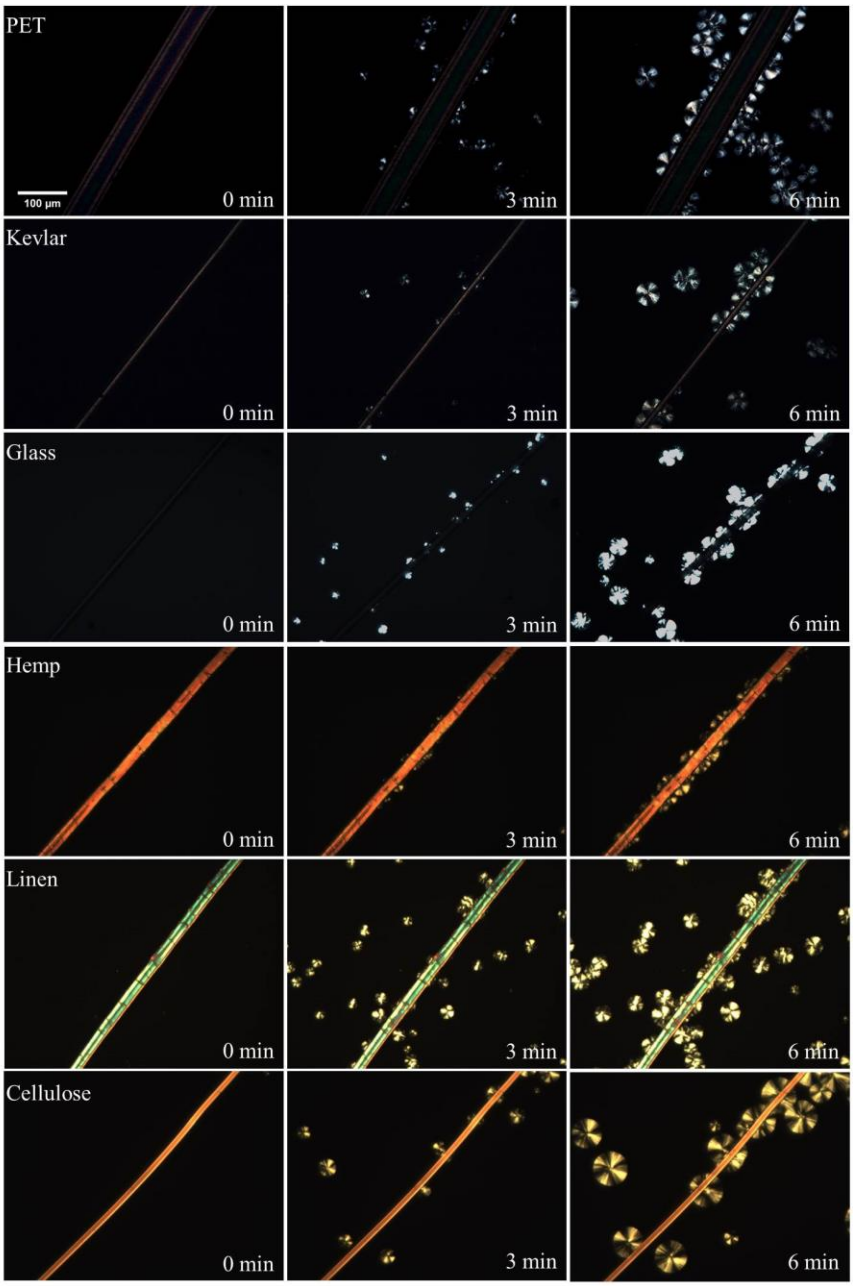

Figure 3.3 Optical micrographs of PLLA after crystallization at 125 °C for indicated time with embedded PET, Kevlar, Glass, Hemp, Linen, Cellulose fibers.

The effect of crystallization temperature on nucleation can be deduced by comparing the morphology developed on the fiber surface after a given holding time at different undercoolings (Figure 3.4). As expected, the nucleation rate increases with decreasing crystallization temperature, as judged by the increased number of nucleated spherulites on the fiber surface at the same time. Notably, when T_c is equal to 142.5 °C (or lower) for SC fiber and 110 °C (or lower) for carbon fiber, TCL develops as a result of the high density of nuclei on the fiber surface. In fact, when the distance between adjacent nuclei on the fiber surface is very small, the growth of crystals is spatially restricted, and the lamellae can only propagate

perpendicularly to the fiber surface. We highlight the large undercooling dependence of the nucleation process, since the extremely different sporadic and TCL morphologies are obtained by varying the crystallization temperature of 5 °C only. Analogous results have been obtained for other commercial and natural fibers, in other specific ranges of temperatures due to intrinsically different nucleating ability (Figure 3.5).

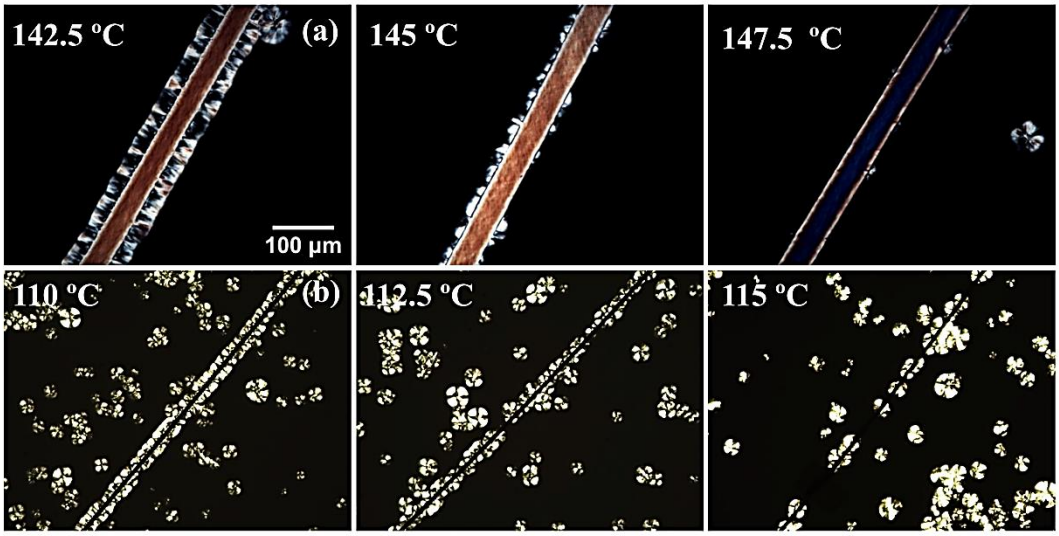

Figure 3.4 (a) Crystallization of PLLA on SC fiber at 142.5, 145 and 147.5 °C for 10 min; (b) crystallization of PLLA on carbon fiber at 110, 112.5 and 115 °C for 5 min.

Such observations are well in line with previous work on fiber induced nucleation on iso-polypropylene (i-PP) composites.[59, 112-117] For example, at 140 °C, transcrystalline layer was observed for i-PP in contact with Teflon fiber, but not for i-PP/Kevlar fiber composite. The latter fiber was able to induce TCL when polypropylene crystallized at 135 °C.[115] The maximum crystallization temperature at which transcrystalline morphology could be obtained was proposed as an estimate of fiber-nucleation ability towards i-PP.[59]

Figure 3.6 compares the crystalline morphology of PLA on other different synthetic fibers (i.e., PET, Kevlar), inorganic fiber (i.e., glass) and natural fiber (i.e., hemp). The same crystallization temperature and time is considered to allow a better evaluation of nucleating efficiency of the different substrates. After 8 min at 130 °C, sporadically nucleated PLLA spherulites can be observed on the surfaces of carbon, PET, kevlar, glass and hemp fibers, while a clear TCL develops on SC fiber substrate. Linen and cellulose fiber display a crystalline morphology analogous to the one of hemp (not shown). A qualitative comparison of the POM micrographs in Figure 3.6 suggests that carbon fiber exhibits the lowest nucleating ability, and SC fiber has by far the highest, while the other substrates display intermediate nucleation efficiency. The easy development of PLA transcrystallinity on SC

crystals was also evidenced by Li et al, who were able to change the interfacial crystallization of PLA/ramie fiber composites from sparsely dispersed spherulites to TCL, by physically decorating the surface of ramie fiber with stereocomplex crystallites adsorbed from solution.[165]

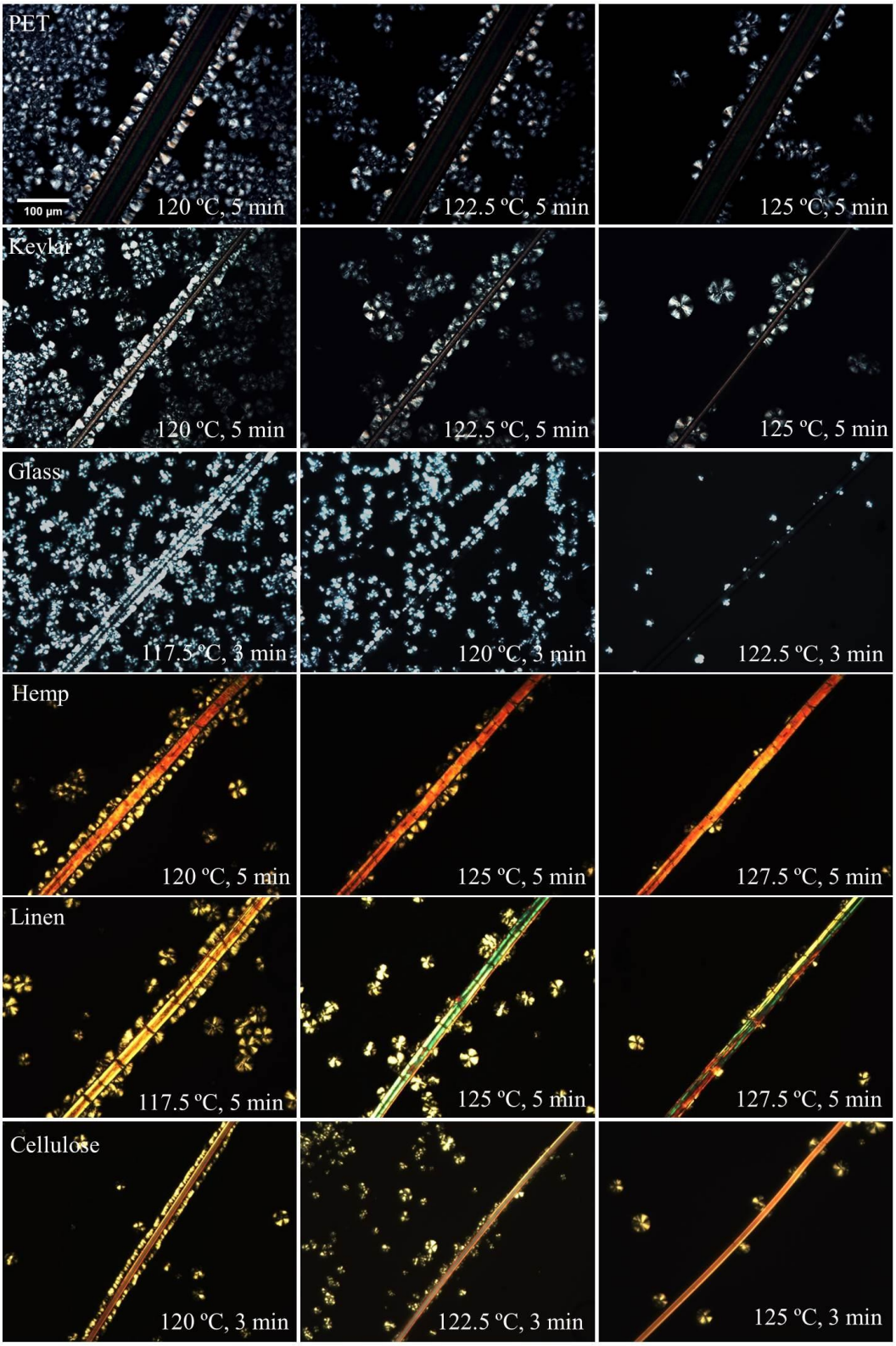

Figure 3.5 Optical micrographs of PLLA after crystallization on PET, Kevlar, Glass, Hemp, Linen, Cellulose fiber surfaces at given temperatures for indicated time.

In order to take into account the differences in the available nucleating surface, due to different fiber diameters, and the time evolution of the nucleation process, a quantitative assessment of nucleation rate at various undercooling is presented in the following section.

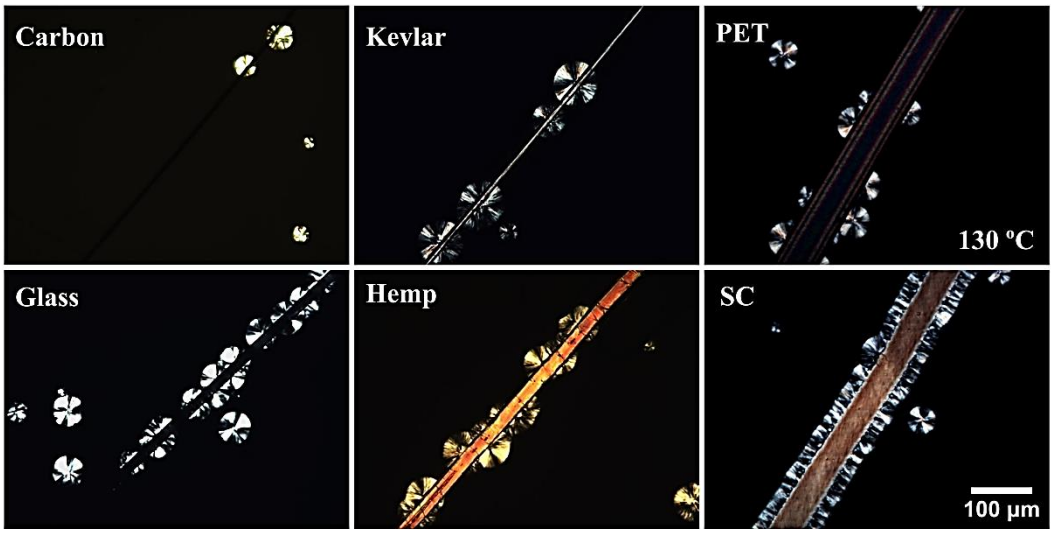

Figure 3.6 POM micrographs of PLLA morphology after crystallization for 8 min at 130 °C in contact with the indicated fiber substrates.

3.3.2 Quantitative Evaluation of the Nucleation Process of PLLA on Different Fiber Substrates

From optical microscopy observations, such as those shown in Figure 3.2, we can derive quantitative information on the nucleation kinetics on the fiber. In Figure 3.7(a), the number of PLLA developing spherulites per unit area of SC fiber (defined as nucleation density) is plotted as a function of time for different undercoolings. In order to calculate the nucleation density, the overall lateral surface of the fiber is considered, being the fiber diameter always lower than polymer sample thickness. A linear increase is observed, allowing a straightforward definition of the nucleation rate as the slope of the fitting line.

A distinct decrease of the nucleation rate as the crystallization temperature is increased can be seen, as expected for the classical heterogeneous nucleation process, and observed in different i-PP/fiber composite in the literature.[59, 112-117] We note that, at low crystallization temperatures where the TCL develops, the direct counting of the number of nuclei is not possible. On the other hand, above a certain crystallization temperature, the nucleation density on the fibers become too low for obtaining statistically meaningful results in few experiments. The experimentally accessible temperature window depends on the considered fiber.

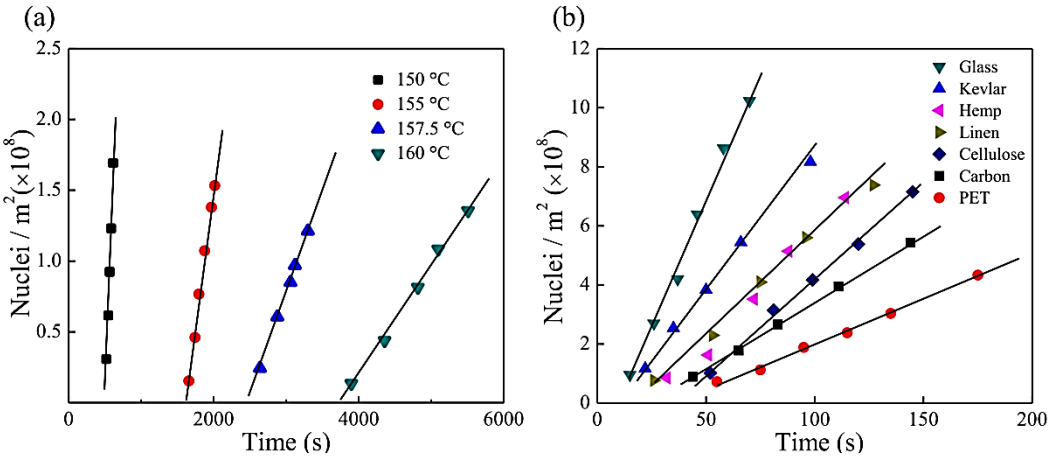

Figure 3.7 (a) Nucleation density of PLLA on SC fiber substrate as a function of time for specimens crystallized at the different indicated temperatures; (b) time evolution of the nucleation density of PLLA during crystallization at 130 °C, on the different indicated fibers. The displayed data are selected representative examples of the nucleation experiments.

The nucleation process of PLLA on different fiber substrates are also compared for the same crystallization temperature of 130 °C in Figure 3.7(b). A certain difference in the nucleation rate can be appreciated, although the differences in slope are much less relevant than those observed for SC fiber at different temperatures (compare the scales of Figure 3.7(a) and (b)). In particular, the nucleation rate at 130 °C on PET and carbon fibers is distinctly lower than that on glass or Kevlar fiber, while all the natural fibers (hemp, linen and cellulose) are characterized by remarkably similar slopes. We note that each isothermal crystallization experiment has been repeated multiple times (at least three), and the measured nucleation rate showed a good reproducibility with relative standard deviation of the order of 10 %. For the sake of clarity, only representative examples of single measurements are displayed in Figure 3.7. Nucleation kinetics data of PLLA on the different fibers can be analyzed in light of the theory of heterogeneous nucleation. Accordingly, the nucleation rate per unit area of substrate, *I,* can be expressed by:[166]

$$Log\ I = Log\ I_0 - \frac{U^*}{2.303R(T_c - T_\infty)} - \frac{16\sigma\sigma_e\Delta\sigma {T_m^0}^2}{2.303kT_c\left(\Delta T\Delta h_f f\right)^2} \qquad (3.1)$$

The parameters appearing in Equation 3.1 are defined as follows: I_0 is a temperature independent constant, R is the gas constant, T_∞ is the limiting temperature at which the polymer segmental motion cease (= T_g – 30), U^* is the activation energy for the diffusion of crystallizing elements across the phase boundary, ΔT is the undercooling (= $T_m^0 - T_c$), T_m^0 is equilibrium melting temperature of PLLA, Δh_f is the enthalpy of fusion per unit volume of bulk crystal at T_m^0 and f is a correction factor (= $2T_c/(T_c+T_m^0)$) which describes the temperature dependence of the fusion enthalpy. σ and σ_e are the lateral and fold surface energy of the

crystal/melt interfaces, while the parameter $\Delta\sigma$ is interfacial free energy difference which accounts for the substitution of a substrate/melt interface with a crystal/substrate and a crystal/melt interfaces (see later for details).

Values of U^*, T_∞, Δh_f, and $\sigma\sigma_e$ for PLLA can be taken from the literatures as 1500 cal/mol, 300 K, 111.08 × 10^3 kJ/m^3 and 7.33 × 10^{-4} J^2/m^4, respectively.[167, 168] The equilibrium melting temperature of the used PLLA grade was determined by extrapolation of the observed crystal melting points measured by POM (Figure 3.8), as a function of crystallization temperature, according to the Hoffman-Weeks method. A value of 475 K is obtained, in good agreement with the literature results.[168, 169]

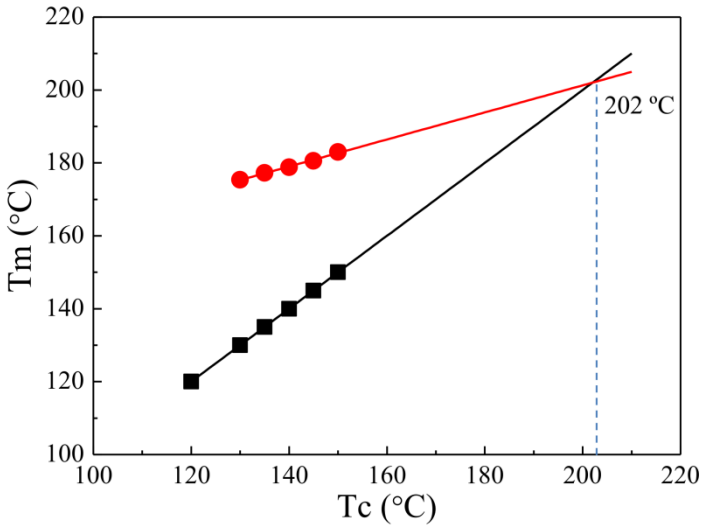

Figure 3.8 Equilibrium melting point of PLLA derived from the Hoffman-Weeks methods.

As mentioned above, $\Delta\sigma$ is defined as $\sigma_{sc} + \sigma_{cm} - \sigma_{sm}$, where σ_{sc} is the substrate-crystal interfacial free energy, σ_{cm} is the side surface free energy of the PLLA crystal, and σ_{sm} is the substrate-melt surface free energy. The interfacial free energy difference, $\Delta\sigma$, has commonly been used in the literature to characterize and evaluate the nucleating ability of different surfaces towards specific polymers.[33, 170, 171] More specifically, this approach has been also used to characterize the nucleation activity of various fiber in polypropylene (PP), polyethylene (PE) and poly(caprolactone) (PCL) composites.[58, 59, 112-117, 134] From Equation 3.1, it is apparent that the lower the $\Delta\sigma$, the lower will be the energy barrier for nucleation on the given substrate, and thus the higher its nucleation ability.

In order to derive the values of $\Delta\sigma$ for the nucleation of PLLA onto different fiber, the nucleation kinetics data are analyzed and plotted in a linearized form of Equation 3.1 in Figure 3.9. The values of $\Delta\sigma$ can be determined from the slopes of the fitting lines, while the intercepts of the lines result in the determination of the parameter I_0 (see Equation 3.1). The results for the different composites are shown in Table 3.1.

Figure 3.9(a) reveals that the data can be divided in two groups. Stereocomplex PLLA fiber is clearly the most efficient nucleating substrate. In fact, although nucleation rates values lower than the rest of the fiber were measured, these were achieved in a much lower range of undercooling, i.e., at higher crystallization temperatures. Indeed, at the crystallization temperatures which were explored for the other fibers, SC substrate always resulted in TCL formation. Moreover, the temperature dependence of the nucleation rate was distinctly the lowest among all the fibers, indicating a lower free energy barrier for nucleation on the stereocomplex crystal surface. Most of the natural and synthetic fibers presented quantitatively similar nucleation kinetics, although some differences could be appreciated by considering the most appropriate crystallization temperature region (see Figure 3.9(b)). Variation of more than one order of magnitude of the nucleation rates can yet be appreciated between for instance glass and PET fibers, or by tuning slightly the undercooling for each of the composite.

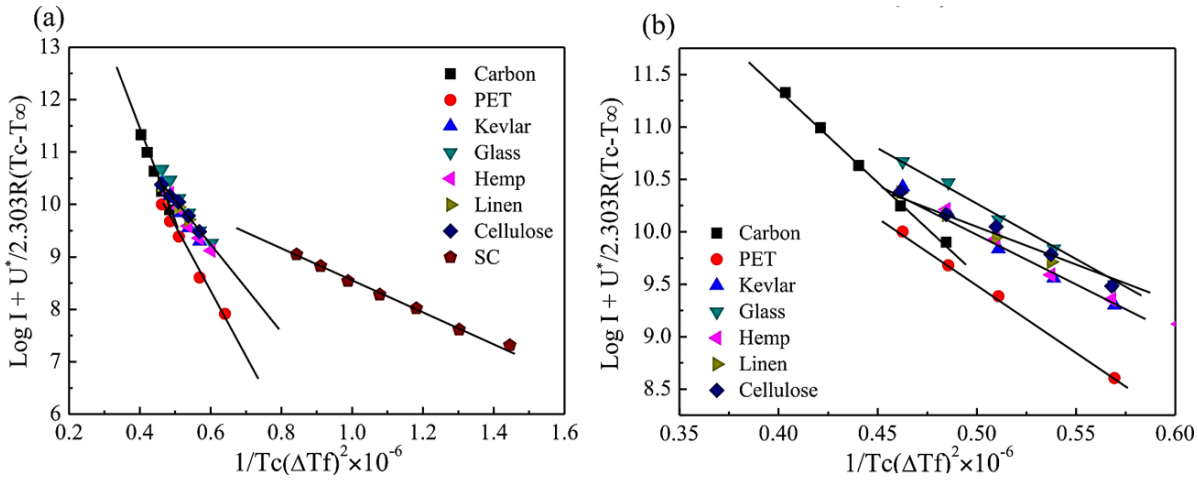

Figure 3.9 Variation of nucleation rate I with degree of undercooling (a), according to Equation 3.1, to determine the interfacial free energy difference ($\Delta\sigma$) for the different fibers; (b) enlarged view of Figure 3.9(a). The displayed data are average values from at least three measurements.

From Table 3.1 we can appreciate that similar values of $\Delta\sigma$, ranging from about 15 to 19 mJ/m^2, were obtained for the majority of the investigated fibers, with two noteworthy exceptions. The interfacial free energy difference of carbon and SC fiber are in fact about 24 and 4.3 mJ/m^2, respectively, in agreement with the different nucleation efficiencies deduced from the POM morphological observations. We highlight that what could seem a relatively small difference in the $\Delta\sigma$ among the substrates, reflects in a very large difference in nucleation rate. In fact, the ratio between the interfacial free energy differences of the various fiber corresponds to the ratio of free energy barrier for nucleation (ΔG^*). Being the nucleation rate exponentially dependent on the magnitude of ΔG^*, at a given undercooling and all the

other parameters being equal, we deduce that the nucleation rate per unit area of stereocomplex PLA fiber would be, for instance, more than 80 times larger than that on the surface of the glass fiber.

The values of $\Delta\sigma$ reported hereby for the nucleation of PLLA on different fibers lay in the same range of the ones found for i-PP on a variety of fibers (4 - 16.7 mJ/m^2).[59] In particular, SC fibers display very high nucleating activity towards PLLA, similarly to Teflon fibers for i-PP, the best substrate reported so far for that polymer.

Ishida et al. studied the nucleation of PCL and PE on ultra-high modulus polyethylene fibers, and derived the value of interfacial free energy difference by analyzing the undercooling dependence of the induction time for the appearance of the transcrystalline layer.[58, 134] Extremely low values of $\Delta\sigma$, i.e. 0.15 - 0.30 mJ/m^2 were obtained. However, these cases are rather peculiar. In fact, in the all-PE composite,[58] due to the fact that the same crystals constitute both the fiber and the matrix, a secondary nucleation (i.e., crystal growth), rather than heterogeneous nucleation model, should more appropriately describe the phenomenon. For PE fiber in PCL matrix, the extremely low values of $\Delta\sigma$ is attributed to the existence of epitaxy among the two polymer crystals, as demonstrated by Yan et al.[172, 173] We recall that no epitaxial relationship has been found for PLLA α-phase crystals and stereocomplex PLA crystal,[164] thus justifying the relatively high value of interfacial free energy difference observed in the present fiber-induced nucleation experiments. The origin of the different nucleating efficiency of the various fibers is tentatively investigated in the following paragraphs.

Table 3.1 Fiber features (diameter and roughness) and measured PLA nucleation parameter ($\Delta\sigma$ and I_0 from Equation 3.1, T_{max} for transcrystallinity development)

Type of Fiber	Diameters (um)	R_q (nm)	$\Delta\sigma$ (mJ/m^2)	T_{max} (ºC)	$Log\ I_0$ (nuclei/m^{2}s)
PET	51	28	19.3	120±1	15.4
Kevlar	12	12	19.3	121±1	15.3
Glass	18	16	18.7	118±1	15.4
Hemp	20	26	16.7	120±1	14.7
Linen	23	32	15.9	117±1	14.6
Cellulose	12	32	14.9	119±1	14.2
Carbon	7	19	24.1	108±1	17.5
SC	45	57	4.3	142.5	11.5

3.3.3 Role of Fiber Surface Roughness and Wettability

Surface topography, or roughness, has always been recognized to have a role in fiber-

induced nucleation in polymer composites,[59, 115, 128, 174, 175] and more generally, in heterogeneous nucleation.[176-182] For example, a decrease in induction time and interfacial free energy difference parameter of heterogeneous nucleation was found for i-PP crystallizing in contact with copper sheets of increasing roughness (in the micrometer scale).[178]

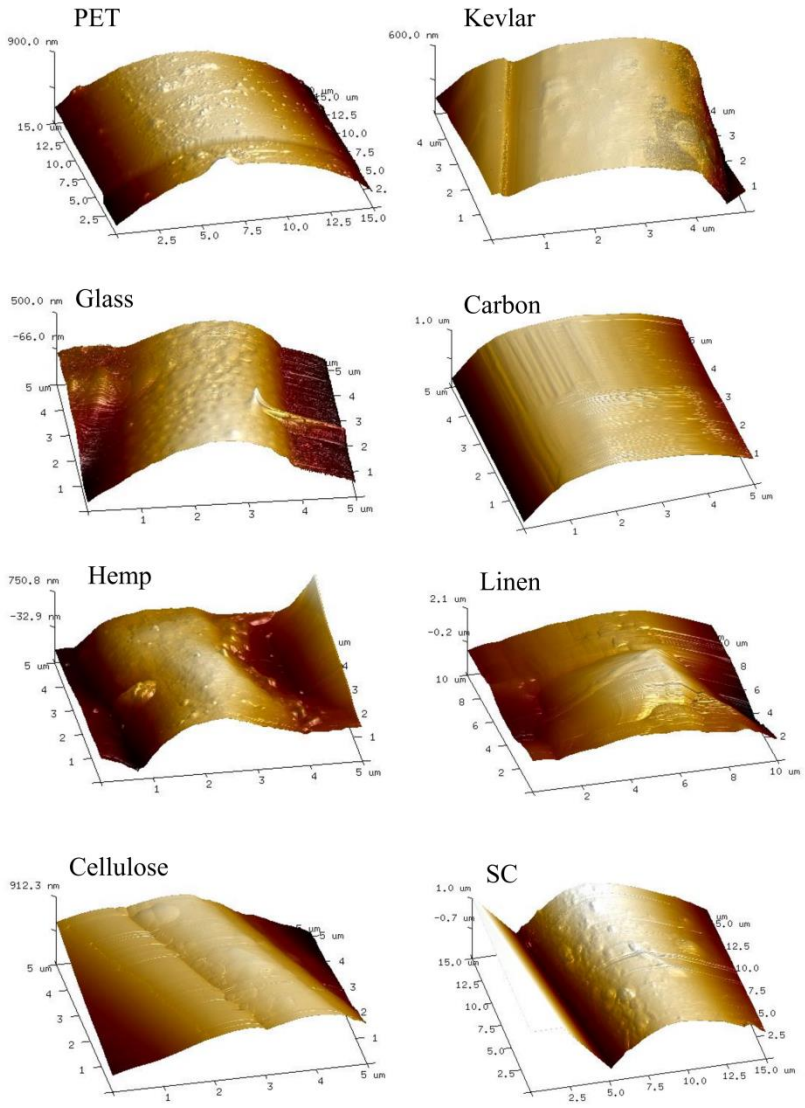

Figure 3.10 AFM height images of different fiber surfaces.

In the case of fiber-induced nucleation, it can be shown via atomic force microscopy (AFM) analysis that the fiber surface is always non-uniform and small “ridges” and “valleys” are usually present.[183] Such a surface topography has been suggested to enhance polymer nucleation for two possible reasons. On one hand, thermal stress develops at the fiber interface upon cooling, and might induce local orientation of polymer chain segments, providing efficient seeds for nucleation. Such thermal stresses are expected to be larger at deep “valleys” with respect to a smooth surface.[115, 117] On the other hand, it should be

considered that the free energy barrier required to form a viable nucleus on a flat surface is always larger than that of nucleation in a groove (tertiary nucleation).[59, 166] As a result, such nucleation in surface grooves is usually preferred.

Therefore, the surface topography of the investigated fiber was probed by means of AFM. Representative AFM images are reported in Figure 3.10 and some examples of characteristic height profiles are provided in Figure 3.11. The line scans have been properly subtracted of the overall fiber curvature, as described in the Method section of the manuscript.

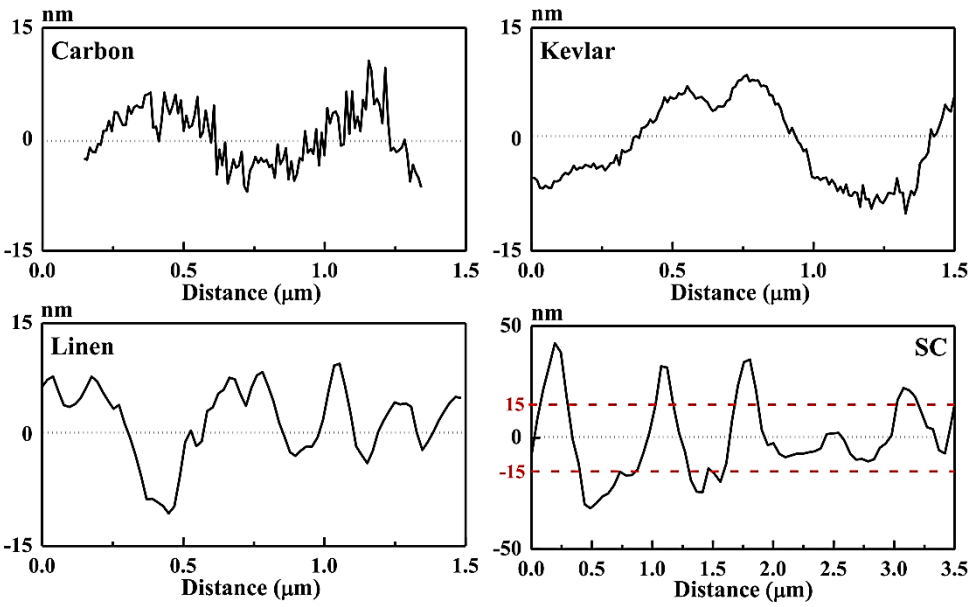

Figure 3.11 Examples of surface height profiles derived from analysis of AFM images. Carbon, Kevlar and Linen fibers are reported on an extended y-axis scale (30 nm), while the y-scale of the SC fiber is 100 nm. For the sake of comparison, the height scale of the other fibers is indicated by red dashed line in the height profile plot of the SC fiber.

All the fibers present characteristic “ridges” and “valleys” features, with typical height variation below 30 nm, with the exception of SC fibers (see Figure 3.12, for height profiles of the additional fibers). In fact, stereocomplex PLA fibers present peaks on their surfaces which are characterized by a larger height variation. A particular topography is also observed in carbon fibers, in which small scale and sharp ridges and valleys occurs with high frequency, superposed to a smoother height variation of the surface.

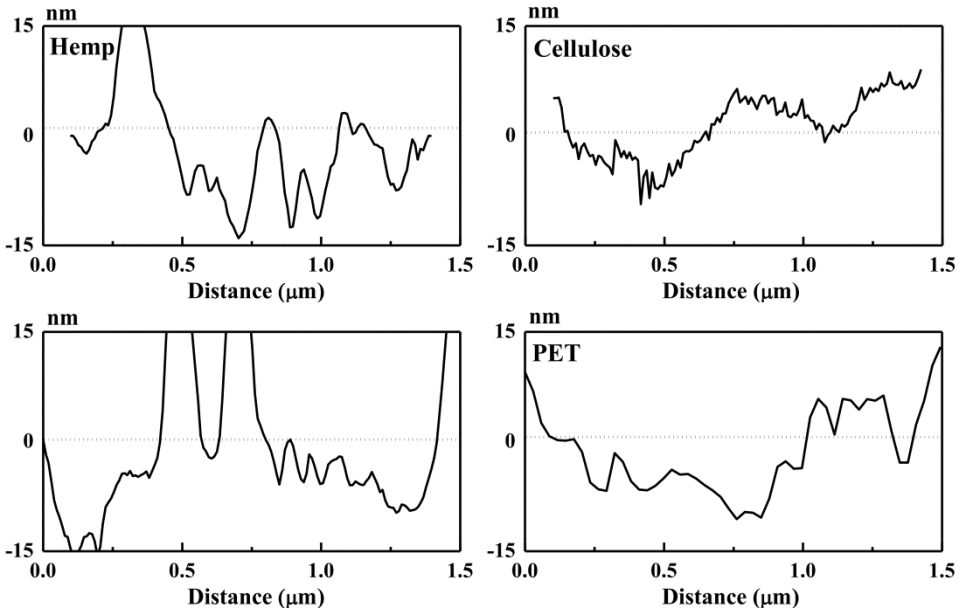

Figure 3.12 Surface height profiles derived from the analysis of AFM images.

From the height profiles as shown in Figure 3.11 and 3.12, the root mean square roughness (RMS or R_q) can be calculated. The values for the different fibers are reported in Table 3.1. Roughness values range from 12 to 32 nm for all the considered fibers except for stereocomplex PLA fiber, which presents a higher roughness (R_q equal to 57 nm), as deduced from Figure 3.11.

From the data reported Table 3.1, the effect of surface roughness on the parameters of the heterogeneous nucleation model can be explored. Figure 3.12(a) reports the interfacial free energy difference form nucleation experiments, as a function of the fiber surface roughness. A general trend of decreasing $\Delta\sigma$ with increasing the roughness of the fiber can be appreciated, indicating that fiber-induced nucleation is favored on non-smooth fibers. This result is in agreement with the commonly proposed association of transcrystallinity development with fiber surface topography,[59, 112-117] and with the measured decrease of interfacial free energy difference for i-PP nucleation on rougher copper substrates.[178]

However, we note that there is no clear simple relation between $\Delta\sigma$ and R_q. In particular, carbon and stereocomplex PLA fibers deviate from the general trend, having respectively a higher and lower interfacial free energy difference than the one that would pertain to their surface roughness value. It should be considered that the sole mean roughness value might not be sufficient to fully characterize a complex surface topography with respect to its nucleation ability. This aspect was clearly evidenced by Lin et al.,[184] who showed that i-PP nucleates faster on Teflon surfaces characterized by a higher fractal dimension but lower overall roughness.

Moreover, it is expected that, for a given surface topography, interactions between the

crystallizing matrix and the surface, dictated by the polymer and substrate chemistry, should also play a role in inducing nucleation. Despite the importance of the interactions via intermolecular forces between the substrates and the matrix, this role has been insufficiently documented in the literature of fiber-induced polymer crystallization, and even the absence of any surface chemistry effect on nucleation has been claimed [128]. On the other hand, the concept is instead rather well accepted in the nucleation of organic or inorganic molecules, especially from solution. [181, 185] The role of fiber matrix-interaction, or wettability, in PLLA nucleation will be tentatively addressed further on.

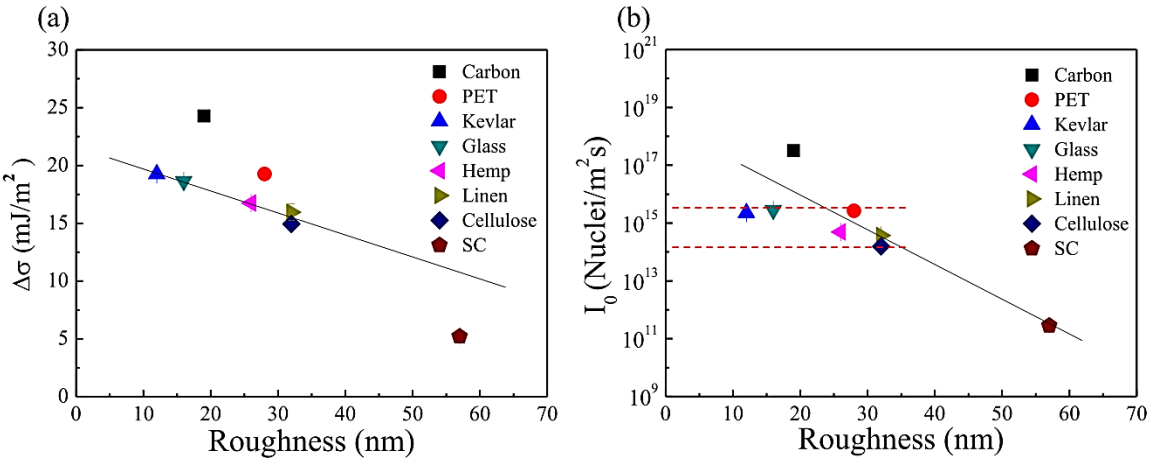

Figure 3.12 (a) Interfacial free energy difference, $\Delta\sigma$, and (b) Log I_0 derived from Equation 3.1, as a function of roughness for all the investigated fibers. The drawn lines are just a guide to the eyes.

From Figure 3.9, it can be deduced that the pre-exponential factor (intercept of the fitting lines with the y-axis), varies with the type of fiber. Such variation is confirmed by the data in Table 3.1. The pre-exponential parameter of the nucleation rate equation (I_0) is a temperature-independent frequency term which is commonly considered to be linked to molecular and transport properties of the nucleating material.[186]

In Figure 3.12(b), the derived I_0 is plotted as a function of fiber surface roughness. A large variation with the type of considered fiber is apparent: while for the majority of the fibers I_0 is in the order of 10^{15} nuclei/m^{2}s, a variation of several orders of magnitude is observed for SC and carbon fibers. In particular, the lowest value is found for stereocomplex PLA fibers, while it is about 10^6 times larger for carbon fiber. To the best of our knowledge, such differences in the pre-exponential factor of the heterogeneous nucleation rate equation have not been highlighted before in other studies of fiber-induced polymer nucleation.

It must be deduced that such kinetic term does not depend uniquely on the crystallizing macromolecule, but rather on the specific polymer/substrate pair. In fact, by considering that I_0 represents a frequency per unit area, it is plausible to hypothesize which it takes into

account the "effective" nucleating area of the fiber. We recall that to derive the quantitative nucleation rate data, the macroscopic area of the fiber has been considered. Therefore, from the measured value of I_0, we must deduce that the carbon fiber possesses a much higher density of "potentially active" nucleation sites on his surface, with respect to that of stereocomplex PLA fiber. This notwithstanding, the overall nucleation kinetics might be lower, due to the higher energy barrier term (related to the value of $\Delta\sigma$). However, the definition of an "active nucleation site" remains elusive, and it must be linked to the matching between the critical nucleus size at a certain undercooling and the exact surface topography. We can thus speculate that the successions of ridges and valleys at that specific length scale in the carbon fiber provides abundant preferred nucleation sites for PLLA. In contrast the SC fiber, despite possessing a much higher average roughness, has fewer active sites due to the lack of grooves of adequate size.

Despite the interesting correlations found between nucleation kinetics parameters and surface roughness, it has been recognized in the studies of heterogeneous nucleation that molecule-substrate interactions are of great importance. A straightforward way to quantify these interactions is the characterization of the substrate wettability by the crystallizing substance, by means of contact angle measurements. In fact, Turnbull used the melt-substrate contact angle to compute the decrease in the free energy barrier for heterogeneous nucleation with respect to the homogeneous case.[187] Experimentally, contact angle measurements have proven to closely correlate with the nucleation ability of solid substrates in the crystallization of small molecules from solution or melt,[181, 185] including the case of water freezing.[188] More recently, the same concept has been shown also for poly(butylene succinate) (PBS), which shows a smaller contact angle on hexagonal boron nitride nanosheets with respect to graphene, in agreement with the lower nucleating effect of the latter substrate.[189]

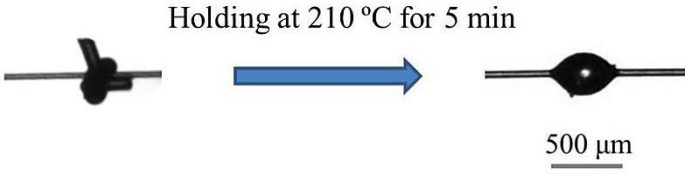

Figure 3.13 Optical micrographs of PLLA knot on SC fiber at room temperature and after annealing at 210 °C for 5 min.

Accordingly, we attempted to carry out PLLA wettability of the different fibers, by creating polymer droplets on their surface, according to the method described in the experimental section of the manuscript, see Figure 3.13 of the supporting information for the

details of sample preparation. Given the similar nucleation activity found for the majority of the fibers, we focused on the synthetic ones, which were more easily handled. Unfortunately, measurement on carbon fiber could not be performed due to its excessive brittleness.

Figure 3.14 shows the typical droplet shapes obtained by melting the PLLA matrix on different fiber substrates. A very similar shape is found for all the commercial fibers, characterized by a droplet/fiber contact angle of around 55°, a value denoting an appreciable wettability.

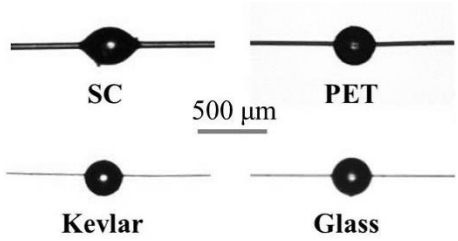

Figure 3.14 Optical micrographs showing the wettability of different fibers by PLLA.

A very different droplet shape is observed for PLLA/SC fiber. In this system PLLA definitely wets the fiber much more, with a contact angle equal to about 40°. The higher wettability of PLA SC fibers by the PLLA matrix is reasonably explained by considering a low interfacial tension between the two, due to the identical chemical nature. Although we are aware of the possible effect of surface roughness on the measured contact angle value, we think that the predominant role may be played by the favorable intermolecular interactions, since no distinct variation of the contact angle is seen for the other synthetic fibers, despite the measurable difference in surface roughness (Table 3.1). Therefore, also in the case of PLLA fiber-induced nucleation, wettability measurements are found to correlate well with the observed nucleation efficiencies of the substrates. As such, this simple method is likely to provide reliable information on fiber-induced nucleation and could potentially be extended to other relevant polymer composites.

3.3.4 Maximum Temperature for Transcrystalline Layer Development

For a given fiber, there is a maximum crystallization temperature (T_{max}) at which a continuous transcrystalline layer develops. Any crystallization temperature below T_{max} will result in TCL morphology, while for $T > T_{max}$ sporadic nucleation occurs. It has been shown for i-PP/fiber composites, that such T_{max} is related to the interfacial free energy difference: the lower $\Delta\sigma$, the higher T_{max}, given the lower free energy barrier that need to be overcome to form a viable nucleus on the fiber surface.[59]

The values of T_{max} obtained for the investigated fibers are reported in Table 3.1, and

displayed as a function of $\Delta\sigma$ in Figure 3.15(a). A general linear correlation can be seen, analogously to that reported for i-PP. With the variation of $\Delta\sigma$ from 24.1 to 4.3 mJ/m^2, T_{max} increases of more than 30 °C, from 108 °C for carbon fiber to 142 °C for stereocomplex fiber. Thus, also for PLLA, the parameter T_{max} provides a measure of the nucleating ability of a given fiber.

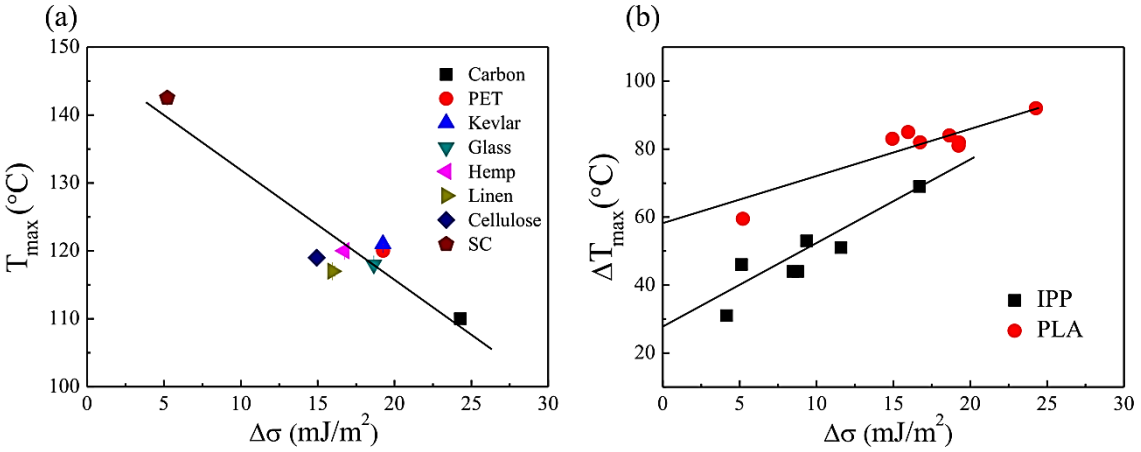

Figure 3.15 (a) T_{max} for TCL development in the various fiber as a function of $\Delta\sigma$ values; (b) comparison of the data in 8(a) with literature data for i-PP.[59] In this case, the undercooling is correlated with the $\Delta\sigma$, for a more direct visualization of the different polymers.

It is worthwhile to compare the behavior of PLLA with published results of i-PP.[59] However, given the different crystallization temperature range which characterizes the two polymers, instead of the maximum temperature for TCL development, the corresponding undercooling (ΔT_{max}) is considered, taking into account the equilibrium melting point of PLLA and i-PP. The results are shown in Figure 3.15(b). It can be seen that for a given interfacial free energy difference $\Delta\sigma$, much higher undercoolings are required to grow a transcrystalline morphology in PLLA, with respect to i-PP. Since $\Delta\sigma$ takes into account the free energy required to nucleate a monolayer of the crystal in contact with the fiber surface, we might deduce that the TCL formation is not completely controlled by this step of the nucleation process, i.e., the growth of further crystalline layers on top of the first one, up to the attainment of a nucleus of supercritical sizes must be the controlling factor. This different energy barrier is related to the energetics of secondary nucleation and chain diffusion, and is indeed expected to be different, depending on the considered semicrystalline polymer.

3.4 Conclusions

The nucleating ability of different fibers towards PLLA was successfully described with a classical heterogeneous nucleation model, and the observed differences could be quantified in

terms of the interfacial free energy difference, $\Delta\sigma$. Among all the considered synthetic and natural fibers, stereocomplex PLA fibers show by far the highest nucleating efficiency. A general trend of decreasing $\Delta\sigma$ with the increase of surface roughness could be grasped, although carbon and SC fibers displayed relevant deviations.

Thus, we can infer that roughness cannot be considered the sole or most important parameter which contributes in determining the nucleating efficiency of fibers in polymer composites, as often assumed in the literature. In fact, the different wetting behavior of the fiber by PLA melt, suggests that chemical interactions between the fiber and the polymer, can also be of importance. Moreover, the surface topography/roughness is suggested to affect the availability of active nucleation sites on the fiber surface, as deduced by the largely different nucleation pre-exponential factors, I_0, measured for the various fibers. Finally, a clear relationship between $\Delta\sigma$ and T_{max}, the maximum crystallization temperature at which a transcrystalline layer could be induced, was also observed.

This work extends the classical studies of fiber-induced nucleation and transcrystallinity in composites to a different polymer-fiber system, and highlights some open issues which need to be addressed for a comprehensive understanding of the heterogeneous nucleation of polymer crystals on natural and synthetic fibers.

Chapter 4. Crystallization of i-PP Micro-Droplets in Immiscible Blends

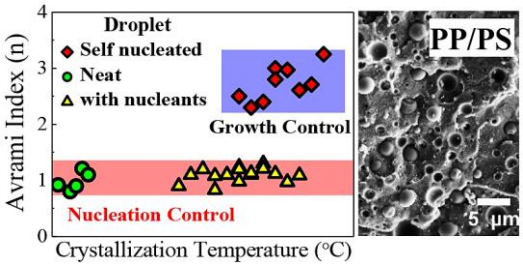

4.1 Introduction

Heterogeneous nucleation uses foreign preexisting surfaces to reduce the free energy barrier opposing primary nucleation.[190] The lower overall free enthalpy would then lead to a faster nucleation rate, which is of great significance for industrial applications. Nucleating additives are routinely used in industry to shorten the injection-molding cycles, and to improve the optical and mechanical properties of the products due to reduced crystal aggregates size.[191-194]

One of the most extensively studied polymers, for what concerns heterogeneous nucleation, is isotactic polypropylene (i-PP). For this material, two distinct classes of nucleating additives are commonly used: particulate systems, which are dispersed into the polymer and remain as solid particles in the polymer melt (such as talc, sodium benzoate, organophosphates, etc.[191, 195]) and soluble systems, such as sorbitol and its derivatives, which can dissolve in the polymer melt upon heating and phase separate upon cooling to produce the heterogeneous nucleating substrate.[196, 197]

A commonly accepted explanation for the acceleration of nucleation by means of nucleating agents, invokes ‘‘epitaxy’’ between NAs and polymer crystals.[198, 199] For example, Lotz et al. and Yoshimoto et al. have successfully disclosed the epitaxial relationship between i-PP α-form crystal and different nucleating agents, by means of atomic force microscopy (AFM) and transmission electron microscopy (TEM).[94, 200]

According to Fillon et al.[95, 96] a convenient Nucleation Efficiency scale (NE), defined in Equation 4.1, can be used for comparing the increase in non-isothermal crystallization temperature of a nucleated sample with that of the neat polymer, and with the one obtained by self-nucleating the same material at the ideal self-nucleation temperature.

$$NE = 100\frac{T_{NA} - T_0}{T_{Max} - T_0} \quad (4.1)$$

In this equation, T_0 and T_{NA} are the crystallization temperatures of the bulk material and of the material compounded with the nucleating agents, respectively, while T_{Max} is the maximum crystallization temperature achievable when a polymer is self-nucleated to the maximum level, without producing any detectable annealing of the original crystals, that is, at the ideal self-nucleation temperature (i.e., $T_{s,ideal}$).

However, due to the combined effect of nucleation and growth processes in determining the overall crystallization of the bulk material, the so-derived efficiency scale remains a useful, but empirical, evaluation method. Ideally, one would need to probe the effect exclusively due to the nucleation step, and compare the different substances on the basis of the free energy barrier for the formation of a critical nucleus on their surfaces.

When semi-crystalline polymers are ideally confined into isolated micro- or nano-domains, e.g., in immiscible blends or block-copolymers, nucleation could be the rate-determining step in the overall crystallization process (that includes both nucleation and growth). This can be evidenced by probing the overall crystallization of the system, which displays a first order kinetics.[37, 201-203] The study of crystallization within droplets dates back to 1880 when Van Riemsdyk [204] investigated the crystallization of gold droplets. He found a significant depression of the crystallization temperature of the droplets in comparison to bulk gold. Since then, many researchers have performed related studies in different materials, such as metals, water, alkenes and polymers.[44, 205-209] Typically, dispersed droplets will exhibit multiple crystallization exothermic peaks.[210-213] This phenomenon, known as fractionated crystallization,[40, 212, 214-219] arises from the presence of numerous dispersed droplets each possibly containing a different number of heterogeneous nuclei or nuclei with different efficiency. Therefore, each exothermic peak represents a population of droplets including a given nucleating heterogeneity, which can become active at a certain undercooling. At large undercoolings the droplets can nucleate at the surface, i.e, at the interface with the matrix, or homogeneously, when the nuclei are formed within the volume of the droplet by spontaneous aggregation of the polymer chains. If the droplets are very small and their number much larger (i.e., orders of magnitude) than the available heterogeneities of the material in bulk, they crystallize exclusively by surface or homogeneous nucleation, i.e., a single crystallization peak is observed at temperatures close to the glass transition.[203]

Thus, the study of droplets crystallization can be a potentially fruitful approach for evaluating the nucleation kinetics of heterogeneously nucleated polymers.[209, 212, 218,

220, 221] Indeed, when nucleating agents are present in droplets which otherwise would nucleate homogeneously, it is anticipated that the resulting fractionated crystallization can provide further insight into the nucleation process of the heterogeneous additives.

This strategy was adopted by Hoffmeir and Perepezko,[37] who took advantage of the droplet emulsion technique to produce Sn metal droplets containing particles of different metal oxides. The heterogeneous nucleation activity of the various compounds was then evaluated upon cooling in terms of the achieved undercooling. Analogously, in semi-crystalline polymers, Santana and Müller [222] successfully altered the fractionated crystallization of i-PP droplets dispersed into polystyrene (PS) matrix, by addition of a phtalocyanine blue pigment to the blend. Langhe et al.[212] applied this method more extensively to investigate the effect of several α- and β- phase nucleating agents, in droplets obtained by the breakup of i-PP nanolayers in a PS matrix. When the NAs were solid particles only i-PP droplets larger than a minimum size could be efficiently nucleated.[212]

Although not yet directly applied to this aim, the method of nucleating isolated droplets seems also promising to derive the nucleation free energy barrier, by studying the crystallization kinetics of the system. In this work, the nucleation process of isotactic polypropylene droplets dispersed in a polystyrene matrix and containing various nucleating agents (i.e., sodium benzoate, NA-11, quinacridone quinone), has been investigated by isothermal step crystallization and melting with Differential Scanning Calorimetry (DSC). Given the fact that crystallization kinetics in such systems is dominated by (heterogeneous) nucleation, the nucleating efficiency of the various heterogeneous NAs are then quantitatively compared on the basis of the derived free energy barrier for critical nucleus formation, ΔG^*. Moreover, self-nucleation of neat PP/PS blend is also studied in detail, enabling to derive an "intrinsic" nucleation efficiency scale based on the ratio of the free energy barrier, ΔG^*, of the various nucleation processes (i.e., homogeneous nucleation, heterogeneous nucleation on different substrates) with respect to that of self-nucleation.

4.2 Experimental Section

4.2.1 Materials

A commercial isotactic polypropylene (i-PP, HD601 CF) kindly provided by Borealis Polyolefine GmbH, with a weight average molecular weight (M_w) of 365 kg/mol and a polydispersity index (M_w/M_n) of 5.4 was used. The atactic polystyrene employed here, with melt flow rate of 3.4 g/10min, was purchased from Sigma-Aldrich.

The NAs employed in this work were sodium benzoate (SB), purchased from Sigma-Aldrich, and an organophosphate salt, (sodium 2,2'-methylene bis-(4,6-di-tert-butylphenyl) phosphate), commercially named NA-11. Both NAs promote the formation of α-form i-PP crystals. Moreover, a β-crystal nucleating agent, quinacridone quinone (QQ), was also used. The NA-11 and QQ nucleating compounds were also kindly provided by Borealis Polyolefine GmbH.

4.2.2 Blend Preparation

All the samples were prepared in a Brabender batch mixer at 210 ºC, with a rotor speed of 50 rpm for 10 min. The nucleating agents were first compounded with polypropylene and then the obtained masterbatches were blended with polystyrene at a constant concentration by weight (i-PP/PS 15/85 wt-%). The compositions of the prepared blends are shown in Table 4.1.

Table 4.1 Composition of the prepared blends.

Sample Label	NA11	OO	SB	PP	PS
	(wt.-% in PP)			(wt.-%)	
PP/PS	0	0	0	15	85
PP/PS/NA11-2	2	0	0	-	-
PP/PS/SB-2	0	0	2	-	-
PP/PS/QQ-2	0	2	0	-	-
PP/PS/NA11-0.1	0.1	0	0	-	-
PP/PS/NA11-0.25	0.25	0	0	-	-
PP/PS/NA11-0.5	0.5	0	0	-	-

4.2.3 Scanning Electron Microscope (SEM)

The morphology of the prepared blends was observed by Field-Emission Scanning Electron Microscope (Supra 40 VP model, Zeiss, Germany) at an accelerating voltage of 1 kV. The specimens were submerged in liquid nitrogen and fractured cryogenically. All samples were thinly sputter-coated with carbon using a Polaron E5100 sputter coater.

4.2.4 Differential Scanning Calorimetry (DSC)

Samples of approximately 3-5 mg were encapsulated in aluminum pans and analyzed by DSC, with a DSC1 STARe System (Mettler-Toledo, Switzerland), under a constant nitrogen flow of 20 mL/min. The DSC instrument was calibrated with indium. The detailed thermal

protocols are described in the following.

4.2.5 Standard Run by Differential Scanning Calorimetry

All the samples were first heated to 210 ºC, held there for 3 min to erase any previous thermo-mechanical history, and then cooled to 25 ºC and subsequently heated again to 210 ºC at a scan rate of 10 ºC/min.

4.2.6 Self-nucleation Experiments

Self-nucleation experiments, first developed for DSC by Fillon et al.[95, 223], and recently reviewed by Michell et al.[224], involved partial melting of a crystalline standard state followed by recrystallization, which takes advantage of the self-nuclei created during this first thermal treatment. For neat PP/PS blend, the standard self-nucleation process was first performed to identify the three self-nucleation domains, as defined in the literature.[216, 223] The detailed procedure is described as following: (a) erasure of crystalline history by heating the blends to 210 ºC for 3 min; (b) cooling down to −10 ºC at 10 ºC/min to create a standard crystalline state; (c) heating at 10 ºC/min to different self-nucleation temperatures (T_s) and holding for 5 min; (d) cooling scan from T_s to −10 ºC at a rate of 10 ºC/min, to detect the effect of thermal treatment on the crystallization behavior of the blends; (e) DSC heating scan from −10 ºC to 210 ºC at a rate of 10 ºC/min. Three domains can be defined, on the basis of the re-crystallization and melting behavior. *Domain I*, where T_s is so high that nor crystalline fragments, neither crystalline memory is left; *Domain II*, where T_s is high enough to melt most of the crystals, while still produces self-nuclei, detected by the shift of the subsequent crystallization temperature to higher values compared to those of *Domain I*. Until now, the nature of self-nuclei is still controversial, since the self-nucleation phenomenon has been attributed to a residual local segmental orientation in the melt, to the effects of non-equilibrium entanglement density or to the survival of stable remnants of pre-existing crystals.[71, 223, 225-231] *Domain III*, locates at T_s low enough that only partial melting takes place, meanwhile part of the crystals still remain intact. Therefore, the unmolten crystals will be annealed during the 5 min holding at T_s, while the molten part of the material produces self-nuclei in the subsequent cooling process.

4.2.7 Isothermal Step Crystallization

The isothermal crystallization kinetics of droplets was determined by the indirect method, Isothermal Step Crystallization.[232, 233] Self-nucleated or heterogeneously nucleated i-PP droplets were first heated to 210 ºC, held for 3 min to erase crystalline history, and then

cooled down directly to crystallization temperature (T_c) at a rate of 10 ºC/min. For neat PP/PS blend, samples were also cooled down to T_c from different self-nucleation temperatures T_s in *Domain II*. Then, isothermal crystallization was performed at T_c for different times for all the samples, and the crystalline fraction developed in the crystallization process was indirectly measured by quantifying the melting enthalpy in the subsequent heating scan.[232, 233]

4.2.8 Polarized Light Optical Microscopy

The crystal growth rate of bulk i-PP sample was studied with a Polyvar Pol optical microscope under crossed polarizers. Micrographs were acquired by using a computer-controlled digital camera (Optika), and the thermal program was imposed and controlled by a calibrated Mettler-Toledo hot-stage. Thin polymer film samples with thickness around 20 - 50 μm were prepared between microscope coverslips; then they were melted at 210 ºC for 3 min and cooled (10 ºC/min) down to isothermal crystallization temperature, where the evolution of the morphology was observed.

4.3 Results and Discussion

4.3.1 Morphology of Immiscible Blends

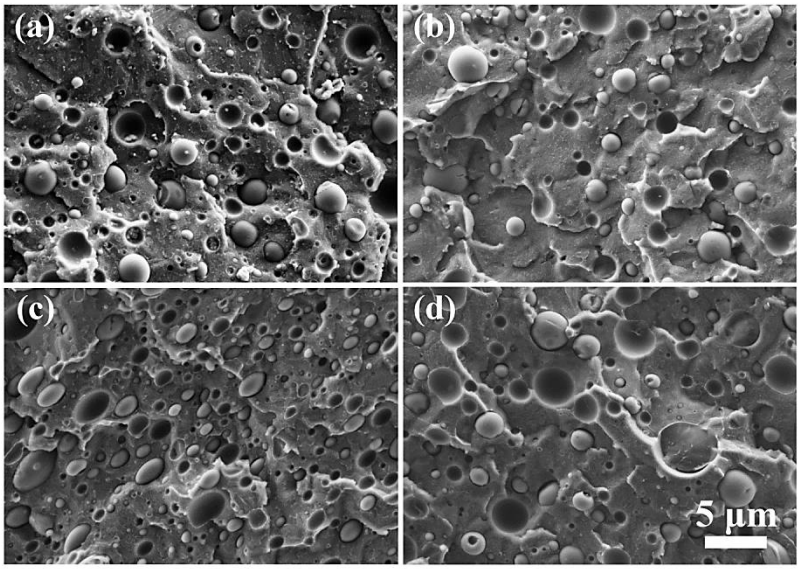

Figure 4.1 SEM micrographs of the prepared blends: (a) PP/PS; (b) PP/PS/NA11-2; (c) PP/PS/SB-2; (d) PP/PS/QQ-2.

Representative SEM micrographs of the fractured surfaces of the prepared polymer blends are shown in Figure 4.1. The minority component, isotactic polypropylene, is well dispersed in the polystyrene matrix and exhibits a characteristic droplet morphology. The number and

volume average diameter (d_n and d_v), dispersity (D), volume fraction of dispersed phase (X_v) and particle number per cm^3 (Ni) were calculated in Figure 4.2 according to standard equations proposed in the literature,[40] by measuring more than 200 particles from different regions of the various samples.

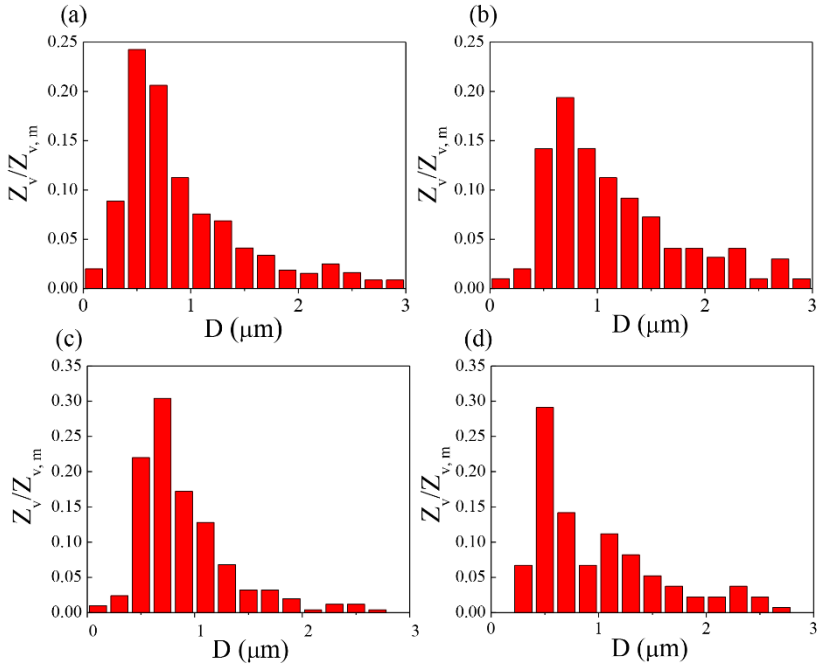

Figure 4.2 Size distribution of i-PP droplets in PS blends: (a) PP/PS; (b) PP/PS/NA11-2; (c) PP/PS/SB-2; (d) PP/PS/QQ-2.

The values are collected in Table 4.2. The spherical micro-domains in the neat PP/PS blends possess a number-average diameter d_n of approximately 1.0 μm and an average concentration, N_i, of 3 $\times 10^{11}$ cm^{-3}. The blends with NAs present similar morphology in comparison with the neat blends, namely average droplet size and concentration of domains. This will thus allow to neglect, as a first approximation, the effect of polydispersity and morphology on crystallization, when comparing differently nucleated i-PP droplets.

Table 4.2 Morphological characterization of the prepared blends.

	d_n (μm)	d_v (μm)	D	X_v	N_i (cm^{-3})
PP/PS	0.98	2.60	2.67	0.18	3.23×10^{11}
PP/PS/NA11-2	1.11	3.64	3.27	0.18	4.70×10^{11}
PP/PS/SB-2	0.88	2.47	2.81	0.18	2.34×10^{11}
PP/PS/QQ-2	1.06	3.17	2.99	0.18	4.09×10^{11}

4.3.2 Results of Standard DSC Run

The DSC scans resulting from cooling and heating at a rate of 10 ºC/min, for bulk i-PP, neat PP/PS blend, and nucleated PP/PS/NA11-2, PP/PS/SB-2, PP/PS/QQ-2 blends are

compared in Figure 4.3.

Fractionated crystallization can be interpreted as due to the crystallization of distinct droplet populations containing different nucleating heterogeneities. If very active nucleating impurities are present in the droplets, these will crystallize at low supercooling, similar to what occurs in the bulk. Meanwhile, droplets containing less efficient impurities will nucleate at higher supercooling, which is characteristic of the nucleating efficiency of the given heterogeneity. Finally, droplets that do not contain any impurities will nucleate at the largest supercooling - typically by homogeneous nucleation or by nucleation at the interface with the matrix phase. Thus, the exothermic peaks at 70 ºC and 100 ºC found in the neat PP/PS blend can be ascribed to the heterogeneous nucleation of i-PP droplets on less efficient impurities (100 °C) or onto PS surface (70°C), since homogeneous nucleation of polypropylene is expected to occur around 35-40 ºC (depending on the microdomain size), according to previous literature results.[212, 216, 234]

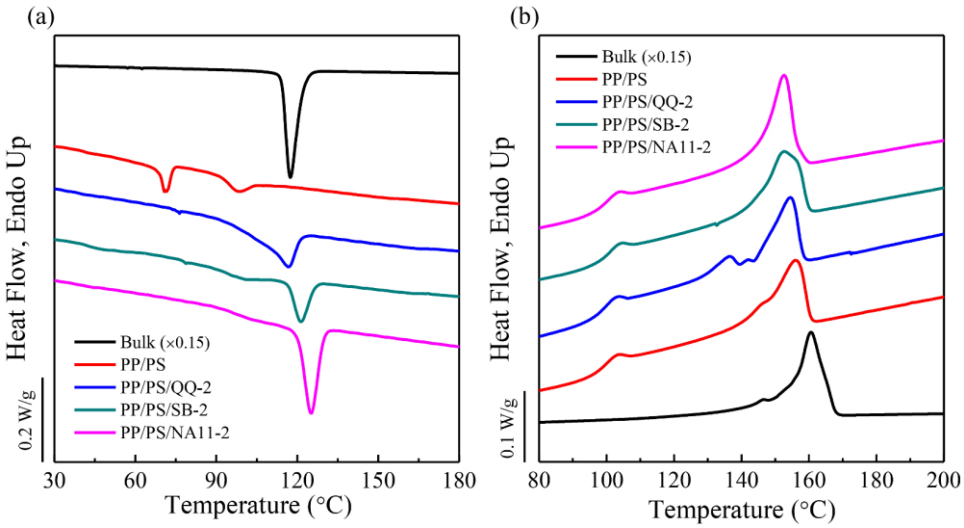

Figure 4.3 Cooling (a) and heating (b) curves of bulk i-PP and of the prepared PP/PS, PP/PS/NA11-2, PP/PS/SB-2, PP/PS/QQ-2 blends.

With the addition of the nucleating agents, the crystallization events at 70 ºC and around 100 ºC tend to disappear, while a new exotherm, close to 120 °C, becomes evident. The exact shape and position of this crystallization peak, which occurs at temperatures slightly above that of the bulk non-nucleated i-PP, depends on the particular employed nucleating agent. It is thus natural to assign this peak to the crystallization of nucleated i-PP droplets. We also note that the melting curves of the samples are substantially analogous, beside the presence of a double melting peak for the i-PP droplets nucleated with Quinacridone Quinone, with the lower melting endotherm reasonably assigned to the presence of a certain amount of trigonal β-polymorph in the crystallized sample.

The effect of varying nucleating agent concentration in the immiscible blends is shown in Figure 4.4. At very low concentration (0.1 wt%), the behavior of the nucleated blend shows no differences with respect to that observed for the neat PP/PS sample (except for the presence of a new small exotherm at 45 ºC, which could be explained by the crystallization of a small population of clean droplets that are able to undergo homogeneous nucleation). On the contrary, when the same amount of NA-11 is added to bulk polypropylene, a clear nucleation effect is evidenced (not shown). This indicated that either the quantity of NAs is insufficient to nucleate the exceedingly large number of droplets, or that part of it is transferred from the compounded polypropylene to the bulk of PS matrix, diminishing the actual concentration available in the i-PP droplets.[235]

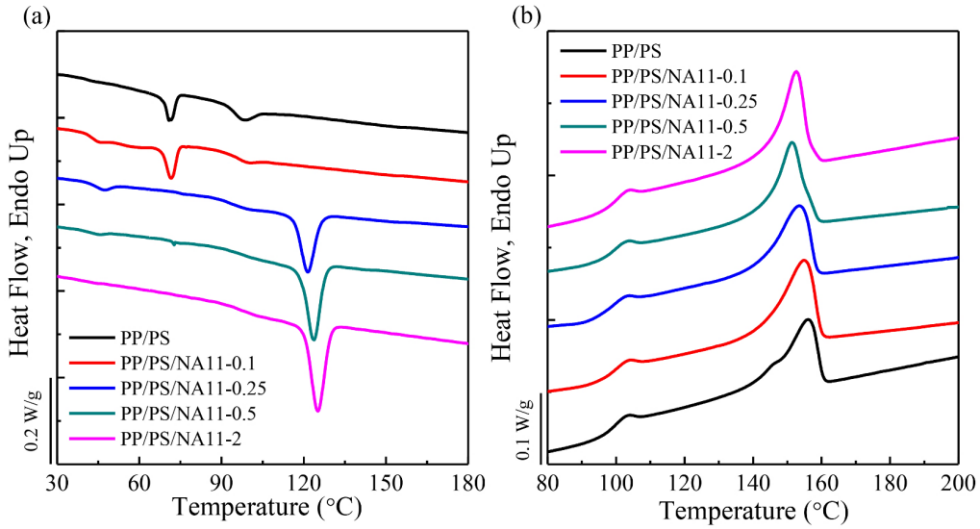

Figure 4.4 Cooling (a) and heating (b) curves of the PP/PS/NA11 blends with different concentrations of NA11.

For higher concentrations, a dual effect is observed: on one hand a slight increase of crystallization temperature, on the other hand a clear increase of the area of the high temperature peak, indicating a larger amount of nucleated droplet and/or a faster crystallization kinetics due to the higher average number of nucleation seeds per droplet.[236] Moreover, in the blends containing low amounts of nucleating agent, at about 45-50 °C one can notice a small exothermic peak, which can be attributed to the fraction of heterogeneity free droplets with smaller diameter, given the observed polydispersity in the size distribution (Table 4.2). Interestingly, such peak also disappears when the concentration of NA-11 is sufficiently high, in agreement with the expectations, since a higher concentration of heterogeneities is required to nucleate the smaller droplets.[237, 238]

4.3.3 Self-nucleation Results

In 1995, Morales et al.[215] applied the self-nucleation technique to a blend of immiscible polymers with a crystallizable minor phase, and they successfully verify for the first time that fractionated crystallization is due to the lack of heterogeneous nuclei in the droplets of the dispersed phase. Since then, several researchers have employed the same technique to various immiscible blends.[37, 40, 211, 216, 218, 239] The results of self-nucleation protocol applicated to our neat PP/PS blend are provided in Figure 4.5, where the cooling scans of the sample from the indicated T_s, and the subsequent heating scans are shown.

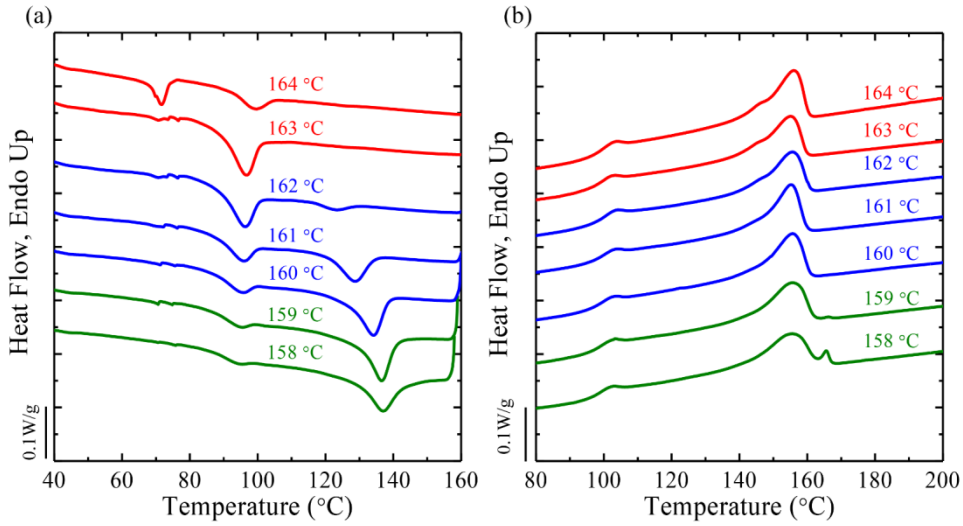

Figure 4.5 (a) DSC cooling scans from the indicated Ts values for the neat PP/PS blend; (b) subsequent DSC heating scans performed after the cooling runs shown in (a). The different colours of the curves represent the different self-nucleation Domains: Domain I (red), Domain II (blue) and Domain III (green).

On the basis of the DSC crystallization and melting traces shown in Figure 4.5, the aforementioned different self-nucleation *Domains* will be discussed. Until self-nucleation temperatures down to 164 °C, the cooling curve is identical to the one obtained in the DSC standard run (cooling from 210 °C), and the system is therefore in *Domain I*. Starting from a T_s of 163 °C, the lowest temperature exotherm disappears, while the one around 100 °C becomes sharper and more defined. Although this might be considered as first sign of the occurrence of self-nucleation, and hence the cross-over to *Domain II*, we conventionally set the *Domain I/Domain II* boundary at 162 °C, where a peak at distinctly higher crystallization temperatures (around 120 °C) starts to appear. Such peaks become progressively larger with decreasing T_s, at the expenses of the crystallization event at 100 °C. No changes in the melting endotherm after re-crystallization from the self-nucleated melt can be appreciated, down to a T_s equal to 159 °C. This temperature thus demarks the *Domain II/Domain III* boundary. The ideal self-nucleation temperature in this case is 160 ºC, as this is the

temperature that causes the maximum self-nucleation (i.e., maximum increase in T_c values or in nucleation density) without annealing, or the minimum T_s temperature within *Domain II*.

For a better visualization, Figure 4.6 reports the recorded crystallization temperature (for the highest temperature exotherm) as a function of T_s, superposed on the standard melting endotherm of the material. It can be seen that *Domain II* is located just at the end of the melting endotherm, as typically found in the case of isotactic polypropylene.[224]

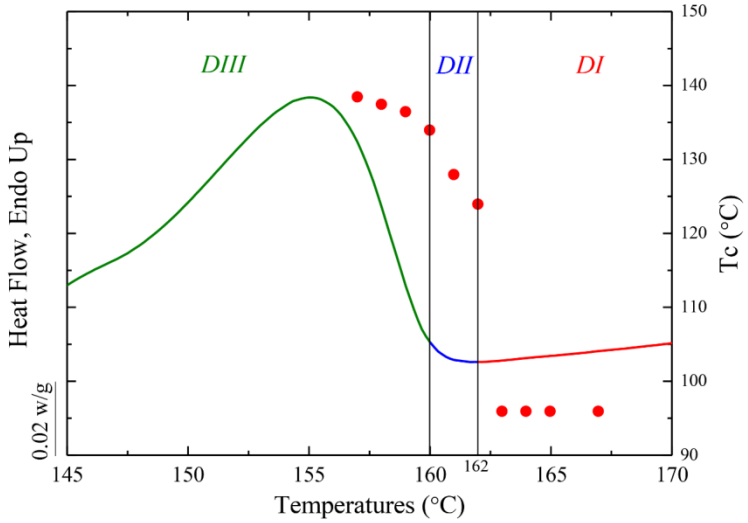

Figure 4.6 Representation of the self-nucleation domains for the PP component within a neat PP/PS blend superimposed on top of the standard DSC melting trace. Data points represent crystallization peak temperatures (plotted using the right-hand y-axis) as a function of Ts values (on the x-axis).

Self-nucleation is a common phenomenon in polymer crystallization, where recrystallization of a semi-crystalline polymer depends strongly on the nature of its initial melt state. Several interpretations have been proposed for its explanation, including the existence of a precursor metastable state, local clustering of chain segments in the melt, and topological effects due to entanglements.[71, 223, 225-231] Under the assumption that the self-nucleated melt state is an intermediate state between isotropic melt and the crystal, it can be shown that the transition between this heterogeneous melt and the crystalline state becomes faster than the direct crystallization from the isotropic melt. In particular, the accelerated crystallization was attributed by Muthukumar to a faster primary nucleation.[225, 228]

On the other hand, Lorenzo and Müller[240] have estimated the nucleation and growth contributions to the overall crystallization energy barrier for isothermally crystallized PPDX (polyparadioxanone), PCL (polycaprolactone) and PE (polyethylene) samples, crystallized from different melt states (i.e., varying the self-nucleation temperature). They demonstrated that, after SN at the ideal temperature, the primary nucleation step is entirely completed and the overall crystallization rate data obtained by DSC contain information on crystal growth

(or secondary nucleation) only. In order to understand whether the same situation holds when the material is dispersed as microdroplets, instead of being in the bulk, and for the subsequent quantitative evaluation of the nucleation efficiency of different nucleating agents, the overall crystallization rate of self-nucleated PP/PS blend at various isothermal temperatures is measured.

The melting curves of neat PP/PS blend isothermally step crystallized for different times at 146 °C after SN at 160 °C are shown in Figure 4.7(a), while Figure 4.7(b) presents the evolution of the relative melting enthalpy (which are proportional to the crystallization enthalpy) as a function of time, at different crystallization temperatures.

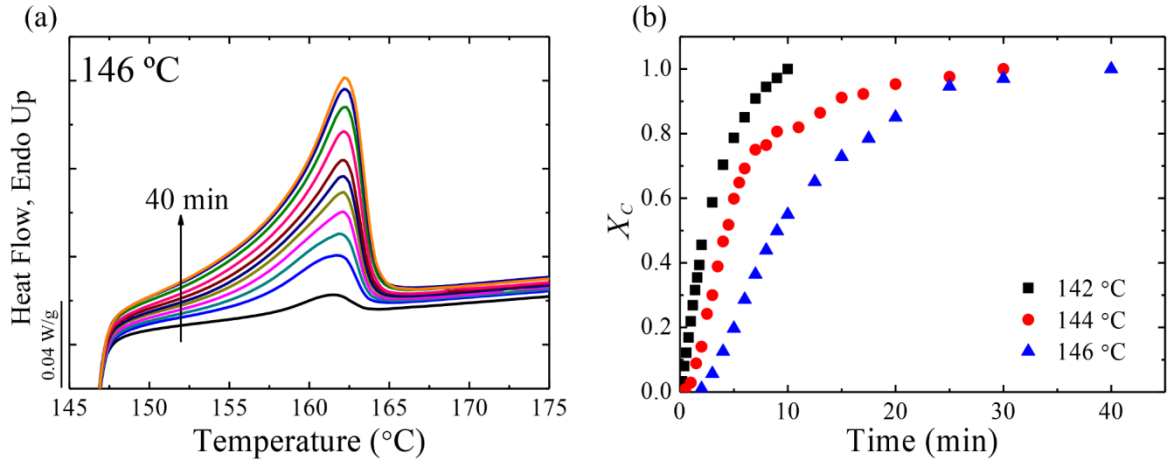

Figure 4.7 (a) Melting after isothermal step crystallization of PP droplets within neat PP/PS blend crystallized for different times at T_c = 146 ºC after self-nucleation at T_s = 160 ºC; (b) evolution of the relative crystallization enthalpy as a function of the overall crystallization time at the indicated temperatures.

The melting curves of PP/PS blend isothermal step crystallized for different times at 146 °C after SN at 160 °C are shown in Figure 4.7(a), while Figure 4.7(b) presents the evolution of the relative crystallization enthalpy as a function of time, at different crystallization temperatures. The isothermal crystallization kinetics is quantitatively compared with the classical Lauritzen and Hoffman model (LH), which provides an expression for the linear growth rate (G) as a function of supercooling. According to the theory, the growth rate can be expressed as:

$$Log\ G = Log\ G_0 - \frac{U^*}{2.303R(T_c - T_\infty)} - \frac{K_g}{2.303T_c\Delta Tf} \tag{4.2}$$

where G_0 is a growth rate constant, R is the gas constant, T_∞ is the limiting temperature at which the polymer segmental motion ceases, U^* is the activation energy for the diffusion of crystallizing elements across the phase boundary, ΔT is the undercooling ($= T_m^0 - T_c$), T_c is the

crystallization temperature, and f is a correcting factor ($= 2T_c/(T_c + T_m^0)$). K_g is the nucleation constant, which is proportional to the energy barrier for secondary nucleation. Values of U^*, T_m^0 and T_∞ for α-form i-PP crystal can be taken from the literature, respectively being 6280 J mol^{-1}, 458 K, 232 K.[241]

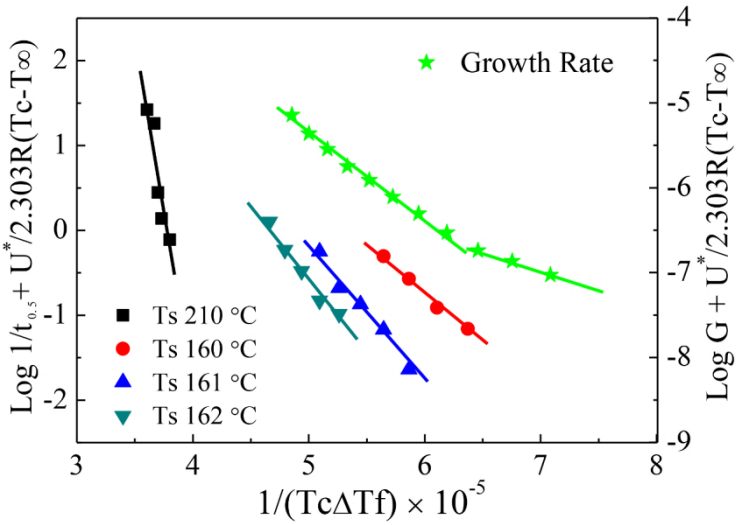

Figure 4.8 Lauritzen and Hoffman plots for DSC determined overall crystallization rate (expressed as the reciprocal of the half-crystallization time) of neat and self-nucleated i-PP droplets and for PLOM spherulitic growth rate data for bulk i-PP. Solid lines are the fits to the theoretical model (Equation 4.1).

Even though the LH treatment was originally developed for describing crystal growth only, it has been widely employed to describe overall crystallization process, due to its suitability to fit the data.[240, 242-245] When isothermal crystallization kinetics data obtained by DSC are employed, instead of growth rate, the energy barrier reflected by the "apparent" K_g^τ value is that for the overall crystallization, which contains contributions from both primary nucleation and crystal growth.

Table 4.3 Values obtained by fitting the isothermal data of i-PP, obtained either from PLOM (growth rates) or DSC (overall crystallization rate).

Method	T_c Range (°C)	$K_g \times 10^{-4}$ (K^2)
POM (K_g^G)	130 -144	24.3
	144 -150	12.9
DSC (K_g^τ)		
T_s=160	142 -150	26.5
T_s=161	136 -144	36.6
T_s=162	130 -138	40.5
T_s=210	106 -112	193.2

Figure 4.8 shows how the LH theory was applied to fit the overall crystallization kinetics data ($1/t_{0.5}$) as a function of T_c for neat and self-nucleated i-PP droplets. The calculated K_g values are listed in Table 4.3, together with those obtained by LH theory applied to the spherulitic growth rates for the same material in bulk.

We can observe a good agreement between the value of K_g^{τ} of ideally self-nucleated i-PP droplets (T_s = 160 °C) obtained by overall crystallization via DSC, and that for spherulitic growth measured by PLOM (K_g^{G}). This is also evidenced in Figure 4.8, where the two slopes of the LH plots for the ideally self-nucleated i-PP droplets data and for the growth rate data are nearly identical, although a shift of the *Regime II-Regime III* transition temperature is present in the growth rata data of bulk material but not observed for self-nucleated droplet overall crystallization. It thus seems that self-nucleation caused a shift of *Regime III* crystallization to lower supercooling values. As such, the overall crystallization of droplets self-nucleated at the ideal temperature shows a negligible energy barrier for primary nucleation, and the kinetics is dominated by secondary nucleation-controlled crystal growth. On the other hand, with the increase of T_s, the value of K_g^{τ} increases continuously, indicating a more important contribution of primary nucleation to the overall crystallization rate, since not 100 % of the i-PP droplets are nucleated, and part of the droplets are without “seeds”. A similar trend was reported by Feng et al. for polypropylene homopolymer and copolymers.[246]

4.3.4 Heterogeneous Nucleation of i-PP Droplets

Differently from self-nucleation, where self-seeds are efficiently injected into the droplets and the barrier for primary nucleation is overcomed, nucleation is still the rate-determining step for the overall crystallization of i-PP micro-droplets containing nucleating agents. In fact, in this system, as it will be shown further in this section, the time necessary for growing crystallites to cover the entire droplet volume is much shorter than the primary nucleation time. In the case of nucleation-controlled crystallization, the overall rate follows a first order kinetics and can be described by the equation:

$$1 - X/X_{max} = exp(-Ivt) \tag{4.3}$$

where X/X_{max} is the fraction of droplets already crystallized, I represent the average nucleation rate and v the droplet volume.

The melting curves of PP/PS/NA11-2, PP/PS/QQ-2 blends after isothermal step crystallization for different times at the indicated temperatures are shown in Figure 4.9(a) and

(b), respectively. The melting enthalpy increases gradually with the crystallization time. Notably, for the PP/PS/QQ-2 blend in Figure 4.9(b), two melting peaks appear during the heating process, differently from the other blends containing α-nucleating agents. The low temperature peak at around 145 °C is identified as the melting peak of β-crystals, while the second peak around 156 °C is due to the melting of α-phase, most likely generated by β-α recrystallization process occurring during heating.[212, 247, 248]

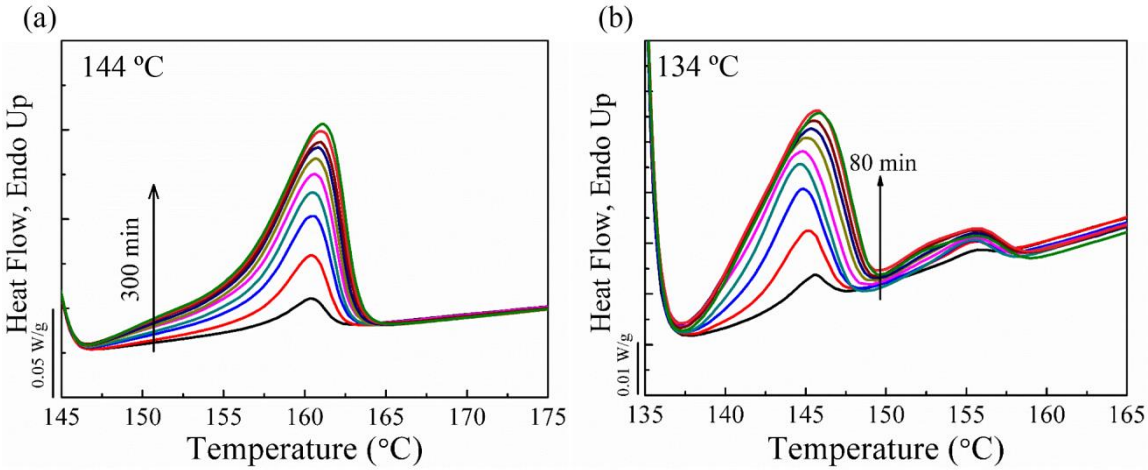

Figure 4.9 Melting of PP/PS/NA11-2 (a) and PP/PS/QQ-2 (b) blends after isothermal step stepwise crystallization at 144 ºC (NA11) and 134 ºC (QQ) for different times.

In order to verify the comply to a first order kinetics for heterogeneously nucleated droplets, the data obtained from the isothermal step crystallization was further analyzed by the Avrami equation:

$$1 - V_c(t) = exp(-k(t-t_0)^n) \tag{4.4}$$

where, t_0 the induction time, n the Avrami index, and k the overall crystallization rate constant (i.e., containing contributions from both nucleation and growth), and V_c is the relative transformed volume fraction, calculated from the enthalpy-based weight fraction of crystals, w_c, according to:

$$V_c = \frac{w_c}{w_c + \frac{\rho_c}{\rho_a}(1-w_c)} \tag{4.5}$$

where ρ_c and ρ_a are the densities of the crystalline and amorphous fraction, respectively.

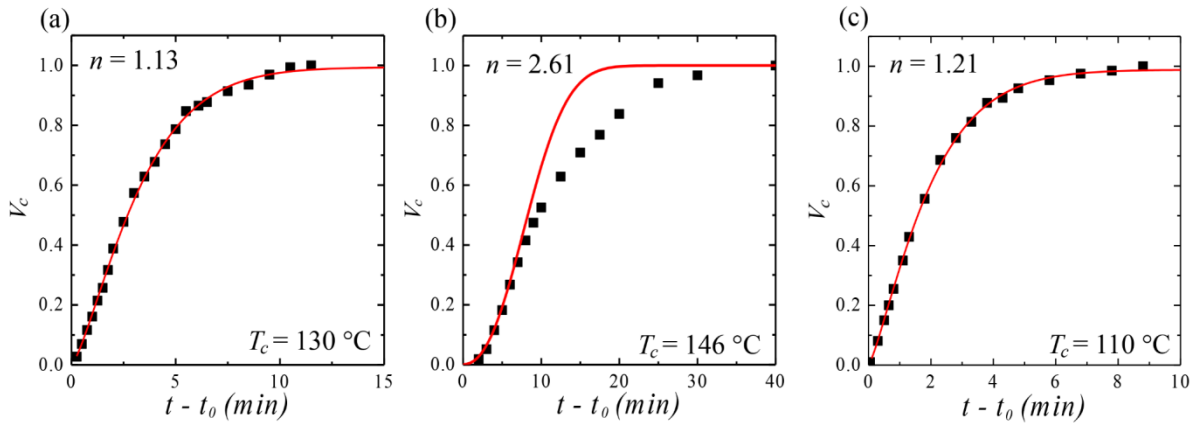

Figure 4.10 Evolution of the crystalline volume fraction as a function of effective overall crystallization time for: (a) PP/PS/NA11-0.25; (b) self-nucleated i-PP droplets from T_s 160 °C (Domain II); (c) self-nucleated i-PP droplets from T_s 210 °C (Domain I).

Even though not so many data are available for the early stages of crystallization (i.e., for conversions between 3 and 20 %), the analysis of the data was performed according to the suggestions provided by Lorenzo et al.[249] Examples of the fittings for heterogeneously nucleated droplets and for droplets self-nucleated from different T_s are shown in Figure 4.10.

For heterogeneously nucleated droplets (with the nucleating agent NA-11), the Avrami index is close to 1.0, reflecting a first order kinetics, consistently with nucleation being the rate-determining step for the overall crystallization. We note that this exponent is obtained in spite of the fact that the most effective NA, from all those tested in this work, was employed. This means that NA-11 is not as efficient as PP self-nuclei produced at the ideal self-nucleation temperature, as expected on the basis of the respective differences in T_c values during cooling from $T_{s,ideal}$ or from a melt containing NA-11.

On the other hand, ideally self-nucleated i-PP droplets in Figure 4.10(b), show an Avrami exponent close to 3, indicating a situation closer to the one in bulk i-PP sample, where predetermined nuclei grow as 3-D spherulites (even when droplets are only 1 μm in size). Self-nuclei are in fact present in every droplet (when the SN is performed at a T_s = 160 °C) and are so efficient that all the nucleation step occurs instantaneously during SN, hence the overall crystallization is dominated by the rate-determining growth rate. However, with increasing T_s from 160 °C to 210 °C in Figure 4.10 (c), all the memory effect is erased (*Domain I*) and the droplets no longer contain self-seeds. As such, primary nucleation becomes again the rate-limiting step of crystallization, and the Avrami index correspondingly changes from 3 to 1.

Figure 4.11 reports the fitted Avrami index for all the prepared blends and crystallization conditions, in order to validate the above describe trends. Remarkably, it is clearly seen that both the droplets containing the different nucleating agents and those of the neat blend cooled

from *Domain I*, crystallize with a first order kinetics. Despite that, in both cases, nucleation controls the overall kinetics, a large difference in the explorable range of supercoolings exist, due to difference in the nucleating efficiency of heterogeneous nucleants (T_c =125-145 °C) and pre-existing impurities/PS surfaces (T_c =100-115 °C).

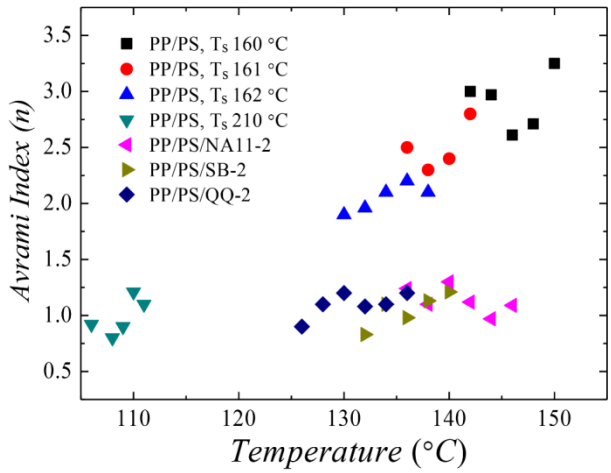

Figure 4.11 Avrami indexes for pure PP/PS blend with different self-nucleation temperatures (T_s), and for PP/PS/NAs blends as function of crystallization temperature (T_c).

Crystallization of self-nucleated droplets show instead a sigmoidal kinetics with *n* between 2 and 3, compatible with predetermined nucleation and two- or three-dimensional crystal growth. With decreasing T_s, both the achievable crystallization temperature range and the Avrami index increase. The lower exponent for partially self-nucleated samples might indicate a certain contribution of primary nucleation to the overall crystallization energy barrier, as previously discussed (Figure 4.8 and Table 4.3).

It is noted that, while first-order crystallization kinetics has been already reported by Dalnoki-Veress for droplets heterogeneously nucleated on the surface of amorphous or semicrystalline substrates,[50, 250] this is to our knowledge the first example showing the expected trend in the case of droplets containing nucleating particles. Similarly, the change from sigmoidal to first-order kinetics in droplets self-nucleated in *Domain II/Domain I* is also evidenced for the first time.

It should be stressed that first order kinetics can be obtained for both homogeneously and heterogeneously[50] nucleated droplets, as the origin of the change in kinetics (from sigmoidal to first order) is the switch to nucleation control in the overall crystallization kinetics.

To further test the different role of the nucleation and growth stages in the two cases, a dimensionless number can be considered. This number is the ratio between the time required

for a crystal growing in a droplet of volume V to completely solidify the micro-domain, i.e., the "growth time" ($V^{1/3}/G$), and the time for nucleation to occur in the same droplet ($1/(IV)$). For this calculation, we consider the volume average droplet diameter and assume that the crystallization of i-PP droplets occurs by a mononuclear mechanism, i.e., one nucleus per droplet. The value of nucleation rate I is taken by fitting the isothermal crystallization data with Equation 4.3, while for the self-nucleated system, the half-crystallization time is considered (assuming it equal to the nucleation time, for testing the hypothesis of solidification controlled by nucleation also in this case).

The data obtained for the different systems and at various crystallization temperatures are shown in Figure 4.12. For i-PP droplets containing nucleating agents, as well as for the neat blend where i-PP nucleates on impurities or at PS interfaces, the ratio is much lower than 1. In particular, the time for a nucleation event to occur in a droplet is 10 - 100 times larger than the time it would take to grow a micro-spherulitic crystal inside the same domain. This confirms that in these cases the nucleation is the rate-determining step in the overall crystallization kinetics. The same is not true, instead, for droplets self-nucleated at T_s = 160 °C, where the ratio is always very close to unity, suggesting that the droplets are basically nucleated instantaneously, and that the solidification rate is controlled by the time required to grow the i-PP micro-spherulitic crystals inside the microdomains.

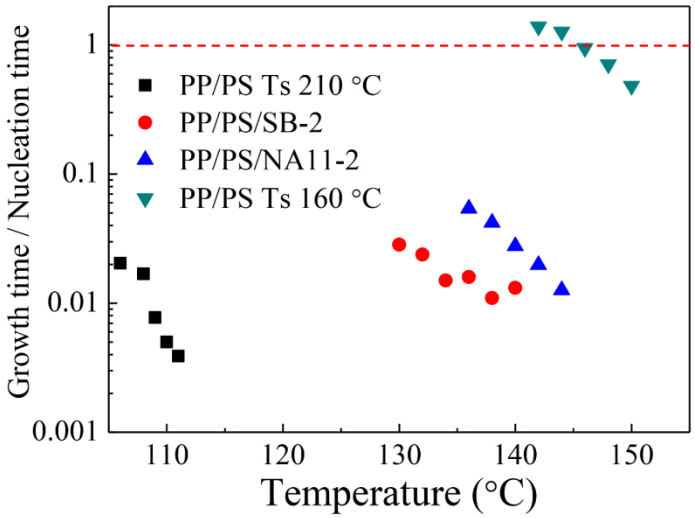

Figure 4.12 Comparison between growth time and nucleation times at different temperatures for i-PP droplets in the indicated systems.

These important results suggest that self-nucleated melts present a negligible primary nucleation barrier, differently from what is foreseen by recent theoretical framework for the interpretation of melt-memory effects in polymer crystallization.[228] The data are consistent with the retention of chain clusters in the self-nucleated melt, possessing the supercritical size

at the chosen crystallization temperature, and thus being able to spontaneously (and immediately) grow. Our findings show that this behavior, already reported for self-nucleation experiments in bulk polymers,[240] can still hold for dispersed and isolated micro-domains with average size of one micrometer.

On the other hand, crystallization of the i-PP droplets with NAs is dominated by nucleation, as nucleation is the rate-determining step (and approximately first order kinetics are observed in all the samples with NAs). Therefore, when we plot $\ln(1-X/X_{max})$ versus time using isothermal step crystallization data, a line with slope $-Iv$ is found. For the sake of simplicity, given the small difference between volume and weight-based transformed fraction, the raw melting enthalpies have been used to calculate X/X_{max} in the following data analysis. Some examples are shown in Figure 4.13, for NA-11 and QQ nucleating agents crystallized at various temperatures. For PP/PS/QQ-2 blend, only the melting enthalpy of the first peak, attributed to the β-form, is considered. An obvious decrease of the nucleation rate (we have neglected any contribution of growth rate, given the results presented in Figure 4.13 and their analysis) with increasing temperature can be observed.

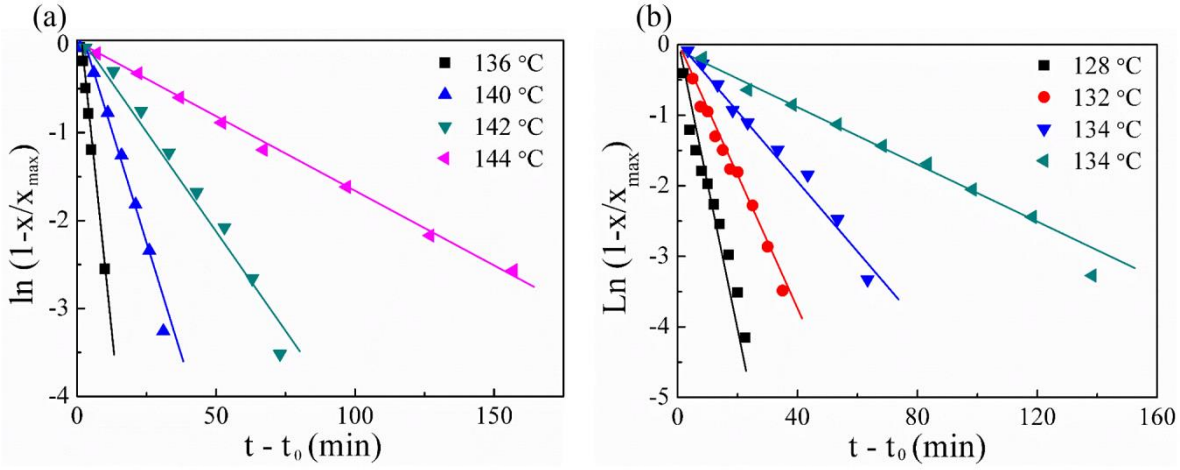

Figure 4.13 Nucleation kinetics at different temperatures for PP/PS/NA11-2 (a) and PP/PS/QQ-2(b) blends. Induction times are subtracted for the sake of clarity.

According to the heterogeneous nucleation theory, the nucleation rate I of i-PP on different substrates can be expressed by:

$$Log\ I = Log\ I_0 - \frac{U^*}{2.303R(T_c - T_\infty)} - \frac{16\sigma\sigma_e\Delta\sigma T_m^{0\,2}}{2.303kT_c(\Delta T\Delta h_f f)^2} \qquad (4.6)$$

where I_0 is a constant independent of temperature, T_m^0 is the equilibrium melting temperature of i-PP, Δh_f is the enthalpy of fusion per unit volume of bulk crystal at T_m^0, σ and σ_e are the lateral and fold surface free energies of the crystals, respectively. The parameter $\Delta\sigma$ is

denoted as the interfacial free energy difference, which accounts for the substitution of a substrate/melt interface with a crystal/substrate and a crystal/melt interface with the formation of the nucleus. The interfacial free energy difference, $\Delta\sigma$, has been commonly used to characterize and evaluate the nucleating ability of different substrates toward a given polymer. The lower the value of $\Delta\sigma$, the higher the nucleating ability of the corresponding surface will be. As stated above, $\Delta\sigma$ is defined as $\sigma_{sc} + \sigma_{cm} - \sigma_{sm}$, where σ_{sc} is the substrate-crystal interfacial free energy, σ_{cm} is the side surface free energy of the i-PP crystal, and σ_{sm} is the substrate-melt surface free energy.

For the application of Equation 4.6 to our data, values of Δh_f and $\sigma\sigma_e$ for α-form i-PP crystal were taken from the literature as 208 J cm^{-3} and 732 erg^2 cm^{-4},[241] while the other parameters are mentioned earlier in the text. For evaluating the data of PP/PS/QQ-2 blend, the used values of T_m^0, Δh_f and $\sigma\sigma_e$ for β-form i-PP are 443 K, 194.9 J cm^{-3}, 520 erg^2 cm^{-4}, respectively.[251-253]

Figure 4.14 reports the values of the nucleation rate of i-PP droplets in the various neat and nucleated blends. From the slope of the fitting lines, according to the heterogeneous nucleation theory, (Equation 4.6) the interfacial free energy difference, $\Delta\sigma$, can be derived. The values of $\Delta\sigma$ for the different nucleating agents are calculated and shown in Table 4. The peak at around 100 ºC (see Figure 4.3) during the fractioned crystallization of neat PP/PS blend is attributed to the presence of some impurities. For the sake of comparison with other NAs, we consider these impurities as a less efficient α-form nucleating agent, and the corresponding $\Delta\sigma$ is also obtained from isothermal kinetics data of neat blend crystallization.

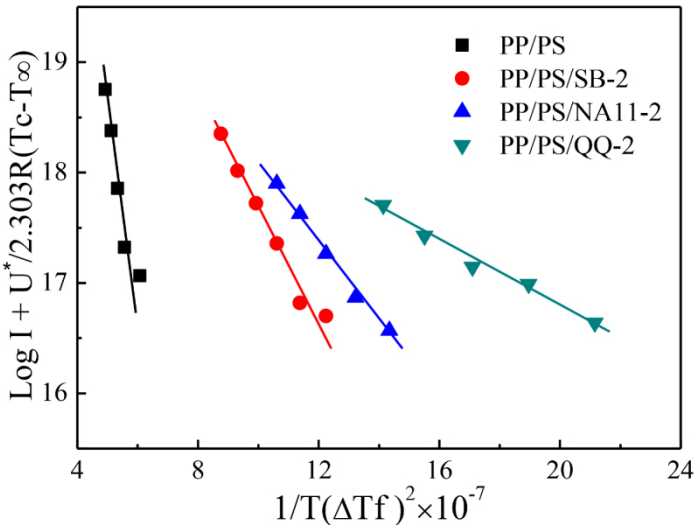

Figure 4.14 Temperature dependence of nucleation rate of i-PP droplets in different blends (neat or containing NAs) according to Equation 4.6.

It can be seen from Table 4.4 that $\Delta\sigma$ increases in the order: PP/PS/NA11-2 < PP/PS/SB-2

< PP/PS (Impurities), which corresponds to an analogous decrease in the nucleation efficiency of the different surfaces. Obviously, the PP/PS/QQ-2 blend cannot be directly compared with the other α-nucleating agents, since quinacridone quinone promotes the formation of β-form crystals.

Table 4.4 Values of T_c, $\Delta\sigma$ and NE determined from nucleation study for i-PP on different substrates.

Type of substrate	T_c (ºC)	NE (Eq. 3.1, %)	$\Delta\sigma$ (erg/cm^2)	ΔG^* (kJ/mol)	$NE^{\Delta G}$ ($\Delta G^*/\Delta G_0^*$)
Self-nuclei	134	100	-	40.9	1.00
NA-11	125	85	4.22	66.2	1.62
SB	121	79	5.72	87.1	2.13
QQ (β crystal)	117	-	1.96	57.2	1.39
Impurities	98	43	11.18	184.5	4.51
Homogeneous nucleation	40	-	-	378.4	9.25

In order to verify that the obtained nucleating efficiency scale is independent from the nucleating agent concentration, the temperature dependence of nucleation rate for PP/PS/NA11-2 and PP/PS/NA11-0.25 blends is compared in Figure 4.15. The higher nucleation rates for PP/PS/NA11-2 blend can be explained by a higher number of heterogeneous nuclei per droplet. However, the interfacial free energy difference, $\Delta\sigma$, derived from the slope of the lines in the plot, on the basis of the heterogeneous nucleation theory, does not change for the two systems. In fact, $\Delta\sigma$ is an intrinsic property of the substrate, independent of nucleating agent concentration.

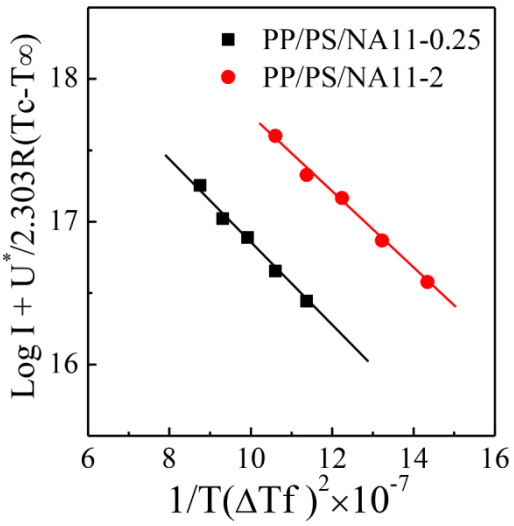

Figure 4.15 Nucleation rate as a function of temperature for PP/PS/NA11-2 and PP/PS/NA11-0.25 blends according to heterogeneous nucleation theory (Equation 4.6).

It is of interest to compare the derived value of interfacial free energy difference with analogous data reported in the literature. The nucleation efficiency of various fibers towards i-PP has been evaluated by using Equation 4.5 by Wang et al.[59] The values ranged from 17 erg cm^{-2} for syndiotactic polystyrene fibers, to about 5 erg cm^{-2} for the highly nucleating poly(tetrafluoroethylene) (PTFE) ones. Thus, the values of $\Delta\sigma$ for SB and NA-11 are comparable or slightly lower to the one of PTFE fiber, the best nucleating fiber. This result is in line with the expectations since both nucleating agents promote epitaxial nucleation with i-PP α-phase.[94, 200] Different values of interfacial free energy differences have been found for the same NAs in previous literature works, including a recent publication by our group.[93, 254] However, the discrepancies are justified by the use of different methods or nucleation models. This notwithstanding, the ratio of the free energy barriers of the two nucleating agents that can be derived from the present work and previous literature is within 15 %.

The particularly low value of $\Delta\sigma$ found for the QQ nucleating agent should not be surprising. In fact, considering that the two modifications grow at very similar rates,[251] and that the β-phase always crystallizes at lower supercoolings with respect to the α-form, a much larger β-phase heterogeneous nucleation rate compared to α-phase nucleation rate on common impurities is required for the trigonal β-modification to prevail, on a volume basis, in the final sample.

The obtained $\Delta\sigma$ data for the different substrates can be conveniently used to define a nucleation efficiency scale. An empirical efficiency scale for classifying the nucleating agents was proposed by Fillon et al. (Equation 4.1),[95, 96] by comparing the increase of non-isothermal crystallization temperature of a nucleated sample with respect to that obtained by self-nucleating the same material at the optimal T_s. This methodology can also be applied to our blended samples. Accordingly, the crystallization temperatures for blends containing NAs (T_{NA}) is obtained from the standard non-isothermal cooling procedure while the maximum crystallization temperature, T_{max}, which is around 134 ºC, is obtained for self-nucleated droplet crystallizing from the ideal self-nucleation temperature (160 ºC). Eventually, the standard non-isothermal crystallization temperature of neat droplets at 70 ºC is taken as T_0. The values of nucleation efficiency according to Equation 4.1 are reported in Table 4.4 for our samples.

Alternatively, the average nucleation barrier in the crystallization temperature range 130 - 142 ºC for blends containing NAs can be calculated on the basis of the obtained interfacial free energy difference, $\Delta\sigma$. However, as previously discussed, for an ideally self-nucleated

system, self-nuclei seem to be already present in the droplets at the beginning of the crystallization process, i.e., a barrierless primary nucleation occurs, and the overall crystallization process kinetics is controlled by crystal growth only. Thus, being the growth step unavoidable, for a meaningful comparison the nucleation barrier for secondary nucleation, as derived from the obtained K_g values, should be considered. Therefore, in Table 4.4 the energy barriers for heterogeneous nucleation on the various substrates and for self-nucleation (secondary nucleation) are reported as well. For the sake of comparison, the homogeneous nucleation free energy barrier is also calculated, according to: $\Delta G^* = 32\sigma\sigma_e T_m^{0\,2}/(\Delta h_f \Delta T)^2$, and using the aforementioned parameters for the crystalline α-phase. Clearly, the energy barrier for self-nucleation is the lowest, and that for heterogeneous nucleation on different substrates is still much lower than for the homogeneous nucleation case.

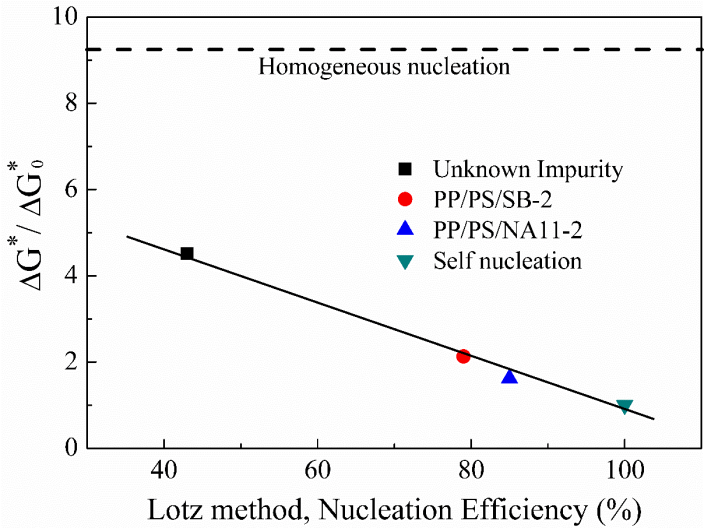

Figure 4.16 Correlation between the ratio of ΔG^* of heterogeneous nucleation on different substrates to that of secondary nucleation (ΔG_0^*) and Lotz's empirical nucleation efficiency scale.

Eventually, on the basis of the nucleation barriers for the different nucleated blends, an "absolute" or "intrinsic" nucleation efficiency scale can be derived, considering the ratio of ΔG^* between the given nucleation process and that of secondary nucleation (ΔG_0^*). In Figure 4.16, the ΔG^* ratio is correlated with the empirical NE values derived from Equation 4.1. It can be seen that the two values are in fact intimately related. A decrease in nucleation efficiency from 100 to 40 % corresponds to an increase in the free energy barrier ratio from 1 to above 4.

More interestingly, from interfacial free energy difference derived by isothermal crystallization measurements and related to various nucleants/impurities (Table 4.4), and by taking into account that fractionated crystallization upon immiscible blends with droplet

morphology is commonly interpreted as the result of nucleation-controlled crystallization, we can tentatively explore the relation between a given non-isothermal crystallization temperature and the $\Delta\sigma$ of the substrate which originates the related fractionated crystallization peak.

Therefore, in Figure 4.17, a working line for fractionated crystallization of i-PP droplets in immiscible blends is proposed. The curve is constructed from the data of Table 4.4, considering the $\Delta\sigma$ and crystallization peak temperature on cooling for the various NAs and unknown impurities. In addition, the T_c of the neat PP/PS blend self-nucleated at the optimum temperature can be related to an "apparent" $\Delta\sigma$. In fact, as shown above, in this specific case the crystallization kinetics is only associated with crystal growth (i.e., the nucleation barrier is equal to that of secondary nucleation). However, we can calculate the corresponding $\Delta\sigma$ of a hypothetical "self-nucleus substrate" which would result in the same energy barrier we have measured. Of course, this is just a convenient assumption, to be able to report the self-nucleation data on the same plot as those of the various nucleating surfaces in Figure 4.17.

We can finally see that all the four filled experimental symbols in Figure 4.17, derived from heterogeneous nucleation or self-nucleation data, nicely fall into a single line, with the higher T_c values corresponding to lower values of interfacial free energy difference. Now, the validity of this correlation curve for i-PP fractionated crystallization in the particular PP/PS blends under investigation can be tested.

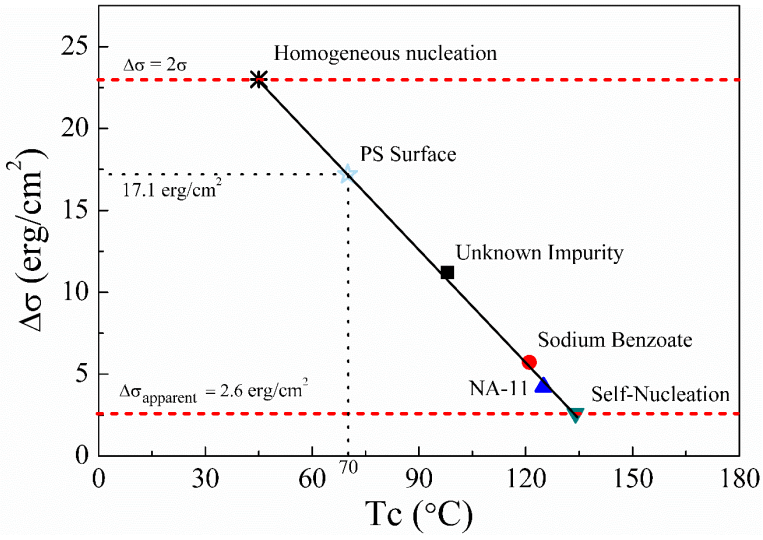

Figure 4.17 A plot of $\Delta\sigma$ versus T_c for various NAs to reveal their nucleating abilities for i-PP crystallization.

At first, we note that the homogenous nucleation temperature range for i-PP droplets can be correctly predicted. In fact, from the theory of heterogeneous nucleation, we know that the nucleation energy barrier on a given substrate becomes equal to that of homogeneous

nucleation in the bulk when the $\Delta\sigma$ equals two times the lateral surface energy of the crystal (2σ).[255] If the working curve of Figure 4.17 is extrapolated to $\Delta\sigma = 2\sigma$, a non-isothermal crystallization temperature of about 45 °C is obtained, perfectly in line with the typical values reported in the literature for homogeneous nucleation of i-PP droplets.[256] We underline that the temperature of crystallization in systems where homogeneous nucleation dominates is related to the droplet volume. Therefore, the curve derived in Figure 4.17 is supposed to be strictly valid for ensembles of i-PP droplets with similar average size and polydispersity as those reported in Table 1.

Eventually, the constructed correlation line can be used to derive the interfacial free energy difference of the impurity or nucleating surface giving rise to a particular fractionated crystallization peak. For example, the fractionated crystallization peak at 70 °C measured for neat PP/PS blend (Figure 4.3) corresponds to a $\Delta\sigma$ of 17.1 erg/cm^2. Interestingly, this value is very close to the one found by Wang et al.[59] for the nucleation i-PP on the surface of syndiotactic polystyrene fibers (16.7 erg/cm^2). On the basis of this similarity, the fractionated crystallization peak at 70 °C in neat PP/PS blend is likely to be caused by the nucleation of the i-PP droplets at the interface with the atactic polystyrene matrix.

4.4 Conclusion

The crystallization kinetics of heterogeneously nucleated i-PP droplets dispersed in PS matrix was quantitatively investigated by DSC. The overall crystallization exhibits a first-order kinetics, as previously observed in the literature for the case of homogeneously nucleating microdomains. It was demonstrated that this is related to a heterogenous nucleation-controlled crystallization, enabling us to assess directly the kinetics of the nucleation process. Different temperature dependences of nucleation rate were found for the various samples, corresponding to variations in the free energy barrier for nucleation, ΔG^*. Considering the ratio of the free energy barrier for heterogeneous nucleation on different substrates with respect to that of secondary nucleation appears to be a reasonable method to derive an “absolute” nucleation efficiency scale, which correlates well with the empirical nucleation efficiency scale derived by Fillon et al..[95, 96] Finally, knowing the interfacial free energy difference for the heterogeneous nucleation of several nucleating agents or substrates in PP/PS immiscible blends with droplet morphology, a working curve which relates this parameter to the non-isothermal crystallization temperature measured for fractionated crystallization of these blends is derived. A linear relation between $\Delta\sigma$ and T_c holds, throughout the explored temperature range and down to the region dominated by

homogeneous nucleation (i.e., for impurity-free droplets).

The proposed approach shows the ability to derive quantitative and important information for the scouting of nucleating agents with improved efficiency, other than the potential to be used to study polymorph-selective substrates for i-PP β-phase.

Chapter 5. Differential Scanning Calorimetry Study of Cross-Nucleation in Isotactic Poly(1-butene)

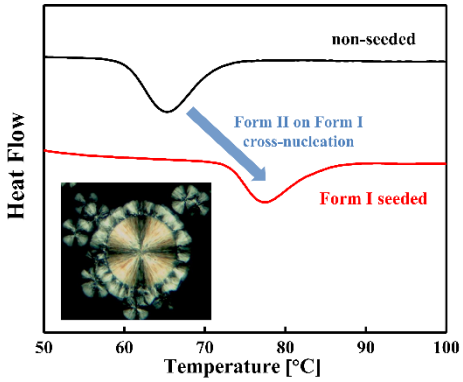

5.1 Introduction

Polymorphism, the ability of a material to crystallize into different crystallographic structures, is a widespread phenomenon both in small[257] and macro-molecular[258, 259] systems. Examples of extremely rich polymorphism can be found for instance in 5-methyl-2-[(2-nitrophenyl)amino]-3-thiophenecarbonitrile (ROY), which displays ten different known structures, and the semi-crystalline polymer poly(vinylidene fluoride) (PVDF), for which five polymorphs have been found.[102, 260] Naturally, polymorphism can lead to much diverse characteristics, thus playing an important role in determining the final performance of products.[257] For example, the same semi-crystalline polymer can be brittle or ductile at room temperature, depending on the prevailing crystalline structure.[261, 262] Thus, being able to understand the mechanism of polymorphic crystallization and control the polymorph formation is of paramount importance.

Much emphasis is put on the nucleation step: for instance, by “seeding” the melt or solution with crystals of the desired polymorphic modification. In polymers, the use of polymorph-selective heterogeneous nucleating agents is effective and an industrially appealing solution to control structure formation. For example, γ-quinacridone red pigment is a very good β-nucleating agent for isotactic polypropylene[263], KBr can help to obtain the γ-modification of Poly(vinylidene fluoride) (PVDF)[264], while hexagonal boron nitride nanosheets (BNNSs) significantly facilitate the formation of α-form crystal of poly(butylene adipate) (PBA).[265]

In view of a more comprehensive understanding of polymorphic nucleation, cross-nucleation[100] i.e., the nucleation of one polymorph on another crystalline substrate of the

same substance but with different structure, is of importance.

It has been found that in order to observe nucleation of a "daughter" phase on the surface of a "parent" polymorph, the first one must always grow faster than the latter, while the relative thermodynamic stability of the two structures is not a determining factor.[101, 266-271] The topic was extensively explored by Yu et al. for small organic molecules such as D-Mannitol and ROY, both in spontaneous and seeded crystallization.[102, 266, 268] A quantitative determination of cross-nucleation kinetics in D-Mannitol/poly(vynilpyrrolidone) mixture, achieved by analysis of the crystallized morphology, indicated that the nucleation rate increases with the undercooling and the content of additive. [266]

More recently, sporadic works on cross-nucleation in semi-crystalline polymers also appeared.[272, 273] Cavallo and Alfonso have shown that much more overlooked examples exist in the polymer crystallization literature.[274-276] Moreover, the systematic extension of the quantitative approach to cross-nucleation to different macromolecules (isotactic poly(1-butene), polypivalolactone and isotactic polypropylene)[107-109, 276, 277], allowed to understand that the nucleation of one polymorph on another can be regarded as a special case of heterogeneous nucleation, unless the parent phase grows at rates comparable to those of the daughter polymorph.[108, 109]

All the wealth of information so far obtained on cross-nucleation has been exclusively gathered by optical microscopy analysis of the developing morphology. On the other hand, typical studies of heterogeneous nucleation process, especially in semi-crystalline polymers, are commonly based on Differential Scanning Calorimetry (DSC). Despite that Polarized Optical Microscopy (POM) has revealed to be an intuitive and informative approach, its quantitative application is limited to systems in which the two polymorphs display distinguishable and optically resolvable morphologies. In particular, the size of the cross-nuclei and distance between them should be adequate to allow their direct observation and counting. Therefore, in this work we explore the possible use of DSC to investigate the effect of cross-nucleation on crystallization. Cross-nucleation of Form II-on-Form I in seeded crystallization of isotactic poly(1-butene) was chosen as a case study. The crystallization kinetics of Form II is accelerated by the presence of Form I seeds, both in non-isothermal and isothermal conditions, to an extent which is dependent on the amount of Form I' crystal surface available. The simple approach can potentially be extended to other polymorphic small organic molecules and semi-crystalline polymers.

5.2 Experimental

5.2.1 Materials and Methods

The polymer used in this work was a commercial Ziegler-Natta isotactic poly(1-butene) (i-PBu), kindly provided by Lyondell-Basell (tradename BR200), with a weight-average molar mass (M_w) of 850 kg/mol and a polydispersity index of 6.8.

To prepare the in-situ seeded samples, i-PBu films of about 150 μm thick were prepared in between two glass slides, by manual compression on a heating stage held at 180 °C. The appropriate thermal protocol for sample preparation (described later on in the text) was imposed by a calibrated Mettler Toledo FP-82 microscope hot-stage. The initial crystallization and final morphology of the samples were checked by means of Polarized optical microscopy using a Polyvar Pol optical microscope under crossed polarizers. Micrographs of the seeded samples before cross-nucleation experiments were acquired by using a computer-controlled digital camera (Motic 2.0).

The actual cross-nucleation experiments were performed by Differential Scanning Calorimetry. A flat disk of approximately 5 mm diameter and weight of about 4 mg was cut from the seeded i-PBu films and placed in an aluminum pan. The calorimetric characterization of isothermal and non-isothermal crystallization of the samples was performed with a Perkin-Elmer DSC 7, under a constant nitrogen flow of 20 ml/min. Temperature and heat flow were calibrated using a standard indium sample.

5.2.2 Sample Preparation and Cross-Nucleation Experiment: Thermal Protocol

In the case of i-PBu polymorphism, it is well known that the metastable tetragonal modification (Form II) is kinetically favored, and the only one obtained upon melt crystallization. Afterwards, upon room temperature aging, it slowly transforms into the thermodynamically stable trigonal Form I.[278, 279]

In order to investigate the effect of Form I polymorph's surface on Form II crystallization, samples of i-PBu containing different concentrations of Form I spherulites of various sizes were prepared. To this aim, a modification of previously developed in-situ seeding strategy[107] for i-PBu was adopted, as briefly sketched in Figure 5.1.

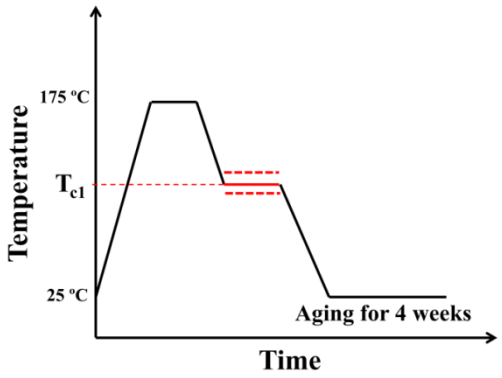

Figure 5.1 Schematic diagram of the thermal history applied for sample preparation.

The film was first heated to 175 °C and annealed for 3 min, to erase crystalline thermal history. Subsequently, the sample was cooled down to selected temperatures, T_{c1}, and allowed to crystallize for a given time. Large Form II spherulites are obtained, with their average concentration and size turned by varying the chosen crystallization temperature and time. After the high temperature crystallization step, the film was quenched to room temperature (by dipping it in a water bath), at which the remaining amorphous material solidified in small Form II crystals. Then, the samples are allowed to transform into Form I by room temperature aging for approximately 4 weeks.

The result of this process is a dual morphology sample, consisting of large Form I spherulites of high-melting point, surrounded by microcrystalline and low-melting point spherulites of the same structure. The DSC melting curve of such sample is shown in Figure 5.2(a). The as prepared sample presents a relatively sharp melting peak around 125 °C and a broad peak at lower temperature, around 118 °C. These peaks correspond to thicker and thinner lamellar crystals of Form I, respectively.

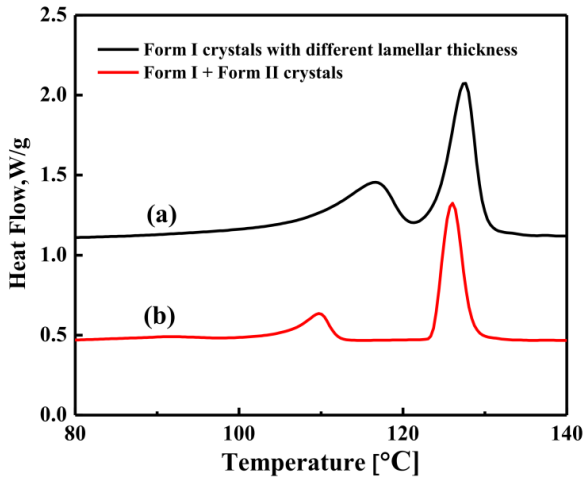

Figure 5.2 DSC heating scans for: (a) as-prepared (4 weeks aged) sample; (b) partially molten and re-crystallized sample before cross-nucleation experiment.

Before the actual cross-nucleation experiment, the as-prepared sample is submitted to a thermal treatment directly in the DSC, in order to erase the thinner Form I crystals from the systems, and thus excluding possible self-nucleation effects. To this aim, the samples were first heated to 122 °C (corresponding to the valley between the two Form I melting peaks) and held there for 3 minutes, before cooling down to room temperature. The molten part of the material recrystallizes into Form II. After this temperature protocol, the difference in melting temperatures between the Form I seed and the rest of the material is enhanced, as demonstrated in Figure 5.2(b). The cross-nucleation experiments are thus performed on this sample, containing Form I seeds and lower-melting point Form II crystals.

To probe the effect of Form I seed on Form II re-crystallization, the above conditioned sample was first annealed to 120 °C for 3 min, to erase any possible memory effect of previous Form II crystals, while leaving intact Form I spherulitic seeds. Subsequently, the crystallization kinetics of seeded i-PBu was probed either in non-isothermal conditions (by cooling at a rate of 10 °C/min to room temperature) or in isothermal experiments at selected temperatures (T_{c2}) for adequate times (see Figure 5.3).

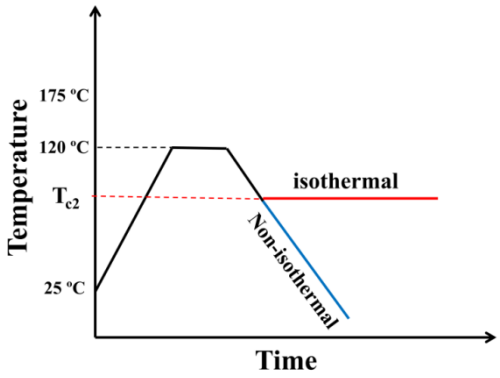

Figure 5.3 Schematic diagram of the thermal history adopted for cross-nucleation experiments with the DSC.

5.3 Results and Discussion

5.3.1 Characteristics of Form I Seeded i-PBu Samples

Some examples of the morphology of Form I-seeded i-PBu samples prepared in different conditions are shown in Figure 5.4. The concentration and size of spherulitic seed can be varied independently by tuning the crystallization temperature T_{c1} (Figure 5.1) and time. Although the spherulites are mostly isolated, a certain degree of impingement can be present. As the subsequent Form II cross-nucleation occurs on the surface of Form I spherulites, it is reasonable to characterize each seeded sample by quantifying the relative amount of available

Form I surface.

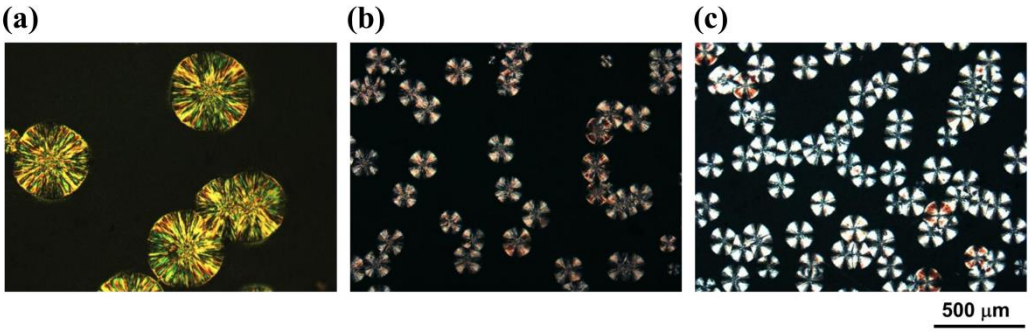

Figure 5.4 Examples of micrographs of Form I-seeded samples partially crystallized under different conditions: (a) T_c = 97 °C, t = 112 min; (b) T_c = 92 °C, t = 10 min; (c) T_c = 88 °C, t = 6 min.

Considering disk-like Form I spherulites, with cross-nucleation of Form II occurring on their lateral surface, the approximate amount of specific seed's surface (i.e., surface of Form I seeds per unit of i-PBu sample volume) is given by:

$$\frac{S_{seed}}{V} = 2\pi \cdot t \cdot R_{avg} \cdot N \tag{5.1}$$

where t represents the sample thickness; R_{avg}, the average spherulite radius; N, the number of spehrulites per unit volume.

The main characteristics of the prepared Form I-seeded samples are reported in Table 5.1. The values of average seed's radius (R_{avg}) and nucleation density (seed's concentration) are derived from the analysis of POM micrographs and refer to at least ten spherulites and 4 different area of the sample. The samples have an average thickness of 150 micrometers, which is optimized for the subsequent DSC measurement, while the approximate S_{seed}/V covers a range of about one order of magnitude. It should be noted that these values can be considered as approximate only for several reasons: i) the assumption of disk-like spherulite is strictly correct only for $R_{avg} >> t/2$; ii) all the lateral surface of the seed is considered available for cross-nucleation, neglecting the fraction of area impinged with neighboring morphologies; iii) the actual cross-nucleation probably occurs only on Form I lamellae, the total area should thus be corrected by the crystallinity of the seeds. Nevertheless, the estimated S_{seed}/V is expected to be a fairly adequate parameter to establish a correlation between seed morphology for a given sample and the cross-nucleation effect.

Table 5.1 Characteristics of Form I seeded i-PBu samples.

Sample code	$T_{c,seed}$ (°C)	$t_{c,seed}$ (min)	Sample thickness (μm)	Nucleation density (spherulites/cm^3)	Average Radius (μm)	S_{seed}/V (m^{-1})
S_{seed}/V_01	97	112	170	6.6E+3	209	1.5E+03
S_{seed}/V_02	97	112	140	1.1E+4	220	2.2E+03
S_{seed}/V_03	98.5	120	140	1.0E+4	337	3.0E+03
S_{seed}/V_04	92	10	175	8.2E+4	86	7.7E+03
S_{seed}/V_05	92	20	175	6.6E+4	129	9.3E+03
S_{seed}/V_06	88	6	160	1.2E+5	78	9.4E+03
S_{seed}/V_07	88	6	160	1.4E+5	86	1.2E+04
S_{seed}/V_08	80	2	150	1.7E+5	81	1.3E+04

5.3.2 Self-Nucleation of Form II and Seeded Form I Crystals

In order to safely exclude possible Form II self-nucleation, that would not allow to distinguish the sole role of Form I seeds surface on i-PBu re-crystallization, preliminary self-nucleation experiments were performed both on as-crystallized Form II and Form I-seeded samples.

To this aim, a standard self-nucleation procedure[223, 224] was followed. The standard crystalline state was created by annealing the sample at 140 °C (or 120 °C for Form I-seeded sample) for 3 min, before cooling to 30 °C at 10 °C/min. At this stage, the sample was heated to a selected self-nucleation temperature (holding time of 5 minutes), and the subsequent crystallization temperature upon cooling at 10 °C /min was recorded.

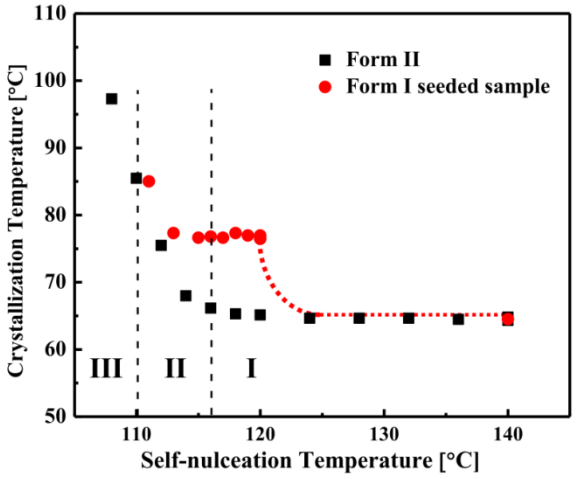

Figure 5.5 Effect of self-nucleation temperature on re-crystallization for i-PBu samples containing exclusively Form II and some amount of Form I seeds. Self-nucleation domains are indicated with dashed vertical lines. The red dashed line describes the expected self-nucleation behavior of Form I seeded samples. [280]

The effect of self-nucleation temperature on crystallization temperature for both Form II and Form I-seeded samples is shown in Figure 5.5. The limits of the self-nucleation

domains[223, 224], corresponding to the absence of memory effects (I), exclusive self-nucleation (II) and self-nucleation and annealing of surviving crystals (III) are indicated with dashed vertical lines.

Standard Form II i-PBu samples exhibit no self-nucleation effects for melt-temperatures above about 117 °C. In the same domain I, the sample containing Form I seeds crystallizes about 10 °C higher than as-crystallized Form II i-PBu. Thus, this larger nucleation effect (i.e., Tc values upon cooling from the melt are proportional to the active heterogeneity density in the material) can be attributed almost exclusively to the nucleating ability of Form I surfaces, since no crystalline memory effect of Form II crystal is found in this temperature range. The self-nucleation domain II related to the original Form II crystals begins at slightly lower temperatures for Form I-seeded i-PBu, with respect to as-crystallized Form II. This is due to the overwhelming effect of cross-nucleation on self-nucleation: the memory effect starts to be noticeable only at self-nucleation temperature low-enough to produce a number of nuclei comparable to those provided by the Form I seed's surfaces. The constancy of crystallization temperature with melt-annealing temperature above ca. 114 °C in Form I seeded i-PBu thus indicate that we can neglect any self-nucleation contribution to the measured crystallization enhancement with respect to non-seeded samples in that temperature range. The chosen melt temperature of 120 °C is therefore appropriate also for i-PBu with low Form I S_{seed}/V, being located in domain I also for the as-crystallized Form II samples.

We note that if Form I seeded samples are heated above the seed's melting point, the standard Form II crystallization kinetics is restored. This has been verified by non-isothermal crystallization from a melt-temperature of 140 °C (see Figure 5.6). The exact temperature of disappearance of seed's nucleation effect has not been tested. However, on the basis of previous work on Form I self-nucleation,[280] it is expected to be around 125 °C, as suggested by the dashed red line of Figure 5.5.

5.3.3 Non-isothermal Crystallization of i-PBu with Seeded Form I Crystal

Selected examples of non-isothermal crystallization curves of i-PBu with different Form I S_{seed}/V are reported in Figure 5.6(a) and compared with that of a non-seeded sample.

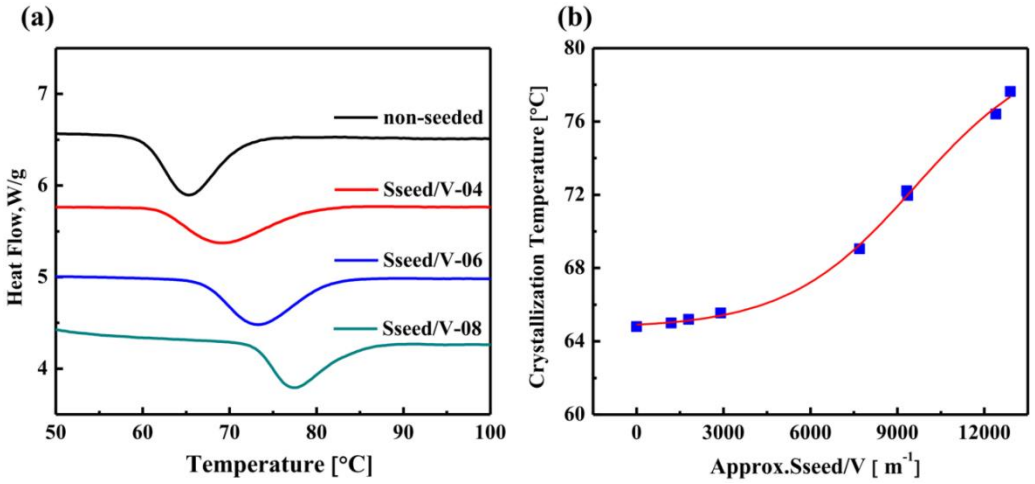

Figure 5.6 (a) DSC cooling scans for i-PBu with different seed's surface per unit volume, for sample code see Table 5.1; (b) peak crystallization temperature as a function of the approximate S_{seed}/V. The line is drawn to guide the eyes.

A distinct change in the crystallization behavior as detected with DSC is noticed with the increase of the amount of specific Form I surface, i.e., going from sample *S_{seed}/V-04* to *S_{seed}/V-08* (see Table 5.1). A broadening of the exothermic peak, with respect to the relatively sharp non-seeded i-PBu is observed. In particular, a high crystallization-temperature tail is evident in the Form I seeded samples, together with an overall shift of the peak towards lower undercooling.

The peak crystallization temperature measured for all the seeded sample is shown as a function of the approximate specific seed's surface area in Figure 5.6(b). With the increase of Form I surface per unit volume, the crystallization temperature stays roughly constant, until about S_{seed}/V = 6000 m^{-1}, and then increases steadily. A maximum increase of peak temperature of more than 10 °C, with respect to non-seeded sample, is revealed for i-PBu with S_{seed}/V slightly above 10000 m^{-1}. No apparent saturation of the crystallization temperature value is detected in the explored range of seed's area, suggesting that a larger nucleating effect could be attained by injecting in the system a higher amount of Form I crystals' surface per unit volume.

The almost negligible nucleation at low S_{seed}/V values can be understood by considering that two distinct types of nucleation contribute to the overall crystallization kinetics of Form II in the seeded system. In fact, Form II crystals can grow both from nuclei developed by heterogeneous nucleation on the surface of foreign materials in the bulk of the sample, and by cross-nuclei originated by the purposely added Form I spherulitic seeds. As long as the concentration of cross-nuclei is lower than that of naturally occurring heterogeneous Form II nuclei, the effect of the extra seed surface on crystallization cannot be noticed. When more and more specific Form I area is present, the cross-nucleation process effectively dominates

the crystallization, and the nuclei formed via heterogeneous nucleation on other surfaces become negligible. A similar situation is encountered in other cases in which two or more nucleation mechanisms are active: for instance, the presence of nucleating agents hides the effect of flow-induced nucleation[280], and the weak nucleation induced by pressure pulses is masked by quiescent heterogeneous nucleation at low undercoolings.[281]

By comparison of the results in Figure 5.6(b) and the self-nucleation tests of Form II (Figure 5.5), is it possible to estimate the nucleation efficiency of Form I spherulites towards Form II. According to Lotz et al.[95], a convenient nucleating efficiency scale can be built by conventionally attributing 0 and 100 % efficiencies to the neat polymer and to ideally self-nucleated sample (i.e., that nucleated at the lowest temperature within domain II, a condition that yields the maximum generation of self-nuclei), respectively.

Considering the maximum crystallization temperature obtained with the highest content of Form I seed specific area, a nucleation efficiency of 60 % can be calculated. We note that this nucleation efficiency is rather high, comparable to that of most polymer nucleating agents,[34] but is not outstanding. While a very efficient nucleation could be in principle expected, given the identical chemistry of the nucleating and crystallizing substrates, we note that the "degree of dispersion" of the in-situ produced Form I seeds is by far not optimal. In fact, all the common nucleating additives generally exhibit sub-micrometer particle size. It should be noted that when high degree of dispersion is achieved, such as in specially prepared nanocomposites, the nucleation efficiency can even exceed 100 %, a condition termed super-nucleation.[34] As such, while at this stage it is not possible to derive an "intrinsic" nucleation efficiency of i-PBu Form I towards Form II, a fairly good nucleation capability is demonstrated and the important role of dispersion underlined.

5.3.4 Isothermal Crystallization of i-PBu with Seeded Form I Crystal

The crystallization of Form I seeded i-PBu was additionally probed in isothermal conditions. Figure 5.7(a) presents typical crystallization isotherms of samples with varying amounts of seed surface, as well as non-seeded, at 140 °C. A clear acceleration in the crystallization rate is observed as the specific content of Form I crystals area in the sample is increased, with peak crystallization time decreasing from values of around 6 minutes for neat i-PBu to less than 2 minutes when S_{seed}/V exceeds 10000 m^{-1}.

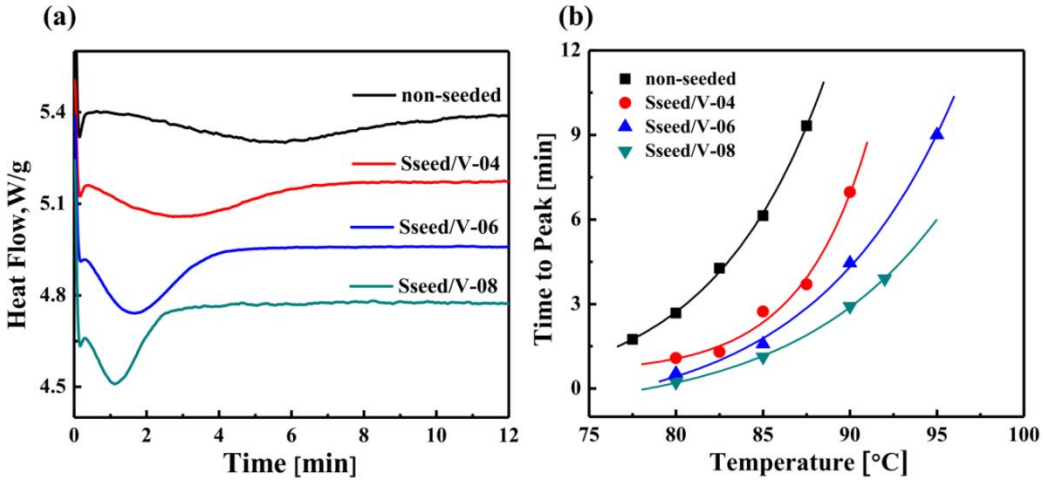

Figure 5.7 (a) DSC crystallization exotherms recorded during isothermal crystallization at 85 °C of i-PBu with varying content of seed surface; (b) peak crystallization times as a function of temperature for different seeded i-PBu samples.

The characteristic crystallization peak times obtained for i-PBu with varying S_{seed}/V crystallized at different temperatures is shown in Figure 5.7(b). Form I seeds allow Form II to crystallize with a faster rate at lower undercoolings. Noticeably, the effect of cross-nucleation is more evident at the highest crystallization temperatures, where the nucleation on foreign heterogeneities is more difficult.

The kinetics parameters of the cross-nucleation process cannot be straightforwardly derived from the isothermal crystallization DSC curves, as those shown in Figure 5.7(a). In fact, as previously mentioned, two concomitant nucleation processes are active during the crystallization. While the nucleation on bulk heterogeneities may be typically predetermined, i.e., it can be considered that the concentration of heterogeneous nuclei is constant at a given temperature within a certain time interval, cross-nucleation on form I spherulites is "pseudo-homogeneous", with the surface density of Form II nuclei linearly increasing with time.[107-109] Moreover, the amount of seeds surface available for cross-nucleation is similarly time-dependent, being progressively occupied by Form II morphologies growing on the substrate or impinging from neighboring seeds. Therefore, the application of a simple crystallization model, such as Avrami, is meaningless. More complex kinetic equations, accounting at least for the parallel action of the dual nucleation mechanism, could in principle be derived, but their test on these DSC cross-nucleation data is out of the scope of the manuscript.

5.4 Conclusions

In order to advance the quantitative understanding of the cross-nucleation phenomenon, in this work we propose a Differential Scanning Calorimetry investigation method. The

approach is applied to the seeded cross-nucleation of i-PBu Form II-on-Form I. A clear enhancement of Form II crystallization kinetics, with respect to non-seeded samples, is detected. The method is validated by measuring samples with Form I spherulites of various sizes and concentration. A strict correlation between the polymorphic seed morphology and the subsequent crystallization behavior is established. The crystallization of Form II becomes progressively controlled by the presence of Form I seeds, rather than by accidentally present foreign surfaces, as the specific amount of Form I area in the sample is increased.

In future works, the proposed method can be tested in other cross-nucleating systems, particularly in conditions where the crystallizing daughter phase morphologies are below the optical resolution.

Chapter 6. Conclusions and Outlook

The aim of this research thesis was to improve the understanding of heterogeneous nucleation in semicrystalline polymers and contribute with new experiments and approaches to the scientific problems related to the evaluation of the nucleating ability of solid substrate, also of importance for industrial application. In particular, the thesis addressed the nucleation behavior of some important polymers (i.e., poly(lactide), isotactic polypropylene) on various commonly used substrates (fibers and nucleating agents). Moreover, a special nucleation phenomenon, known as cross-nucleation, between different polymorphs in isotactic poly(1-butene) was also studied.

The main outcomes of these works and potential outlook can be summarized as follows:

In Chapter 3, the nucleation process of biodegradable poly(lactide) on a series of fibers was studied by means of in-situ polarized optical microscope during crystallization. Several synthetic and natural fibers (PET, carbon, Kevlar, glass, hemp, linen and cellulose) were employed, and compared to custom-spun fiber of stereocomplex enantiomeric PLA blend. Meaningful differences in the nucleating ability towards PLA could be found for all the considered fibers. Stereocomplex PLA fibers display extremely high nucleating efficiency, with the development of a continuous transcrystalline morphology on their surface, up to high crystallization temperatures. Quantitative measurement of the nucleation rate allowed a comparison of the different fiber substrates in the light of classical heterogeneous nucleation theory, by considering the interfacial free energy difference parameter, $\Delta\sigma$, directly related to the nucleation barrier. The topography of the fibers surface was investigated by atomic force microscopy (AFM), and tentatively related to the measured nucleation ability. While a general effect of surface roughness on lowering the heterogeneous nucleation energy barrier can be deduced, deviations can be observed, in particular for carbon and stereocomplex PLA fibers. The different fiber wettability by PLA melt suggests that chemical interactions between the substrate and the crystallizing polymer also play a meaningful role in promoting the nucleation, although this aspect is generally disregarded in the literature - in favor of surface roughness. Moreover, the specific surface topography is shown to largely affect the density of available nucleation sites along the fiber. However, the interplay between surface roughness and chemical interaction between the matrix and fiber in promoting nucleation is quite complex and not easy to be resolved. Therefore, further experiments with chemically or topographically modified model surfaces should be carried out for a better understanding.

In Chapter 4, we have studied nucleating agents (NAs), which are common polymer additives widely used for speeding up processing and tuning the final mechanical properties. Despite their industrial importance, the scouting of different substances in search of highly efficient NAs is still mainly empirical. When semi-crystalline polymers are confined into isolated micro- or nano-domains, nucleation often turns out to be the rate-determining step for the overall crystallization. A novel approach was proposed, according to which, the heterogeneous nucleation process of isotactic polypropylene (i-PP) droplets containing nucleating agents (i.e., sodium benzoate, NA11, quinacridone quinone) dispersed in an immiscible polystyrene matrix has been investigated by isothermal step crystallization and melting with Differential Scanning Calorimetry (DSC). Moreover, self-nucleation of neat i-PP droplets is also studied in detail, enabling to derive an "intrinsic" nucleation efficiency scale based on the ratio of the free energy barrier, ΔG^*, of heterogeneous nucleation on different substrates with respect to that of self-nucleation, which is found equivalent to the secondary nucleation barrier for crystal growth. Such ratio correlates well with the empirical efficiency scale of heterogeneous NAs proposed by Lotz et al. Moreover, having established the interfacial free energy difference parameter ($\Delta\sigma$) governing the heterogeneous nucleation kinetics of i-PP onto different substrates, a simple correlation curve useful to describe non-isothermal fractionated crystallization of i-PP/PS blends with droplet morphology was constructed. It is found that, being fractionated crystallization typically nucleation-controlled, a close correlation between the measured crystallization temperature and $\Delta\sigma$ exist, and it can be conveniently exploited to attribute a particular crystallization peak of immiscible i-PP blends to a heterogeneous nucleating impurity or surface with a given efficiency, or to homogeneous nucleation occurring in the bulk of the phase. The proposed approach in this chapter shows the ability to derive quantitative and important information for the scouting of nucleating agents with improved efficiency, meanwhile, it can be extended to different nucleating systems in the future, for example for searching polymorph-selective nucleants for i-PP β-phase.

In the last Chapter, cross-nucleation of a "daughter" polymorph on another pre-existing ("parent") structure of the same substance was investigated. Polarized Optical Microscopy is commonly used to study both the morphology and the kinetics aspects of cross-nucleation in polymers and small molecules. However, we propose a Differential Scanning Calorimetry (DSC) approach for the quantitative investigation of isotactic poly(1-butene) Form II-on-Form I nucleation. Seeds of trigonal Form I crystal were produced in PB1 samples, and their amount and characteristic size were varied by appropriate choice of the thermal protocol.

DSC isothermal and non-isothermal crystallization measurements of Form I seeded samples were performed, highlighting a meaningful nucleation effect of the stable polymorph on Form II. As expected, the nucleating efficiency is highly dependent on the specific content of Form I seeds (i.e., area of Form I spherulites per unit of sample volume). Depending on the seeding and crystallization conditions, Form II crystallization is dominated either by nucleation on foreign heterogeneous surfaces or on Form I crystals. The described quantitative approach can be extended to the study of cross-nucleation in polymorphic systems in which morphological evidences are not sufficiently informative.

References

[1] R.H. Doremus, Growth and perfection of crystals: proceedings, Wiley1958.
[2] H. Yamakawa, Modern theory of polymer solutions, Harper & Row1971.
[3] P. Till Jr, The growth of single crystals of linear polyethylene, Journal of Polymer Science 24(106) (1957) 301-306.
[4] E. Fischer, Stufen-und spiralförmiges Kristallwachstum bei Hochpolymeren, Zeitschrift für Naturforschung A 12(9) (1957) 753-754.
[5] A. Keller, A. O'connor, Large periods in polyethylene: The origin of low-angle X-ray scattering, Nature 180(4597) (1957) 1289.
[6] D. Bassett, F. Frank, A. Keller, Evidence for distinct sectors in polymer single crystals, Nature 184(4689) (1959) 810-811.
[7] J.D. Hoffman, J. Lauritzen, Crystallization of bulk polymers with chain folding-Theory of growth of lamellar spherulites, Journal of Research of the National Bureau of Standards (4) (1961) 297-+.
[8] J.D. Hoffman, G.T. Davis, J.I. Lauritzen, The rate of crystallization of linear polymers with chain folding, Treatise on solid state chemistry, Springer1976, pp. 497-614.
[9] J. Hoffman, Theoretical aspects of polymer crystallization with chain folds: bulk polymers, Polymer Engineering & Science 4(4) (1964) 315-362.
[10] J.D. Hoffman, R.L. Miller, Kinetic of crystallization from the melt and chain folding in polyethylene fractions revisited: theory and experiment, Polymer 38(13) (1997) 3151-3212.
[11] D. Sadler, G. Gilmer, A model for chain folding in polymer crystals: rough growth faces are consistent with the observed growth rates, Polymer 25(10) (1984) 1446-1452.
[12] D.M. Sadler, Roughness of growth faces of polymer crystals: Evidence from morphology and implications for growth mechanisms and types of folding, Polymer 24(11) (1983) 1401-1409.
[13] M. Hikosaka, K. Tsukijima, S. Rastogi, A. Keller, Equilibrium triple point pressure and pressure-temperature phase diagram of polyethylene, Polymer 33(12) (1992) 2502-2507.
[14] M. Hikosaka, Unified theory of nucleation of folded-chain crystals and extended-chain crystals of linear-chain polymers, Polymer 28(8) (1987) 1257-1264.
[15] M. Hikosaka, Unified theory of nucleation of folded-chain crystals (FCCs) and extended-chain crystals (ECCs) of linear-chain polymers: 2. Origin of FCC and ECC, Polymer 31(3) (1990) 458-468.
[16] W. Hu, D. Frenkel, V.B. Mathot, Intramolecular nucleation model for polymer crystallization, Macromolecules 36(21) (2003) 8178-8183.
[17] W. Hu, Intramolecular crystal nucleation, Progress in Understanding of Polymer Crystallization, Springer2007, pp. 47-63.
[18] G. Strobl, Crystallization and melting of bulk polymers: New observations, conclusions and a thermodynamic scheme, Progress in polymer science 31(4) (2006) 398-442.
[19] G. Strobl, Colloquium: Laws controlling crystallization and melting in bulk polymers, Reviews of modern physics 81(3) (2009) 1287.
[20] G.R. Strobl, G.R. Strobl, The physics of polymers, Springer1997.
[21] G. Strobl, A thermodynamic multiphase scheme treating polymer crystallization and melting, The European Physical Journal E 18(3) (2005) 295-309.
[22] M. Muthukumar, Commentary on theories of polymer crystallization, The European Physical Journal E: Soft Matter and Biological Physics 3(2) (2000) 199-202.
[23] M. Muthukumar, Molecular modelling of nucleation in polymers, Philosophical Transactions of the Royal Society of London. Series A: Mathematical, Physical and Engineering Sciences 361(1804) (2003) 539-556.
[24] B. Wunderlich, Reversible crystallization and the rigid–amorphous phase in semicrystalline macromolecules, Progress in Polymer Science 28(3) (2003) 383-450.
[25] B. Wunderlich, G. Czornyj, A study of equilibrium melting of polyethylene, Macromolecules 10(5) (1977) 906-913.
[26] B. Wunderlich, A. Mehta, The nucleation of polyethylene dendrites from solution, Journal of Materials Science 5(3) (1970) 248-253.
[27] B. Wunderlich, Macromolecular Physics, Academic Press, New York1976.
[28] J.W. Gibbs, H.A. Bumstead, Thermodynamics, Longmans, Green and Company1906.
[29] M. Volmer, Kinetik der phasenbildung, (1939).
[30] W. Kossel, Zur theorie des kristallwachstums, Nachrichten von der Gesellschaft der Wissenschaften

zu Göttingen, Mathematisch-Physikalische Klasse 1927 (1927) 135-143.
[31] D. Turnbull, J.C. Fisher, Rate of nucleation in condensed systems, The Journal of chemical physics 17(1) (1949) 71-73.
[32] S. Glasstone, H. Eyring, K.J. Laidler, The theory of rate processes, McGraw-Hill1941.
[33] A. Chatterjee, F. Price, S. Newman, Heterogeneous nucleation of crystallization of high polymers from the melt. I. Substrate-induced morphologies, Journal of Polymer Science: Polymer Physics Edition 13(12) (1975) 2369-2383.
[34] A.J. Müller, M.L. Arnal, M. Trujillo, A.T. Lorenzo, Super-nucleation in nanocomposites and confinement effects on the crystallizable components within block copolymers, miktoarm star copolymers and nanocomposites, European Polymer Journal 47(4) (2011) 614-629.
[35] R.V. Castillo, A.J. Müller, Crystallization and morphology of biodegradable or biostable single and double crystalline block copolymers, Progress in Polymer Science 34(6) (2009) 516-560.
[36] R.M. Michell, I. Blaszczyk-Lezak, C. Mijangos, A.J. Müller, Confinement effects on polymer crystallization: From droplets to alumina nanopores, Polymer 54(16) (2013) 4059-4077.
[37] A.J. Müller, V. Balsamo, M.L. Arnal, Nucleation and crystallization in diblock and triblock copolymers, Block Copolymers II, Springer2005, pp. 1-63.
[38] A.J. Müller, M.L. Arnal, A.T. Lorenzo, Crystallization in Nano-Confined Polymeric Systems, Handbook of Polymer Crystallization (2013).
[39] O.O. Santana, A.J. Müller, Homogeneous nucleation of the dispersed crystallisable component of immiscible polymer blends, Polymer Bulletin 32(4) (1994) 471-477.
[40] M.L. Arnal, M.E. Matos, R.A. Morales, O.O. Santana, A.J. Müuller, Evaluation of the fractionated crystallization of dispersed polyolefins in a polystyrene matrix, Macromolecular Chemistry and Physics 199(10) (1998) 2275-2288.
[41] M.L. Arnal, A.J. Müller, P. Maiti, M. Hikosaka, Nucleation and crystallization of isotactic poly(propylene) droplets in an immiscible polystyrene matrix, Macromolecular Chemistry and Physics 201(17) (2000) 2493-2504.
[42] R.T. Tol, V.B.F. Mathot, G. Groeninckx, Confined crystallization phenomena in immiscible polymer blends with dispersed micro- and nanometer sized PA6 droplets, part 3: crystallization kinetics and crystallinity of micro- and nanometer sized PA6 droplets crystallizing at high supercoolings, Polymer 46(9) (2005) 2955-2965.
[43] R.L. Cormia, F.P. Price, D. Turnbull, Kinetics of Crystal Nucleation in Polyethylene, The Journal of Chemical Physics 37(6) (1962) 1333-1340.
[44] J.R. Burns, D. Turnbull, Kinetics of Crystal Nucleation in Molten Isotactic Polypropylene, Journal of Applied Physics 37(11) (1966) 4021-4026.
[45] J.I. Uriguen, L. Bremer, V. Mathot, G. Groeninckx, Preparation of water-borne dispersions of polyolefins: new systems for the study of homogeneous nucleation of polymers, Polymer 45(17) (2004) 5961-5968.
[46] Y.-L. Loo, R.A. Register, A.J. Ryan, Polymer Crystallization in 25-nm Spheres, Physical Review Letters 84(18) (2000) 4120-4123.
[47] H.-L. Chen, J.-C. Wu, T.-L. Lin, J.S. Lin, Crystallization Kinetics in Microphase-Separated Poly(ethylene oxide)-block-poly(1,4-butadiene), Macromolecules 34(20) (2001) 6936-6944.
[48] A.J. Müller, V. Balsamo, M.L. Arnal, T. Jakob, H. Schmalz, V. Abetz, Homogeneous Nucleation and Fractionated Crystallization in Block Copolymers, Macromolecules 35(8) (2002) 3048-3058.
[49] M.V. Massa, K. Dalnoki-Veress, Homogeneous Crystallization of Poly(Ethylene Oxide) Confined to Droplets: The Dependence of the Crystal Nucleation Rate on Length Scale and Temperature, Physical Review Letters 92(25) (2004) 255509.
[50] J.L. Carvalho, K. Dalnoki-Veress, Homogeneous bulk, surface, and edge nucleation in crystalline nanodroplets, Physical review letters 105(23) (2010) 237801.
[51] C. Schick, R. Androsch, J.W.P. Schmelzer, Homogeneous crystal nucleation in polymers, Journal of Physics: Condensed Matter 29(45) (2017) 453002.
[52] J.E.K. Schawe, S. Pogatscher, Material Characterization by Fast Scanning Calorimetry: Practice and Applications, in: C. Schick, V. Mathot (Eds.), Fast Scanning Calorimetry, Springer International Publishing, Cham, 2016, pp. 3-80.
[53] E. Zhuravlev, C. Schick, Non-Adiabatic Scanning Calorimeter for Controlled Fast Cooling and Heating, in: C. Schick, V. Mathot (Eds.), Fast Scanning Calorimetry, Springer International Publishing, Cham, 2016, pp. 81-104.
[54] A. Toda, R. Androsch, C. Schick, Insights into polymer crystallization and melting from fast scanning

chip calorimetry, Polymer 91 (2016) 239-263.
[55] C. Schick, R. Androsch, Nucleation-controlled semicrystalline morphology of bulk polymers, POLYMER CRYSTALLIZATION 1(4) (2018) e10036.
[56] L. Mandelkern, Crystallization of Polymers: Volume 2, Kinetics and Mechanisms, Cambridge University Press2004.
[57] M. Muchova, F. Lednický, Induction time as a measure for heterogeneous spherulite nucleation: quantitative evaluation of early-stage growth kinetics, Journal of Macromolecular Science, Part B: Physics 34(1-2) (1995) 55-73.
[58] H. Ishida, P. Bussi, Surface induced crystallization in ultrahigh-modulus polyethylene fiber-reinforced polyethylene composites, Macromolecules 24(12) (1991) 3569-3577.
[59] C. Wang, F.-H. Liu, W.-H. Huang, Electrospun-fiber induced transcrystallization of isotactic polypropylene matrix, Polymer 52(5) (2011) 1326-1336.
[60] J.P. Abdou, K.J. Reynolds, M.R. Pfau, J. van Staden, G.A. Braggin, N. Tajaddod, M. Minus, V. Reguero, J.J. Vilatela, S. Zhang, Interfacial crystallization of isotactic polypropylene surrounding macroscopic carbon nanotube and graphene fibers, Polymer 91 (2016) 136-145.
[61] F. Abraham, S. Ganzleben, D. Hanft, P. Smith, H.-W. Schmidt, Synthesis and Structure–Efficiency Relations of 1,3,5-Benzenetrisamides as Nucleating Agents and Clarifiers for Isotactic Poly(propylene), Macromolecular Chemistry and Physics 211(2) (2010) 171-181.
[62] S. Yoshimoto, T. Ueda, K. Yamanaka, A. Kawaguchi, E. Tobita, T. Haruna, Epitaxial act of sodium 2,2′-methylene-bis-(4,6-di-t-butylphenylene)phosphate on isotactic polypropylene, Polymer 42(23) (2001) 9627-9631.
[63] M. Gahleitner, C. Grein, S. Kheirandish, J. Wolfschwenger, Nucleation of Polypropylene Homo- and Copolymers, International Polymer Processing 26(1) (2011) 2-20.
[64] D.J. Blundell, A. Keller, Nature of self-seeding polyethylene crystal nuclei, Journal of Macromolecular Science, Part B 2(2) (1968) 301-336.
[65] D.J. Blundell, A. Keller, A.J. Kovacs, A new self-nucleation phenomenon and its application to the growing of polymer crystals from solution, Journal of Polymer Science Part B: Polymer Letters 4(7) (1966) 481-486.
[66] J. Rabesiaka, A.J. Kovacs, Isothermal Crystallization Kinetics of Polyethylene. III. Influence of the Sample Preparation, Journal of Applied Physics 32(11) (1961) 2314-2320.
[67] J.H. Magill, Melting behaviour and spherulitic crystallization of polycaproamide (nylon 6), Polymer 3 (1962) 43-51.
[68] G. Vidotto, D. Lévy, A.J. Kovacs, Cristallisation et fusion des polymères autoensemencés, Kolloid-Zeitschrift und Zeitschrift für Polymere 230(2) (1969) 289-305.
[69] B. Fillon, A. Thierry, J.C. Wittmann, B. Lotz, Self-nucleation and recrystallization of polymers. Isotactic polypropylene, β phase: β-α conversion and β-α growth transitions, Journal of Polymer Science Part B: Polymer Physics 31(10) (1993) 1407-1424.
[70] R.M. Michell, A. Mugica, M. Zubitur, A.J. Müller, Self-Nucleation of Crystalline Phases Within Homopolymers, Polymer Blends, Copolymers, and Nanocomposites, in: F. Auriemma, G.C. Alfonso, C. de Rosa (Eds.), Polymer Crystallization I: From Chain Microstructure to Processing, Springer International Publishing, Cham, 2017, pp. 215-256.
[71] B.O. Reid, M. Vadlamudi, A. Mamun, H. Janani, H. Gao, W. Hu, R.G. Alamo, Strong memory effect of crystallization above the equilibrium melting point of random copolymers, Macromolecules 46(16) (2013) 6485-6497.
[72] H. Gao, M. Vadlamudi, R.G. Alamo, W. Hu, Monte Carlo Simulations of Strong Memory Effect of Crystallization in Random Copolymers, Macromolecules 46(16) (2013) 6498-6506.
[73] M. Muthukumar, Communication: Theory of melt-memory in polymer crystallization, The Journal of Chemical Physics 145(3) (2016) 031105.
[74] L. Sangroniz, F. Barbieri, D. Cavallo, A. Santamaria, R.G. Alamo, A.J. Müller, Rheology of self-nucleated poly(ε-caprolactone) melts, European Polymer Journal 99 (2018) 495-503.
[75] L. Sangroniz, D. Cavallo, A. Santamaria, A.J. Müller, R.G. Alamo, Thermorheologically Complex Self-Seeded Melts of Propylene–Ethylene Copolymers, Macromolecules 50(2) (2017) 642-651.
[76] L. Sangroniz, R.G. Alamo, D. Cavallo, A. Santamaría, A.J. Müller, A. Alegría, Differences between Isotropic and Self-Nucleated PCL Melts Detected by Dielectric Experiments, Macromolecules 51(10) (2018) 3663-3671.
[77] C.-M. Wu, M. Chen, J. Karger-Kocsis, Transcrystallization in syndiotactic polypropylene induced by high-modulus carbon fibers, Polymer Bulletin 41(2) (1998) 239-245.

[78] N. Billon, C. Magnet, J. Haudin, D. Lefebvre, Transcrystallinity effects in thin polymer films. Experimental and theoretical approach, Colloid and Polymer Science 272(6) (1994) 633-654.
[79] D.T. Quillin, D.F. Caulfield, J.A. Koutsky, Crystallinity in the polypropylene/cellulose system. I. Nucleation and crystalline morphology, Journal of Applied Polymer Science 50(7) (1993) 1187-1194.
[80] J. Thomason, A. Van Rooyen, Transcrystallized interphase in thermoplastic composites, Journal of materials science 27(4) (1992) 897-907.
[81] A. Misra, B. Deopura, S. Xavier, F. Hartley, R. Peters, Transcrystallinity in injection molded polypropylene glass fibre composites, Die Angewandte Makromolekulare Chemie: Applied Macromolecular Chemistry and Physics 113(1) (1983) 113-120.
[82] B. Wang, T. Wen, X. Zhang, A. Tercjak, X. Dong, A.J. Müller, D. Wang, D. Cavallo, Nucleation of Poly (lactide) on the Surface of Different Fibers, Macromolecules 52(16) (2019) 6274-6284.
[83] A. Ameli, P. Jung, C. Park, Electrical properties and electromagnetic interference shielding effectiveness of polypropylene/carbon fiber composite foams, Carbon 60 (2013) 379-391.
[84] X. Chu, Z. Wu, R. Huang, Y. Zhou, L. Li, Mechanical and thermal expansion properties of glass fibers reinforced PEEK composites at cryogenic temperatures, Cryogenics 50(2) (2010) 84-88.
[85] G.P. Desio, L. Rebenfeld, Effects of fibers on the crystallization of poly (phenylene sulfide), Journal of applied polymer science 39(4) (1990) 825-835.
[86] K. Panyasart, N. Chaiyut, T. Amornsakchai, O. Santawitee, Effect of surface treatment on the properties of pineapple leaf fibers reinforced polyamide 6 composites, Energy procedia 56 (2014) 406-413.
[87] J. Felix, P. Gatenholm, Effect of transcrystalline morphology on interfacial adhesion in cellulose/polypropylene composites, Journal of materials science 29(11) (1994) 3043-3049.
[88] H. Quan, Z.-M. Li, M.-B. Yang, R. Huang, On transcrystallinity in semi-crystalline polymer composites, Composites Science and Technology 65(7-8) (2005) 999-1021.
[89] T. Yilmaz, Influence of annealing duration on the erosive wear behavior of polyphenylenesulphide composites, Journal of materials science 45(9) (2010) 2381-2389.
[90] B. Lotz, J. Wittmann, A. Lovinger, Structure and morphology of poly (propylenes): a molecular analysis, Polymer 37(22) (1996) 4979-4992.
[91] M. Gahleitner, C. Grein, S. Kheirandish, J. Wolfschwenger, Nucleation of polypropylene homo-and copolymers, International Polymer Processing 26(1) (2011) 2-20.
[92] J.C. Wittmann, B. Lotz, Epitaxial crystallization of polymers on organic and polymeric substrates, Progress in polymer science 15(6) (1990) 909-948.
[93] T. Urushihara, K. Okada, K. Watanabe, A. Toda, N. Kawamoto, M. Hikosaka, Acceleration mechanism in critical nucleation of polymers by epitaxy of nucleating agent, Polymer journal 41(3) (2009) 228.
[94] S. Yoshimoto, T. Ueda, K. Yamanaka, A. Kawaguchi, E. Tobita, T. Haruna, Epitaxial act of sodium 2, 2′-methylene-bis-(4, 6-di-t-butylphenylene) phosphate on isotactic polypropylene, Polymer 42(23) (2001) 9627-9631.
[95] B. Fillon, B. Lotz, A. Thierry, J. Wittmann, Self-nucleation and enhanced nucleation of polymers. Definition of a convenient calorimetric “efficiency scale” and evaluation of nucleating additives in isotactic polypropylene (α phase), Journal of Polymer Science Part B: Polymer Physics 31(10) (1993) 1395-1405.
[96] B. Fillon, A. Thierry, B. Lotz, J. Wittmann, Efficiency scale for polymer nucleating agents, Journal of thermal analysis 42(4) (1994) 721-731.
[97] J. Bernstein, J.M. Bernstein, Polymorphism in molecular crystals, Oxford University Press2002.
[98] C.G. Salzmann, P.G. Radaelli, B. Slater, J.L. Finney, The polymorphism of ice: five unresolved questions, Physical Chemistry Chemical Physics 13(41) (2011) 18468-18480.
[99] W. Ostwald, Studies on formation and transformation of solid materials, Z. Phys. Chem 22 (1897) 289-330.
[100] L. Yu, Nucleation of one polymorph by another, Journal of the American Chemical Society 125(21) (2003) 6380-6381.
[101] S. Chen, H. Xi, L. Yu, Cross-nucleation between ROY polymorphs, Journal of the American Chemical Society 127(49) (2005) 17439-17444.
[102] L. Yu, Polymorphism in molecular solids: an extraordinary system of red, orange, and yellow crystals, Accounts of chemical research 43(9) (2010) 1257-1266.
[103] C. Stoica, P. Tinnemans, H. Meekes, E. Vlieg, P.J.C.M. van Hoof, F.M. Kaspersen, Epitaxial 2D Nucleation of Metastable Polymorphs: A 2D Version of Ostwald's Rule of Stages, Crystal Growth &

Design 5(3) (2005) 975-981.
[104] C. Stoica, P. Verwer, H. Meekes, E. Vlieg, P.J.C.M. van Hoof, F. Kaspersen, Heterogeneous 2D nucleation of the stable polymorphic form on the metastable form, Journal of Crystal Growth 275(1–2) (2005) e1727-e1731.
[105] A.J. Lovinger, J.O. Chua, C.C. Gryte, Studies on the α and β forms of isotactic polypropylene by crystallization in a temperature gradient, Journal of Polymer Science: Polymer Physics Edition 15(4) (1977) 641-656.
[106] J. Varga, Supermolecular structure of isotactic polypropylene, Journal of Materials Science 27(10) (1992) 2557-2579.
[107] D. Cavallo, L. Gardella, G. Portale, A.J. Müller, G.C. Alfonso, Kinetics of cross-nucleation in isotactic poly (1-butene), Macromolecules 47(2) (2014) 870-873.
[108] S. Looijmans, A. Menyhard, G.W. Peters, G.C. Alfonso, D. Cavallo, Anomalous temperature dependence of isotactic polypropylene α-on-β cross-nucleation kinetics, Crystal Growth & Design 17(9) (2017) 4936-4943.
[109] D. Cavallo, F. Galli, L. Yu, G.C. Alfonso, Cross-Nucleation between Concomitantly Crystallizing α- and γ-Phases in Polypivalolactone: Secondary Nucleation of One Polymorph on Another, Crystal Growth & Design 17(5) (2017) 2639-2645.
[110] H.-l. ZHENG, Z.-z. LIU, C.-y. LI, B. LU, G.-q. ZHENG, A Review on Crystalline Behaviors of Semi-crystalline Polymer/Carbon Nanotubes Nanocomposites, Shanghai Plastics (2) (2013) 3.
[111] M. Huson, W. McGill, Transcrystallinity in polypropylene, Journal of Polymer Science: Polymer Chemistry Edition 22(11) (1984) 3571-3580.
[112] C. Wang, L. Hwang, Transcrystallization of PTFE fiber/PP composites (I) crystallization kinetics and morphology, Journal of Polymer Science Part B: Polymer Physics 34(1) (1996) 47-56.
[113] C. Wang, Y.-J. Wu, C.-Y. Fang, C.-W. Tsai, Electrospun nanofiber-reinforced polypropylene composites: Nucleating ability of nanofibers, Composites Science and Technology 126 (2016) 1-8.
[114] C. Wang, C. Liu, Transcrystallization of polypropylene on carbon fibres, Polymer 38(18) (1997) 4715-4718.
[115] C. Wang, C.-R. Liu, Transcrystallization of polypropylene composites: nucleating ability of fibres, Polymer 40(2) (1999) 289-298.
[116] C. Wang, C.-Y. Fang, C.-Y. Wang, Electrospun poly (butylene terephthalate) fibers: Entanglement density effect on fiber diameter and fiber nucleating ability towards isotactic polypropylene, Polymer 72 (2015) 21-29.
[117] C. Wang, C. Liu, C. Chen, L. Hawang, Transcrystallinity in PTFE fiber/PP composites, The Journal of Adhesion 67(1-4) (1998) 167-180.
[118] C. He, X. Dong, X. Zhang, D. Wang, D. Xu, Morphology investigation of transcrystallinity at polyamide 66/aramid fiber interface, Journal of applied polymer science 91(5) (2004) 2980-2983.
[119] H. Shi, Y. Zhao, X. Dong, C. He, D. Wang, D. Xu, Transcrystalline morphology of nylon 6 on the surface of aramid fibers, Polymer international 53(11) (2004) 1672-1676.
[120] M. Folkes, S. Hardwick, The mechanical properties of glass/polypropylene multilayer laminates, Journal of Materials Science 25(5) (1990) 2598-2606.
[121] T. Kwei, H. Schonhorn, H. Frisch, Dynamic mechanical properties of the transcrystalline regions in two polyolefins, Journal of Applied Physics 38(6) (1967) 2512-2516.
[122] Y. Qin, Y. Xu, L. Zhang, G. Zheng, X. Yan, K. Dai, C. Liu, C. Shen, Z. Guo, Interfacial interaction enhancement by shear-induced β-cylindrite in isotactic polypropylene/glass fiber composites, Polymer 100 (2016) 111-118.
[123] Y. Qin, Y. Xu, L. Zhang, G. Zheng, K. Dai, C. Liu, X. Yan, J. Guo, Z. Guo, Shear-induced interfacial sheath structure in isotactic polypropylene/glass fiber composites, Polymer 70 (2015) 326-335.
[124] S. Saeidlou, M.A. Huneault, H. Li, P. Sammut, C.B. Park, Evidence of a dual network/spherulitic crystalline morphology in PLA stereocomplexes, Polymer 53(25) (2012) 5816-5824.
[125] T. Gao, S.-J. Zhao, R.-Y. Bao, G.-J. Zhong, Z.-M. Li, M.-B. Yang, W. Yang, Constructing Sandwich-Architectured Poly (L-lactide)/High-Melting-Point Poly (L-lactide) Non-Woven Fabrics: Towards Heat Resistant Poly (L-lactide) Barrier Biocomposites with Full Biodegradability, ACS Applied Bio Materials (2019).
[126] T. Gao, Z.-M. Zhang, L. Li, R.-Y. Bao, Z.-Y. Liu, B.-H. Xie, M.-B. Yang, W. Yang, Tailoring Crystalline Morphology by High-Efficiency Nucleating Fiber: Toward High-Performance Poly (l-lactide) Biocomposites, ACS applied materials & interfaces 10(23) (2018) 20044-20054.
[127] R. Zhao, X. Zhou, G. Dai, Effect of the microstructure of GMT on its mechanical properties,

Polymer composites 23(6) (2002) 1026-1035.
[128] T. Hata, K. Ohsaka, T. Yamada, K. Nakamae, N. Shibata, T. Matsumoto, Transcrystalline region of polypropylene: its formation, structure and mechanical properties, The Journal of Adhesion 45(1-4) (1994) 125-135.
[129] T. Wen, G. Liu, Y. Zhou, X. Zhang, F. Wang, H. Chen, J. Loos, D. Wang, Epitaxy-induced crystallization of olefin block copolymers, Macromolecules 45(15) (2012) 5979-5985.
[130] Z. Guo, S. Li, X. Liu, J. Zhang, H. Li, X. Sun, Z. Ren, S. Yan, Epitaxial crystallization of isotactic poly (methyl methacrylate) from different states on highly oriented polyethylene thin film, The Journal of Physical Chemistry B 122(40) (2018) 9425-9433.
[131] J. Liu, J. Wang, H. Li, D. Shen, J. Zhang, Y. Ozaki, S. Yan, Epitaxial crystallization of isotactic poly (methyl methacrylate) on highly oriented polyethylene, The journal of physical chemistry B 110(2) (2006) 738-742.
[132] K. Cho, D. Kim, S. Yoon, Effect of substrate surface energy on transcrystalline growth and its effect on interfacial adhesion of semicrystalline polymers, Macromolecules 36(20) (2003) 7652-7660.
[133] D. Gray, "Transcrystallization" induced by mechanical stress on a polypropylene melt, Journal of Polymer Science: Polymer Letters Edition 12(11) (1974) 645-650.
[134] H. Ishida, P. Bussi, Induction time approach to surface induced crystallization in polyethylene/poly (ε-caprolactone) melt, Journal of materials science 26(23) (1991) 6373-6382.
[135] K.M. Nampoothiri, N.R. Nair, R.P. John, An overview of the recent developments in polylactide (PLA) research, Bioresource technology 101(22) (2010) 8493-8501.
[136] J.R. Murdoch, G.L. Loomis, Polylactide compositions, Google Patents, 1988.
[137] G.L. Loomis, J.R. Murdoch, Polylactide compositions, Google Patents, 1991.
[138] R. Conn, J. Kolstad, J. Borzelleca, D. Dixler, L. Filer Jr, B. LaDu Jr, M. Pariza, Safety assessment of polylactide (PLA) for use as a food-contact polymer, Food and Chemical Toxicology 33(4) (1995) 273-283.
[139] D.R. Witzke, Introduction to properties, engineering, and prospects of polylactide polymers, (1999).
[140] H. Xu, C. Teng, M. Yu, Improvements of thermal property and crystallization behavior of PLLA based multiblock copolymer by forming stereocomplex with PDLA oligomer, Polymer 47(11) (2006) 3922-3928.
[141] B. Gupta, N. Revagade, J. Hilborn, Poly (lactic acid) fiber: An overview, Progress in polymer science 32(4) (2007) 455-482.
[142] R.M. Rasal, A.V. Janorkar, D.E. Hirt, Poly (lactic acid) modifications, Progress in polymer science 35(3) (2010) 338-356.
[143] H. Liu, J. Zhang, Research progress in toughening modification of poly (lactic acid), Journal of polymer science part B: Polymer Physics 49(15) (2011) 1051-1083.
[144] J. Zhang, Y. Duan, H. Sato, H. Tsuji, I. Noda, S. Yan, Y. Ozaki, Crystal modifications and thermal behavior of poly (L-lactic acid) revealed by infrared spectroscopy, Macromolecules 38(19) (2005) 8012-8021.
[145] L. Xiao, B. Wang, G. Yang, M. Gauthier, Poly (lactic acid)-based biomaterials: synthesis, modification and applications, InTech2012.
[146] H. Tsuji, F. Horii, S.H. Hyon, Y. Ikada, Stereocomplex formation between enantiomeric poly (lactic acid) s. 2. Stereocomplex formation in concentrated solutions, Macromolecules 24(10) (1991) 2719-2724.
[147] X.-F. Wei, R.-Y. Bao, Z.-Q. Cao, W. Yang, B.-H. Xie, M.-B. Yang, Stereocomplex crystallite network in asymmetric PLLA/PDLA blends: Formation, structure, and confining effect on the crystallization rate of homocrystallites, Macromolecules 47(4) (2014) 1439-1448.
[148] Z. Jing, X. Shi, G. Zhang, Competitive stereocomplexation and homocrystallization behaviors in the poly (lactide) blends of PLLA and PDLA-PEG-PDLA with controlled block length, Polymers 9(3) (2017) 107.
[149] Y. Ikada, K. Jamshidi, H. Tsuji, S.H. Hyon, Stereocomplex formation between enantiomeric poly (lactides), Macromolecules 20(4) (1987) 904-906.
[150] H. Tsuji, S.H. Hyon, Y. Ikada, Stereocomplex formation between enantiomeric poly (lactic acid) s. 4. Differential scanning calorimetric studies on precipitates from mixed solutions of poly (D-lactic acid) and poly (L-lactic acid), Macromolecules 24(20) (1991) 5657-5662.
[151] H. Tsuji, Y. Ikada, S.H. Hyon, Y. Kimura, T. Kitao, Stereocomplex formation between enantiomeric poly (lactic acid). VIII. Complex fibers spun from mixed solution of poly (D-lactic acid) and poly (L-lactic acid), Journal of applied polymer science 51(2) (1994) 337-344.

[152] H. Tsuji, F. Horii, M. Nakagawa, Y. Ikada, H. Odani, R. Kitamaru, Stereocomplex formation between enantiomeric poly (lactic acid) s. 7. Phase structure of the stereocomplex crystallized from a dilute acetonitrile solution as studied by high-resolution solid-state carbon-13 NMR spectroscopy, Macromolecules 25(16) (1992) 4114-4118.
[153] H. Tsuji, Y. Ikada, Stereocomplex formation between enantiomeric poly (lactic acid) s. XI. Mechanical properties and morphology of solution-cast films, Polymer 40(24) (1999) 6699-6708.
[154] Y. Fan, H. Nishida, Y. Shirai, Y. Tokiwa, T. Endo, Thermal degradation behaviour of poly (lactic acid) stereocomplex, polymer Degradation and Stability 86(2) (2004) 197-208.
[155] N. Rahman, T. Kawai, G. Matsuba, K. Nishida, T. Kanaya, H. Watanabe, H. Okamoto, M. Kato, A. Usuki, M. Matsuda, Effect of polylactide stereocomplex on the crystallization behavior of poly (L-lactic acid), Macromolecules 42(13) (2009) 4739-4745.
[156] J. Sun, H. Yu, X. Zhuang, X. Chen, X. Jing, Crystallization behavior of asymmetric PLLA/PDLA blends, The Journal of Physical Chemistry B 115(12) (2011) 2864-2869.
[157] M. Hirata, Y. Kimura, Thermomechanical properties of stereoblock poly (lactic acid) s with different PLLA/PDLA block compositions, Polymer 49(11) (2008) 2656-2661.
[158] J. Shao, S. Xiang, X. Bian, J. Sun, G. Li, X. Chen, Remarkable melting behavior of PLA stereocomplex in linear PLLA/PDLA blends, Industrial & Engineering Chemistry Research 54(7) (2015) 2246-2253.
[159] J. Sarasua, A.L. Arraiza, P. Balerdi, I. Maiza, Crystallinity and mechanical properties of optically pure polylactides and their blends, Polymer Engineering & Science 45(5) (2005) 745-753.
[160] H. Tsuji, Poly (lactide) stereocomplexes: formation, structure, properties, degradation, and applications, Macromolecular bioscience 5(7) (2005) 569-597.
[161] H. Tsuji, H. Takai, S.K. Saha, Isothermal and non-isothermal crystallization behavior of poly (L-lactic acid): Effects of stereocomplex as nucleating agent, Polymer 47(11) (2006) 3826-3837.
[162] S.C. Schmidt, M.A. Hillmyer, Polylactide stereocomplex crystallites as nucleating agents for isotactic polylactide, Journal of Polymer Science Part B: Polymer Physics 39(3) (2001) 300-313.
[163] K.S. Anderson, M.A. Hillmyer, Melt preparation and nucleation efficiency of polylactide stereocomplex crystallites, Polymer 47(6) (2006) 2030-2035.
[164] T. Wen, Z. Xiong, G. Liu, X. Zhang, S. de Vos, R. Wang, C.A. Joziasse, F. Wang, D. Wang, The inexistence of epitaxial relationship between stereocomplex and α crystal of poly (lactic acid): Direct experimental evidence, Polymer 54(7) (2013) 1923-1929.
[165] Y.-Y. Liang, J.-Z. Xu, Y. Li, G.-J. Zhong, R. Wang, Z.-M. Li, Promoting Interfacial Transcrystallization in Polylactide/Ramie Fiber Composites by Utilizing Stereocomplex Crystals, ACS Sustainable Chemistry & Engineering 5(8) (2017) 7128-7136.
[166] B. Wunderlich, Macromolecular Physics, Vol. 2, Crystal Nucleation, Growth, Annealing (1976).
[167] B. Kalb, A. Pennings, General crystallization behaviour of poly (L-lactic acid), Polymer 21(6) (1980) 607-612.
[168] R. Vasanthakumari, A. Pennings, Crystallization kinetics of poly (L-lactic acid), Polymer 24(2) (1983) 175-178.
[169] A.J. Müller, M. Ávila, G. Saenz, J. Salazar, Crystallization of PLA-based Materials, Chapter 3 in Poly(lactic acid) Science and Technology: Processing, Properties, Additives and Applications, Royal Society of Chemistry2014.
[170] A. Chatterjee, F. Price, S. Newman, Heterogeneous nucleation of crystallization of high polymers from the melt. II. Aspects of transcrystallinity and nucleation density, Journal of Polymer Science: Polymer Physics Edition 13(12) (1975) 2385-2390.
[171] A. Chatterjee, F. Price, S. Newman, Heterogeneous nucleation of crystallization of high polymers from the melt. III. Nucleation kinetics and interfacial energies, Journal of Polymer Science: Polymer Physics Edition 13(12) (1975) 2391-2400.
[172] C. Yan, H. Li, J. Zhang, Y. Ozaki, D. Shen, D. Yan, A.-C. Shi, S. Yan, Surface-induced anisotropic chain ordering of polycarprolactone on oriented polyethylene substrate: Epitaxy and soft epitaxy, Macromolecules 39(23) (2006) 8041-8048.
[173] H. Chang, J. Zhang, L. Li, Z. Wang, C. Yang, I. Takahashi, Y. Ozaki, S. Yan, A study on the epitaxial ordering process of the polycaprolactone on the highly oriented polyethylene substrate, Macromolecules 43(1) (2009) 362-366.
[174] T. Sukhanova, F. Lednický, J. Urban, Y. Baklagina, G. Mikhailov, V. Kudryavtsev, Morphology of melt crystallized polypropylene in the presence of polyimide fibres, Journal of materials science 30(9) (1995) 2201-2214.

[175] C. Wang, C.R. Liu, Transcrystallization of PTFE fiber/PP composites—III. Effect of fiber pulling on the crystallization kinetics, Journal of Polymer Science Part B: Polymer Physics 36(8) (1998) 1361-1370.
[176] J.C. Wittmann, P. Smith, Highly oriented thin films of poly (tetrafluoroethylene) as a substrate for oriented growth of materials, Nature 352(6334) (1991) 414.
[177] P. Damman, S. Coppée, V.M. Geskin, R. Lazzaroni, What is the mechanism of oriented crystal growth on rubbed polymer substrates? Topography vs epitaxy, Journal of the American Chemical Society 124(51) (2002) 15166-15167.
[178] C. Lin, S. Ding, Y. Hwang, Interfacial crystallization of isotactic polypropylene molded against the copper surface with various surface roughnesses prepared by an electrochemical process, Journal of materials science 36(20) (2001) 4943-4948.
[179] A.J. Page, R.P. Sear, Crystallization controlled by the geometry of a surface, Journal of the American Chemical Society 131(48) (2009) 17550-17551.
[180] Y.-X. Liu, X.-J. Wang, J. Lu, C.-B. Ching, Influence of the roughness, topography, and physicochemical properties of chemically modified surfaces on the heterogeneous nucleation of protein crystals, The Journal of Physical Chemistry B 111(50) (2007) 13971-13978.
[181] G. Di Profio, E. Fontananova, E. Curcio, E. Drioli, From tailored supports to controlled nucleation: Exploring material chemistry, surface nanostructure, and wetting regime effects in heterogeneous nucleation of organic molecules, Crystal Growth & Design 12(7) (2012) 3749-3757.
[182] J. Holbrough, J. Campbell, F. Meldrum, H. Christenson, Topographical control of crystal nucleation, Crystal Growth & Design 12(2) (2012) 750-755.
[183] M.H. Lee, K.J. Yoon, S.W. Ko, Synthesis of a vinyl monomer containing β-cyclodextrin and grafting onto cotton fiber, Journal of Applied Polymer Science 80(3) (2001) 438-446.
[184] C. Lin, Y. Du, Effect of surface topographies of PTFE and polyimide as characterized by atomic force microscopy on the heterogeneous nucleation of isotactic polypropylene, Materials chemistry and physics 58(3) (1999) 268-275.
[185] Y. Zhang, M. Wang, X. Lin, W. Huang, Effect of substrate surface microstructure on heterogeneous nucleation behavior, Journal of Materials Science & Technology 28(1) (2012) 67-72.
[186] F. Price, Nucleation; AC Zettlemoyer, New York: Marcel Dekker, 1969.
[187] D. Turnbull, Kinetics of heterogeneous nucleation, The Journal of Chemical Physics 18(2) (1950) 198-203.
[188] L. Boinovich, A.M. Emelyanenko, V.V. Korolev, A.S. Pashinin, Effect of wettability on sessile drop freezing: when superhydrophobicity stimulates an extreme freezing delay, Langmuir 30(6) (2014) 1659-1668.
[189] Y.-r. Tang, T. Li, H.-m. Ye, J. Xu, B.-h. Guo, The effect of polymer-substrate interaction on the nucleation property: Comparing study of graphene and hexagonal boron nitride Nanosheets, Chinese Journal of Polymer Science 34(8) (2016) 1021-1031.
[190] B. Wunderlich, Macromolecular physics, Elsevier2012.
[191] H. Beck, Heterogeneous nucleating agents for polypropylene crystallization, Journal of Applied Polymer Science 11(5) (1967) 673-685.
[192] S. Nagasawa, A. Fujimori, T. Masuko, M. Iguchi, Crystallisation of polypropylene containing nucleators, Polymer 46(14) (2005) 5241-5250.
[193] D. Libster, A. Aserin, N. Garti, Advanced nucleating agents for polypropylene, Polymers for Advanced Technologies 18(9) (2007) 685-695.
[194] M. Gahleitner, J. Wolfschwenger, D. Mileva, Polymer crystal nucleating agents, (2016).
[195] F. Binsbergen, Heterogeneous nucleation in the crystallization of polyolefins: Part 1. Chemical and physical nature of nucleating agents, Polymer 11(5) (1970) 253-267.
[196] N.Z.N. Ke, Effect of DMDBS on Crystallization Behavior of Polypropylene [J], China Plastics 7 (2008).
[197] K. Sreenivas, R. Basargekar, G. Kumaraswamy, Phase separation of DMDBS from PP: effect of polymer Molecular Weight and Tacticity, Macromolecules 44(7) (2011) 2358-2364.
[198] J. Wittmann, A. Hodge, B. Lotz, Epitaxial crystallization of polymers onto benzoic acid: Polyethylene and paraffins, aliphatic polyesters, and polyamides, Journal of Polymer Science: Polymer Physics Edition 21(12) (1983) 2495-2509.
[199] K. Okada, K. Watanabe, T. Urushihara, A. Toda, M. Hikosaka, Role of epitaxy of nucleating agent (NA) in nucleation mechanism of polymers, Polymer 48(1) (2007) 401-408.
[200] B. Lotz, J.-C. Wittmann, W. Stocker, S. Magonov, H.-J. Cantow, Atomic force microscopy on

epitaxially crystallized isotactic polypropylene, Polymer bulletin 26(2) (1991) 209-214.
[201] Y.-L. Loo, R.A. Register, A.J. Ryan, G.T. Dee, Polymer crystallization confined in one, two, or three dimensions, Macromolecules 34(26) (2001) 8968-8977.
[202] M.V. Massa, K. Dalnoki-Veress, Homogeneous crystallization of poly (ethylene oxide) confined to droplets: the dependence of the crystal nucleation rate on length scale and temperature, Physical review letters 92(25) (2004) 255509.
[203] R.M. Michell, A.J. Mueller, Confined crystallization of polymeric materials, Progress in Polymer Science 54 (2016) 183-213.
[204] A. Van Riemsdyk, Eclair des Essais D'Or, Annales de Chimie et de Physique, 1880, p. 66.
[205] B. Vonnegut, Variation with temperature of the nucleation rate of supercooled liquid tin and water drops, Journal of colloid science 3(6) (1948) 563-569.
[206] D. Turnbull, R. Cech, Microscopic observation of the solidification of small metal droplets, Journal of Applied Physics 21(8) (1950) 804-810.
[207] D. Turnbull, Kinetics of solidification of supercooled liquid mercury droplets, The Journal of chemical physics 20(3) (1952) 411-424.
[208] D. Turnbull, R.L. Cormia, Kinetics of crystal nucleation in some normal alkane liquids, The Journal of Chemical Physics 34(3) (1961) 820-831.
[209] R. Cormia, F. Price, D. Turnbull, Kinetics of crystal nucleation in polyethylene, The Journal of Chemical Physics 37(6) (1962) 1333-1340.
[210] A. Manaure, A. Müller, Nucleation and crystallization of blends of poly (propylene) and ethylene/α-olefin copolymers, Macromolecular Chemistry and Physics 201(9) (2000) 958-972.
[211] M.S. Sánchez, V. Mathot, G.V. Poel, G. Groeninckx, W. Bruls, Crystallization of polyamide confined in sub-micrometer droplets dispersed in a molten polyethylene matrix, Journal of Polymer Science Part B: Polymer Physics 44(5) (2006) 815-825.
[212] D.S. Langhe, J.K. Keum, A. Hiltner, E. Baer, Fractionated crystallization of α-and β-nucleated polypropylene droplets, Journal of Polymer Science Part B: Polymer Physics 49(2) (2011) 159-171.
[213] M.E. Córdova, A.T. Lorenzo, A.J. Müller, L. Gani, S. Tencé-Girault, L. Leibler, The Influence of Blend Morphology (Co-Continuous or Sub-Micrometer Droplets Dispersions) on the Nucleation and Crystallization Kinetics of Double Crystalline Polyethylene/Polyamide Blends Prepared by Reactive Extrusion, Macromolecular Chemistry and Physics 212(13) (2011) 1335-1350.
[214] H. Frensch, P. Harnischfeger, B. Jungnickel, Fractionated crystallization in incompatible polymer blends, Multiphase polymers: blends and ionomers 395 (1989) 101.
[215] R. Morales, M. Arnal, A. Müller, The evaluation of the state of dispersion in immiscible blends where the minor phase exhibits fractionated crystallization, Polymer Bulletin 35(3) (1995) 379-386.
[216] M.L. Arnal, A.J. Müller, P. Maiti, M. Hikosaka, Nucleation and crystallization of isotactic poly (propylene) droplets in an immiscible polystyrene matrix, Macromolecular chemistry and physics 201(17) (2000) 2493-2504.
[217] R. Castillo, M. Arnal, A. Müller, I. Hamley, V. Castelletto, H. Schmalz, V. Abetz, Fractionated crystallization and fractionated melting of confined PEO microdomains in PB-b-PEO and PE-b-PEO diblock copolymers, Macromolecules 41(3) (2008) 879-889.
[218] J. Ibarretxe, G. Groeninckx, L. Bremer, V. Mathot, Quantitative evaluation of fractionated and homogeneous nucleation of polydisperse distributions of water-dispersed maleic anhydride-grafted-polypropylene micro-and nano-sized droplets, Polymer 50(19) (2009) 4584-4595.
[219] A. Müller, V. Balsamo, M. Arnal, T. Jakob, H. Schmalz, V. Abetz, Homogeneous nucleation and fractionated crystallization in block copolymers, Macromolecules 35(8) (2002) 3048-3058.
[220] M. Massa, J. Carvalho, K. Dalnoki-Veress, Direct visualisation of homogeneous and heterogeneous crystallisation in an ensemble of confined domains of poly (ethylene oxide), The European Physical Journal E 12(1) (2003) 111-117.
[221] D.S. Langhe, A. Hiltner, E. Baer, Effect of additives, catalyst residues, and confining substrates on the fractionated crystallization of polypropylene droplets, Journal of Applied Polymer Science 125(3) (2012) 2110-2120.
[222] O. Santana, A. Müller, Homogeneous nucleation of the dispersed crystallisable component of immiscible polymer blends, Polymer Bulletin 32(4) (1994) 471-477.
[223] B. Fillon, J. Wittmann, B. Lotz, A. Thierry, Self-nucleation and recrystallization of isotactic polypropylene (α phase) investigated by differential scanning calorimetry, Journal of Polymer Science Part B: Polymer Physics 31(10) (1993) 1383-1393.
[224] R. Michell, A. Mugica, M. Zubitur, A. Müller, Self-nucleation of crystalline phases within

homopolymers, polymer blends, copolymers, and nanocomposites, Polymer Crystallization I, Springer2015, pp. 215-256.
[225] A.T. Lorenzo, M.L. Arnal, J.J. Sanchez, A.J. Müller, Effect of annealing time on the self-nucleation behavior of semicrystalline polymers, Journal of Polymer Science Part B: Polymer Physics 44(12) (2006) 1738-1750.
[226] J. Xu, Y. Ma, W. Hu, M. Rehahn, G. Reiter, Cloning polymer single crystals through self-seeding, Nature materials 8(4) (2009) 348.
[227] C. Luo, J.-U. Sommer, Frozen topology: Entanglements control nucleation and crystallization in polymers, Physical review letters 112(19) (2014) 195702.
[228] M. Muthukumar, Communication: Theory of melt-memory in polymer crystallization, AIP Publishing, 2016.
[229] L. Sangroniz, D. Cavallo, A. Santamaria, A.J. Müller, R.G. Alamo, Thermorheologically complex self-seeded melts of propylene–ethylene copolymers, Macromolecules 50(2) (2017) 642-651.
[230] L. Sangroniz, F. Barbieri, D. Cavallo, A. Santamaria, R. Alamo, A. Müller, Rheology of self-nucleated poly (ε-caprolactone) melts, European Polymer Journal 99 (2018) 495-503.
[231] L. Sangroniz, R. Alamo, D. Cavallo, A. Santamaría, A. Müller, A. Alegría, Differences between isotropic and self-nucleated PCL melts detected by dielectric experiments, Macromolecules 51(10) (2018) 3663-3671.
[232] V. Balsamo, N. Urdaneta, L. Pérez, P. Carrizales, V. Abetz, A. Müller, Effect of the polyethylene confinement and topology on its crystallisation within semicrystalline ABC triblock copolymers, European polymer journal 40(6) (2004) 1033-1049.
[233] M. Galante, L. Mandelkern, R. Alamo, A. Lehtinen, R. Paukker, Crystallization kinetics of metallocene type polypropylenes: Influence of molecular weight and comparison with Ziegler-Natta type systems, Journal of Thermal Analysis and Calorimetry 47(4) (1996) 913-929.
[234] G. Shi, G. Liu, C. Su, H. Chen, Y. Chen, Y. Su, A.J. Muller, D. Wang, Reexamining the crystallization of poly (ε-caprolactone) and isotactic polypropylene under hard confinement: nucleation and orientation, Macromolecules 50(22) (2017) 9015-9023.
[235] Z. Bartczak, A. Galeski, N. Krasnikova, Primary nucleation and spherulite growth rate in isotactic polypropylene-polystyrene blends, Polymer 28(10) (1987) 1627-1634.
[236] D. Kashchiev, D. Clausse, C. Jolivet-Dalmazzone, Crystallization and critical supercooling of disperse liquids, Journal of colloid and interface science 165(1) (1994) 148-153.
[237] R. Tol, V. Mathot, G. Groeninckx, Confined crystallization phenomena in immiscible polymer blends with dispersed micro–and nanometer sized PA6 droplets, part 1: uncompatibilized PS/PA6,(PPE/PS)/PA6 and PPE/PA6 blends, Polymer 46(2) (2005) 369-382.
[238] R. Tol, V. Mathot, G. Groeninckx, Confined crystallization phenomena in immiscible polymer blends with dispersed micro-and nanometer sized PA6 droplets, part 2: reactively compatibilized PS/PA6 and (PPE/PS)/PA6 blends, Polymer 46(2) (2005) 383-396.
[239] S.E. Fenni, J. Wang, N. Haddaoui, B.D. Favis, A.J. Müller, D. Cavallo, Crystallization and self-nucleation of PLA, PBS and PCL in their immiscible binary and ternary blends, Thermochimica Acta 677 (2019) 117-130.
[240] A. Lorenzo, A. Müller, Estimation of the nucleation and crystal growth contributions to the overall crystallization energy barrier, Journal of Polymer Science Part B: Polymer Physics 46(14) (2008) 1478-1487.
[241] J.D. Hoffman, G.T. Davis, J. Lauritzen, Treatise on solid state chemistry, Plenum Press, New York 3 (1976) 497.
[242] W.S. Lambert, P.J. Phillips, Crystallization kinetics of low molecular weight fractions of branched polyethylenes, Macromolecules 27(13) (1994) 3537-3542.
[243] S. Andjelić, D. Jamiolkowski, J. McDivitt, J. Fischer, J. Zhou, R. Vetrecin, Crystallization study on absorbable poly (p-dioxanone) polymers by differential scanning calorimetry, Journal of applied polymer science 79(4) (2001) 742-759.
[244] A.J. Müller, J. Albuerne, L. Marquez, J.-M. Raquez, P. Degée, P. Dubois, J. Hobbs, I.W. Hamley, Self-nucleation and crystallization kinetics of double crystalline poly (p-dioxanone)-b-poly (ε-caprolactone) diblock copolymers, Faraday discussions 128 (2005) 231-252.
[245] A. Lorenzo, M. Arnal, A. Müller, A. Boschetti-de-Fierro, V. Abetz, Nucleation and isothermal crystallization of the polyethylene block within diblock copolymers containing polystyrene and poly (ethylene-alt-propylene), Macromolecules 40(14) (2007) 5023-5037.
[246] Y. Feng, X. Jin, Effect of self-nucleation on crystallization and melting behavior of polypropylene

and its copolymers, Journal of applied polymer science 72(12) (1999) 1559-1564.
[247] J. Varga, Melting memory effect of the β-modification of polypropylene, Journal of thermal analysis 31(1) (1986) 165-172.
[248] Y. Lu, D. Lyu, D. Cavallo, Y. Men, Enhanced beta to alpha recrystallization in beta isotactic polypropylene with different thermal histories, Polymer Crystallization 2(2) (2019) e10040.
[249] A.T. Lorenzo, M.L. Arnal, J. Albuerne, A.J. Müller, DSC isothermal polymer crystallization kinetics measurements and the use of the Avrami equation to fit the data: Guidelines to avoid common problems, Polymer testing 26(2) (2007) 222-231.
[250] J. Carvalho, K. Dalnoki-Veress, Surface nucleation in the crystallisation of polyethylene droplets, The European Physical Journal E 34(1) (2011) 6.
[251] J. Varga, A. Ille, Y. Fujiwara, βα-bifurcation of growth during the spherulitic crystallization of polypropylene, Periodica Polytechnica Chemical Engineering 34(4) (1990) 255-271.
[252] J. Varga, β-modification of isotactic polypropylene: preparation, structure, processing, properties, and application, Journal of Macromolecular Science, Part B 41(4-6) (2002) 1121-1171.
[253] P. Sajkiewicz, A. Gradys, A. Ziabicki, B. Misztal-Faraj, On the metastability of β phase in isotactic polypropylene: Experiments and numerical simulation, e-Polymers 10(1) (2010).
[254] E. Carmeli, B. Wang, P. Moretti, D. Tranchida, D. Cavallo, Estimating the Nucleation Ability of Various Surfaces Towards Isotactic Polypropylene via Light Intensity Induction Time Measurements, Entropy 21(11) (2019) 1068.
[255] F. Price, Nucleation, Zettlemoyer AC, editor (1969).
[256] D.K. Reid, B.A. Ehlinger, L. Shao, J.L. Lutkenhaus, Crystallization and orientation of isotactic poly (propylene) in cylindrical nanopores, Journal of Polymer Science Part B: Polymer Physics 52(21) (2014) 1412-1419.
[257] J. Bernstein, Polymorphism in molecular crystals, Oxford University Press2002.
[258] F. Danusso, Macromolecular polymorphism and stereoregular synthetic polymers, Polymer 8 (1967) 281-320.
[259] P. Pan, Y. Inoue, Polymorphism and isomorphism in biodegradable polyesters, Progress in Polymer Science 34(7) (2009) 605-640.
[260] A.J. Lovinger, Annealing of poly (vinylidene fluoride) and formation of a fifth phase, Macromolecules 15(1) (1982) 40-44.
[261] M. Gahleitner, D. Mileva, R. Androsch, D. Gloger, D. Tranchida, M. Sandholzer, P. Doshev, Crystallinity-based product design: Utilizing the polymorphism of isotactic PP homo-and copolymers, International Polymer Processing 31(5) (2016) 618-627.
[262] J. Karger-Kocsis, How does “phase transformation toughening” work in semicrystalline polymers?, Polymer Engineering & Science 36(2) (1996) 203-210.
[263] J. Varga, G.W. Ehrenstein, Beta-modification of isotactic polypropylene, Polypropylene, Springer1999, pp. 51-59.
[264] T. Miyazaki, Y. Takeda, M. Akasaka, M. Sakai, A. Hoshiko, Preparation of isothermally crystallized γ-form poly (vinylidene fluoride) films by adding a KBr powder as a nucleating agent, Macromolecules 41(7) (2008) 2749-2753.
[265] Y.-R. Tang, J. Xu, B.-H. Guo, Polymorphic behavior and enzymatic degradation of poly (butylene adipate) in the presence of hexagonal boron nitride nanosheets, Industrial & Engineering Chemistry Research 54(6) (2015) 1832-1841.
[266] J. Tao, L. Yu, Kinetics of cross-nucleation between polymorphs, The Journal of Physical Chemistry B 110(14) (2006) 7098-7101.
[267] C. Stoica, P. Tinnemans, H. Meekes, E. Vlieg, P. Van Hoof, F. Kaspersen, Epitaxial 2D nucleation of metastable polymorphs: A 2D version of Ostwald's rule of stages, Crystal growth & design 5(3) (2005) 975-981.
[268] J. Tao, K.J. Jones, L. Yu, Cross-nucleation between D-mannitol polymorphs in seeded crystallization, Crystal Growth and Design 7(12) (2007) 2410-2414.
[269] L. Yu, Survival of the fittest polymorph: how fast nucleater can lose to fast grower, CrystEngComm 9(10) (2007) 847-851.
[270] C. Desgranges, J. Delhommelle, Molecular mechanism for the cross-nucleation between polymorphs, Journal of the American Chemical Society 128(32) (2006) 10368-10369.
[271] C. Desgranges, J. Delhommelle, Insights into the molecular mechanism underlying polymorph selection, Journal of the American Chemical Society 128(47) (2006) 15104-15105.
[272] Y. Nozue, S. Seno, T. Nagamatsu, S. Hosoda, Y. Shinohara, Y. Amemiya, E. Berda, G. Rojas, K.

Wagener, Cross nucleation in polyethylene with precisely spaced ethyl branches, ACS Macro Letters 1(6) (2012) 772-775.
[273] C. Fraschini, L. Jiménez, B. Kalala, R.E. Prud'homme, Polymorphism and cross-nucleation in poly (1, 3-dioxolan), Polymer 53(1) (2012) 188-195.
[274] J. Wang, Z. Ren, X. Sun, H. Li, S. Yan, The βα growth transition of isotactic polypropylene during stepwise crystallization at elevated temperature, Colloid and Polymer Science 293(10) (2015) 2823-2830.
[275] G.C. Alfonso, P. Moretti, P. Pallenzona, J. Yin, Growth rates of different polymorphs from interspherulitic boundary profiles, Optical Engineering 34(12) (1995) 3385-3392.
[276] D. Cavallo, G.C. Alfonso, Concomitant crystallization and cross-nucleation in polymorphic polymers, Polymer Crystallization II, Springer2015, pp. 1-54.
[277] D. Cavallo, L. Gardella, G. Portale, A.J. Müller, G.C. Alfonso, On cross-and self-nucleation in seeded crystallization of isotactic poly (1-butene), Polymer 54(17) (2013) 4637-4644.
[278] F. Azzurri, A. Flores, G. Alfonso, F. Baltá Calleja, Polymorphism of isotactic poly (1-butene) as revealed by microindentation hardness. 1. Kinetics of the transformation, Macromolecules 35(24) (2002) 9069-9073.
[279] G. Alfonso, F. Azzurri, M. Castellano, Analysis of calorimetric curves detected during the polymorphic transformation of isotactic polybutene-1, Journal of thermal analysis and calorimetry 66(1) (2001) 197-207.
[280] D. Byelov, P. Panine, K. Remerie, E. Biemond, G.C. Alfonso, W.H. de Jeu, Crystallization under shear in isotactic polypropylene containing nucleators, Polymer 49(13) (2008) 3076-3083.
[281] E.M. Troisi, S. Formenti, F. Briatico-Vangosa, D. Cavallo, G.W. Peters, Nucleation induced by "Short-Term Pressurization" of an undercooled isotactic polypropylene melt, European Polymer Journal 85 (2016) 553-563.

Acknowledgment

Time flies, it was my honor to study in “Semicrystalline Polymers” group in Genova.

First of all, I would like to give my thanks to Prof. Dario Cavallo for providing me a chance to continue research, for the polite, generous and patient supervision in the three years. I appreciate all the discussions during my Ph.D. Extremely, I am grateful to you for involving me in various research activities, introducing me to other researchers and spending time to correct my articles and thesis.

I would like to express my deep respect to Prof. Giovanni Carlo Alfonso. Your series of work inspired me a lot when I start research until now. Thank you very much for the discussions in the three years, from which I benefit a lot. I wish you enjoy your retired life very well.

I want to thank Prof. Gerrit Peters and Prof. Ruth Cardinaels, for allowing me to work in your lab and sharing your valuable time with me to discuss every question patiently. Also, I would like to extend my thanks to Prof. Lambert Van Breemen, for giving me freedom and encouragement. Meanwhile, thanks for the help from Stan Looijmans.

I would like to acknowledge Prof. Dujin Wang, Prof. Xia Dong for hosting me very well during my internship in Beijing.

I also would like to acknowledge my collaborators, Prof. Alejandro Müller, Prof. Dujin Wang, Prof. Xia Dong, Prof. Xiuqin Zhang. Thanks for everything you contributed to my Ph.D thesis.

Thanks to the members from “Semicrystalline Polymers” group in Genova: Enrico, Kasha, Filippo, Giulio, especially to Seif.

The friends I have in Genova: Kun Li, Tao Li, Xue Bai, Yao Wang, Tianwen Qi, Wei Fu, Jianan Huang, Wei Wang, Meng Li, et al., and my friends in Eindhoven: You Peng, Yuying Liu, Liyang Wang et al. It is very nice to meet you out of China. Thank you very much for the company and making my life wonderful.

I am grateful to China Scholarship Council (CSC) for the financial support during my Ph.D, giving me a chance to study abroad and experience different cultures. I also appreciate the BIODEST and Erasmus projects, enabling me to do internships in China and Netherlands.

Again, I would like to give my appreciation to all my teachers and supervisors in the past. Thank you so much for educating me.

Finally, I dedicate this thesis to my family, especially my parents. I am far away and indebted to you too much. I hope I can compensate you back in the future.

Publications

1. Wang B, Alfonso G.C, Müller A.J, Cavallo D. Differential scanning calorimetry study of cross-nucleation between polymorphs in isotactic poly (1-butene). ***Polymer International***, 2019, *68*(2), 257-262.
2. Wang B, Müller A.J, Wang D, Cavallo D. Nucleation of Poly (lactide) on the Surface of Different Fibers. ***Macromolecules***, 2019, *52*(16), 6274-6284.
3. Wang B, Cavallo D, Zhang B, Chen J.B. Evolution of chain entanglements under large amplitude oscillatory shear flow and its effect on crystallization of isotactic polypropylene. ***Polymer***, 2019: 121899.
4. Carmeli E, Wang B, Moretti P, Tranchida D, Cavallo D. Estimating the Nucleation Ability of Various Surfaces Towards Isotactic Polypropylene via Light Intensity Induction Time Measurements. ***Entropy***, 2019, *21*(11), 1068.
5. Wei Wang, B Wang, Enrico Carmeli, Zefan Wang, Zhe Ma, Dario Cavallo. Cross-nucleation of polybutene-1 Form II on Form I seeds with different morphology. ***Polymer Crystallization***, 2019, doi.org/10.1002/pcr2.10104.
6. Wang B, Müller, A.J, Cavallo D. Self-nucleation and heterogeneous nucleation of i-PP micro-droplets in immiscible blends. *Submitted to Macromolecules*, ***Under Review***.